NON-STATISTICAL FLUCTUATIONS IN RELATIVISTIC HEAVY-ION COLLISIONS

ABSTRACT

OF THE

THESIS

SUBMITTED FOR THE AWARD OF THE DEGREE OF

Doctor of Philosophy

IN

PHYSICS

By

WASEEM BARI

Under the Supervision of

Prof. Muhammad Irfan

DEPARTMENT OF PHYSICS
ALIGARH MUSLIM UNIVERSITY
ALIGARH (INDIA)

2002

ABSTRACT

The study of nuclear collisions has attracted the attention of the high energy physicists during the recent years. One of the main considerations for undertaking such a study is the possibility of searching for the evidence of the quark-gluon plasma (QGP) in these collisions. QGP is envisaged to have similar characteristics which existed $10^{-6} - 10^{-5}$ seconds after the Big Bang. QGP is also believed to exist in the core of neutron stars. Since the conditions of the Big Bang can not be reached now and the neutron stars are quite far away, relativistic heavy-ion collisions remain the only possibility for looking at the elusive phase of quark-gluon plasma and the fingerprints of its formation.

Study of various features of relativistic heavy-ion collisions became possible only with the advent of several heav-ion accelerators and colliders. The two main machines which are especially dedicated to the study of ultra-relativistic nuclear collisions, especially the production of QGP in the collisions produced by the ion beams from the Relativistic Heavy Ion Collider (RHIC) at BNL and Large Hadron Collider (LHC) at CERN; RHIC became operational in 2000 while LHC is expected to start functioning from early 2005.

In A-A collisions at RHIC and LHC energies, the conditions necessary for the production of QGP might be reached, confirmation of the formation of such a phase of matter would still remains elusive. It is because of the fact that even if QGP is formed at these energies, it will be of very small size and

would survive for very short time; QGP is visualized to be a few fermis in diameter and to survive for $\sim$ 5 to 10 fm/c.

One of the most important probes for the formation of QGP is the occurrence of fluctuations in the multiplicity and pseudorapidity distributions of the relativistic charged particles produced in the collisions of heavy nuclei at ultra-relativistic energies. The idea of considering the occurrence of fluctuations as a probe for QGP formation is based on the fact that if QGP is produced in these collisions, it may give rise to non-linear emission of particles, the effect of which would be reflected in multiplicity distributions in the form of existence of unusual peaks and valleys in these distributions. However, it may be mentioned that the fluctuations may not arise due to QGP formation only, there may be other reasons as well which may be of purely statistical nature. Thus, it is always desirable to separate out the non-statistical contribution to the fluctuations so that some conclusive remark about the physical origin of these fluctuations may be made.

Occurrence of non-statistical fluctuations in the interactions of 4.5A and 14.5A GeV/c ^{28}Si nuclei with emulsion is investigated in terms of scaled factorial moments. The scaled factorial moments are observed to increase linearly with decreasing bin width. Thus, the predicted power law behaviour of the scaled factorial moments has been observed, indicating thereby presence of non-statistical fluctuations in the interactions considered.

Variations of the slopes of $\ln< F_q >$ versus $-\ln\delta\eta$ plots, which characterize

the strength of the intermittency effect, with the order of the moment and the incident energy are examined. The slope parameters are found to increase with increasing order of the moment; their values turn out to be greater for the higher incident energy for each order of the moment.

The fractal nature of the particle emission source is studied in terms of the anomalous dimensions, $d_q(=\frac{\phi_q}{q-1})$. The anomalous dimensions demonstrate an increasing trend with increasing order of the moment. On the other hand, the values of d_q for the interactions caused by the projectile of higher energy are higher as compared to those for the collisions caused by lower energy projectile. Furthermore, the values of the anomalous dimensions for the interactions due to lighter targets (CNO) are observed to be relatively higher in comparison to their corresponding values for the heavier targets (AgBr) for each order of the moment.

In order to examine the occurrence of the non-thermal phase transition in the various interactions considered in the present study, the behaviour of $\lambda_q(=\frac{\phi_{q+1}}{q})$ as a function of the order of the moment, q is studied. Clear minima in the λ_q versus q plots are not observed in all the categories of interactions considered. However, for the interactions of 4.5A GeV/c ^{28}Si nuclei with emulsion, the presence of a distinct minima in the λ_q versus q plots may indicate the existence of non-thermal phase transition.

Multifractality in the interactions considered has been investigated in terms of multifractal moments, $< G_q >$. $\ln < G_q >$ versus $-\ln\delta\eta$ plots show linear

rise upto a certain extent and thereafter the plots get saturated. The observed linearity points towards the existence of multifractality in the interactions considered in the present study. It is worthmentioning that the saturation in the plots is a reflection of the fact that with decreasing bin width, more and more bins contain one or no particle.

The variation of the mass exponents τ_q with the order of the moment is studied. It is observed that the mass exponents increase with the order of the moment. The dynamical component of of the mass exponent is observed to deviate substantially from q-1, which indicates the presence of dynamical fluctuations in the interactions investigated.

Variation of the generalized dimensions, D_q, with the order of the moment, q, is observed to satisfy the condition of multifractality, that is, $D_q > D_{q'}$, where $q < q'$. The generalized dimensions are observed to have positive values for all the orders of the moments. Furthermore, the generalized dimensions are found to exhibit a decreasing trend with increasing order of the moment which is a general property of multifractals.

A qualitative description of the fluctuations is presented in terms of the variation of the spectral function, $f(\alpha_q)$, with the Lipschitz-Holder exponents α_q. The spectral function is observed to be smooth and concave downwards with its maximum lying around $q = 0$. The function is not sharply peaked thereby confirming the non-smooth nature of the multiplicity distribution.

Correlation and clusterization amongst the relativistic charged particles

produced in 4.5A and 14.5A GeV/c ^{28}Si nucleus collisions are investigated in terms of the maximum rapidity density distribution of relativistic charged particles in narrow pseudorapidity bins, $\Delta\eta$. For a fixed $\Delta\eta$, the mean value of the maximum charged particle density is found to decrease exponentially with increasing value of the total pseudorapidity and increase with increasing particle multiplicity. These features are, however, essentially independent of the beam energy. These features, when compared with those obtained for correlation free Monte Carlo event sample, indicate the existence of dynamical correlation and clusterization.

Correlation and irregularities in the relativistic charged particles density distributions in A-A collisions are looked into by studying the nearest neighbour spacing spectra of relativistic charged particles. For this purpose, experimental and simulated data samples over a wide energy range involving different targets and projectiles are analyzed in the frame work of Wigner-Dyson type of Random Matrix Theory. The findings of the presetn study help conclude that the random emission of particles dominates in the central region of the η spectrum and correlation, if any, appears to be suppressed. It may be remarked that in future experiments involving higher beam energies and targets as heavy as lead, random emission, particularly in the mid rapidity region would be the dominant process.

NON-STATISTICAL FLUCTUATIONS IN RELATIVISTIC HEAVY-ION COLLISIONS

THESIS

SUBMITTED FOR THE AWARD OF THE DEGREE OF

Doctor of Philosophy

IN

PHYSICS

By

WASEEM BARI

Under the Supervision of

Prof. Muhammad Irfan

DEPARTMENT OF PHYSICS
ALIGARH MUSLIM UNIVERSITY
ALIGARH (INDIA)

2002

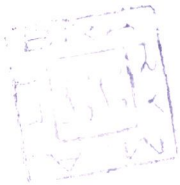

To

MY FATHER
who taught me to be tough

MY MOTHER
who taught me to be patient

and

AMTUL HADI, AMTUL RASHID,
AMBREEN AND ATIYA
who make the best part of my being

Dr. Muhammad Irfan
Professor of Physics
Phone : +91-571-700093
Fax : +91-571-701001
e-mail: hep_amu@rediffmail.com

Department of Physics
Aligarh Muslim University
Aligarh – 202 002
INDIA

Date: May 31, 2002

Certificate

Certified that this thesis entitled, "NON-STATISTICAL FLUCTUATIONS IN RELATIVISTIC HEAVY-ION COLLISIONS", embodies the original work of Mr.WASEEM BARI carried out under my supervision. The work is worthy of consideration for the award of Ph. D. degree.

(**Prof. Muhammad Irfan**)

ACKNOWLEDGEMENTS

It gives me immense pleasure to express with great reverence my deep sense of gratitude to my esteemed teacher and supervisor, Professor Muhammad Irfan for his keen interest in the completion of this work. I must admit that without his able guidance and constructive comments, this Thesis would not have been completed. This would not be an exaggeration if I also admit that in addition to his academic impact on me, his dynamic personality has helped me grow as a responsible person as well.

I am thankful to Professor S. K. Singh, Ex-Chairman, Department of Physics and Professor R. Prasad, Chairman, Department of Physics for providing the facilities of High Energy Physics Laboratory of the Department.

My sincere thanks are due to Professor Mohammad Zafar, Department of physics, AMU, Aligarh for several fruitful discussions I had with him and to Dr. Afzal Ahmad, Department of Applied Physics, AMU, Aligarh for many valuable suggestions. I am indeed indebted to Dr. Shakeel Ahmad, Department of physics, AMU, Aligarh for his continuous help during the completion of this work. I must put on record that his programming skills were quite helpful in carrying out various analyses presented in this Thesis.

I take this opportunity to thank Dr. A. R. Khan, Dr. Shafiq Ahmad and Dr. Tufail Ahmad for their active cooperation.

I wish to extend my gratefulness to the various ALICE collaborators in India and abroad who provided me several opportunities to work in the field of experimental high energy physics. I am especially thankful to Prof. Bikash Sinha, Director, Saha Institute of Nuclear Physics (SINP) and Variable Energy Cyclotron Centre (VECC), Kolkata for allowing me to work with the Experimental High Energy Physics Group of the Institute. I would like to extend my sincere thanks to Prof. Prasanta Sen of SINP, Kolkata for his constant encouragement during my stay at SINP. I am grateful to all the members of the EHP Division of SINP, particularly Prof. Pratap Bhattacharya, Head EHP Division, Dr. Sukalyan Chattopadhyay, Dr. Supratik Mukhopadhyay, Dr. Swapan Sen, Dr. (Mrs.) Nayana Majumdar, Dr. (Mrs.) Tinku Sinha and Mr. Tilak Ghosh for their encouragement and academic as well as moral support they provided during my short stay at SINP. I am also grateful to Dr. Y. P. Viyogi and Dr. Tapan Nayak of VECC, Kolkata for their valuable suggestions from time to time.

I wish to express my indebtedness to my colleagues, Mr. Nazeer Ahmad, Mr. Mohsin Khan and Mr. Danish Azmi, for their cooperation and various helps. Thanks are also due to Mr. Syed Muhammad Mahir and Er. Khalid Imdad for their technical help.

During my stay at Aligarh, several people have been of immense help to

me. I wish I could extend my sincere thanks to all these people. However, if I miss to mention any name who should have been properly thanked, he or she should consider it as a human error and pardon me for the same.

I take this opportunity to extend my gratitude to Dr. Waseem Ahmad Faridi and Mrs. Maisra Faridi, whose affection has always made me feel homely at Aligarh.

My friends have had a great role in making me comfortable in every way. Ms. Nazma Bano, Jawaid Ahmad Lone, Zameer Chacha, Dr. Farooq A. Dar, Khalid Ayaz, Dr. Rafiq Ahmad, Younus Iqbal, Zia A. Khan, K. U. Mahmood Ahmad and Ms. Shameema deserve special thanks for their support and encouragement. I would also like to thank my younger friends, Primrose Bashir, Parvez A. Wani, Ajaz A. Mir, Mushariq Ahmad, Rafiq Hussain and Idrees M. Dar.

I wish to express my deepest sense of gratitude to my brother-in-law, Mr. Abdul Shakoor Tak, who has been very kind and affectionate to my parents during my stay here away from home.

I would like to express my gratitude to all my elders, particularly my uncles, aunts and in-laws, whose blessings and affection have always been available to me.

My wife, who inculcated in me the great feelings of humanism, deserves a huge appreciation and special thanks.

Financial assistance from the Department of Science and Technology (DST) and the Department of Atomic Energy (DAE), Govt. of India, New Delhi is acknowledged with thanks.

Last but not the least, my compassionate parents and my loving sisters deserve the best treat from me. However, writing just a few lines about them would not express adequately my true feelings. So, I prefer to keep these feelings close to my heart.

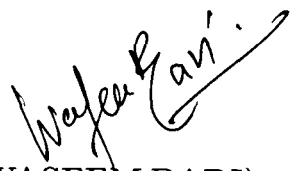

(WASEEM BARI)

PREFACE

The main motivation behind the present study was to examine the occurrence of non-statistical fluctuations in 14.5A GeV/c ^{28}Si-nucleus interactions for it is envisaged that the existence of dynamical fluctuations in multiplicity and pseudorapidity distributions of the relativistic particles produced in heavy-ion collisions would yield invaluable information regarding the source of these particles. It is worthmentioning that the study of non-statistical fluctuations becomes still more important due to the fact that the occurrence of the dynamical fluctuations in these distributions may be one of the many finger prints of the formation of quark-gluon plasma (QGP) in these collisions.

Relevant details about some of the models, which successfully explain important aspects of relativistic nuclear collisions are presented in Chapter I. Furthermore, details about the major facilities available for carrying out study of relativistic heavy-ion collisions are given in the same chapter. Explanation based on theoretical considerations of the various signatures of the formation of QGP in relativistic nuclear collisions is also given.

The details about the emulsion stacks used and the criteria for selecting the events, methods of measurements etc., are given in Chapter II. Results on some general characteristics, like mean multiplicity and multiplicity distributions of various types of charged particles and pseudorapidity distributions of relativistic charged particles produced in the interactions of 4.5A and 14.5A

GeV/c ^{28}Si nuclei with emulsion are also presented in this chapter.

The occurrence of intermittency in the various categories of interactions considered is examined in detail. The method of scaled factorial moments (SFM) proposed by Bialas and Peschanski, is used for studying intermittency. Various interesting aspects of intermittency, like the power law behaviour of the SFM, the intermittency indices and the generalized dimensions are investigated systematically and thoroughly. The possible occurrence of the non-thermal phase transition in these interactions has also been looked into. The occurrence of intermittent patterns is also studied in the framework of the Ginzburg-Landau description of intermittency. Results based on well focussed observations about the above features are presented in Chapter III

Intermittency in relativistic heavy-ion collisions is envisaged to be a reflection of the fractal nature of the particle emitting source. This aspect is studied in terms of the theory of multifractals and the results are presented in Chapter IV. The contribution of the dynamical component of the moments is disentangled by using Monte Carlo generated data samples. Experimental findings are compared with those obtained on the basis of FRITIOF simulated events. The behaviour of the anomalous dimensions shows multifractal nature in the various types of interactions studied. Furthermore, the study of the spectral function reveals non-smooth nature of the multiplicity and pseudorapidity distributions of the particles produced in these interactions. All these results are also presented in Chapter IV

Results of the study of correlations and fluctuations observed on event-by-event basis in rapidity density and rapidity spacing spectra are presented in Chapter V. Monte Carlo simulations are carried out to disentangle the contribution of the dynamical fluctuations from the statistical ones. Furthermore, the extrapolation is made using the event generator FRITIOF to predict the mechanism of multiparticle production in nuclear collisions at RHIC and LHC energies. These are also described in Chapter V.

Summary of the findings of the present study and concluding remarks about some of the interesting features of relativistic nucleus-nucleus collisions are presented in Chapter VI.

CONTENTS

List of Figures

List of Tables

CHAPTER I

INTRODUCTION

Study of nucleus-nucleus collisions at relativistic energies provides an opportunity to understand the properties of the densest and the hottest form of matter that can be produced in the laboratory. The ultimate goal of studying these collisions is to reach the conditions under which the hadronic matter is envisaged to undergo a phase transition to quark-gluon plasma (QGP): the degrees of freedom of the new state are the quarks and gluons. Quark-gluon plasma is believed to have existed in the early Universe [1]; it is also envisaged to exist in the core of the neutron stars [2]. However, the Big Bang occurred long ago and the neutron stars are very far away. So the collisions of heavy nuclei at relativistic energies remain the only possibility to search for the QGP formation [3-6].

In a nucleus-nucleus collision, many nucleon-nucleon collisions are visualized to take place, thereby depositing the energy of the nucleons in the centre-of-mass regions. Since all these nucleon-nucleon collisions take place almost at the same time, due to Lorentz contraction a region of very high energy density is created However, the dynamics of nuclear collisions is very complicated and needs a deep and thorough understanding of the behaviour of nucleon-nucleon collisions It is important to have a clear understanding of the dynamics of nucleus-nucleus collisions in order to make some interesting remarks about the

features of the matter formed in these collisions.

Investigations carried out using heavy-ion beams from SPS, CERN and AGS, BNL during the last several years reveal that the characteristics of relativistic nuclear collisions significantly deviate from what one would have expected on the basis of superposition of independent nucleon-nucleon collisions [7]. Several experimental facts, such as strangeness enhancement [8,9] and large fluctuations in multiplicity and transverse energy distributions [10,11] observed in nuclear collisions cannot be explained in terms of the superposition of nucleon-nucleon collisions.

Study of multiplicity distributions of relativistic hadrons produced in nuclear collisions at high energies and correlations amongst these particles help understand the dynamics of these collisions and mechanism of multiparticle production. Furthermore, study of multiplicity distributions in a limited phase space is of great relevance as this may be quite helpful in searching for the evidence of dynamical fluctuations of an underlying fractal structure [12,13] referred to as intermittency.

Keeping in view the possibility of occurrence of fluctuations and correlations in relativistic nuclear collisions, a thorough study of these aspects is carried out using 4.5A and 14.5A GeV ^{28}Si-nucleus interactions. Various aspects of these collisions are presented in Section 1.4 of this chapter.

1.1 Models of nucleus-nucleus collisions

The occurrence of non-trivial phenomena in relativistic nucleus-nucleus collisions requires introduction of the models put forward to explain the mechanism governing these phenomena. The most important part of the description of these models is focussed on giving the details about the collision geometry, the emission characteristics of the secondaries and the estimation of the energy density of the matter formed during the collisions. Details about some of these models are presented in the following sections.

1.1.1 Wounded nucleon model

Wounded nucleon model [14] explains quite satisfactorily the emission characteristics including angular distribution of the particles produced in relativistic nucleus-nucleus collisions [15]. This model assumes that the number of relativistic charged particles produced in A-A collisions, n_{AA}, should scale with the mean number of wounded or participating nucleons, W. Furthermore, according to this model n_{AA} should scale with $< n_{pp} >$, where n_{pp} represents the number of fast charged particles produced in p-p collisions at an equivalent incident energy. Thus the particle multiplicity in A-A collision at a given projectile energy may be expressed [15] as, $n_{AA}(E) = \frac{1}{2}Wn_{pp}(E)$.

The multiplicity per participating nucleon, $m(= n_{AA}/W)$ is a convenient parameter for comparing the multiplicities for the systems of different sizes because m is independent of W and hence will not depend on the impact pa-

rameter; m depends only on the collision dynamics.

The number of wounded nucleons may be estimated [14] using the following expression:

$$W = A_T \frac{\sigma_{NP}}{\sigma_{PT}} + A_P \frac{\sigma_{NT}}{\sigma_{PT}} = W_T + W_P \quad (1.1)$$

where σ_{PT} is the total inelastic cross-section for the collision of projectile nucleus with target nucleus; σ_{NP} and σ_{NT} are respectively the total inelastic nucleon-projectile nucleus and nucleon-target nucleus interaction cross-sections; A_P and A_T are the masses of the projectile and the target nuclei respectively and W_T and W_P respectively denote the numbers of wounded nucleons of the target and the projectile nuclei.

In order to calculate the values of W for the central A-A collisions, the cross-sections which are the functions of the maximum impact parameter, b_{max} are used. The cross-sections are estimated with the help of Glauber approach [16] using the hadronic cross-sections and the nuclear density functions of the target and projectile nuclei. The value of b_{max} may be calculated using the following expression [15]:

$$\sigma_{part} = \pi b_{max}^2 = \frac{N_{central}}{N_{total}} \quad (1.2)$$

where $N_{central}$ and N_{total} are the numbers of the central and total events respectively for a given sample of A-A collision data. The nuclear collision geometry considered in the FRITIOF [17] may be used to determine the value of the *impact parameter*, b, for each event of the simulated sample. For the central

collisions, the value of b is taken to be less than 5 fm [15]. Furthermore, by using the value of b = 5 fm, W may be evaluated. Hence, using the Glauber calculations, W_P and W_T and hence W may also be easily estimated.

By assuming that the cross-section for the nucleons which have been excited by various interactions is the same as that for the unexcited nucleons, the number of projectile and target interactions, ν_P and ν_T can be estimated from:

$$\nu_T = A_T\sigma_{NN}/\sigma_{NT} \text{ and } \nu_P = A_P\sigma_{NN}/\sigma_{NP}$$

The total number of encounters made by the projectile nucleons with the target nucleus may be calculated using the following relation:

$$\nu = W_P\nu_T = W_T\nu_P$$

Predictions of the wounded nucleon model are reported [15, 18,19] to be in fair agreement with the results of the experimental and FRITIOF data on p-Em, O-Em and S-Em interactions at 200A GeV and 158A GeV Pb-Pb collisions.

1.1.2 Multiple nucleon collision model

Initially, this model was proposed [20] for parameterizing multiplicity distribution observed in high energy hadron-nucleus interactions. Later on, it was extended [21] to explain the data on A-A collisions also.

On the basis of the Additive Quark Model (AQM) [22], it was proposed [23] that relativistic charged particle multiplicities in h-p and h-A collisions,

$< n_s >_{hp}$ and $< n_s >_{hA}$, may be expressed as:

$$< n_s >_{hA} = < n_s >_{hp} N_q$$

where $N_q (= N_c \sigma_{qA}^{in} / \sigma_{hA}^{in})$ denotes the average number of constituent quarks participating in the interaction; N_c is referred to as the number of valence quarks in the projectile and σ_{qA}^{in} and σ_{hA}^{in} represent respectively inelastic quark-nucleus and hadron-nucleus cross-sections.

According to the multiple nucleon collision model [20, 21], the mean multiplicity of relativistic charged particles produced in h-A interactions may be determined using the expression

$$< n_s >_{hA} = N_q \left[a + b \ln \frac{\sqrt{s_A}}{N_q} - c \ln^2 \frac{\sqrt{s_A}}{N_q} \right] - \alpha \qquad (1.3)$$

The parameters a, b and c have been reported [21] to have the values equal to 2.50, 0.28 and 0.53 respectively for both pion and proton projectiles, while the value of α, which is referred to as the leading particle multiplicity, is found [21] to be 0.85.

In the above expression $\sqrt{s_A}$ denotes the total centre-of-mass energy, which according to coherent tube picture [24], is expressible as $s_A = \nu_q s_a$ where $\sqrt{s_a} = \sqrt{s} - m_B - m_T$. $\sqrt{s}$ is the available centre-of-mass energy in a h-N collision and m_B and m_T are respectively the masses of projectile and target. It may be noted that ν_q is the mean number of inelastic collisions made by quarks with the target nucleus and may be calculated using:

$$\nu_q = A \sigma_{qN}^{in} / \sigma_{qA}^{in}$$

where A is the atomic number of the target nucleus and $\sigma_{qN}^{in} = \frac{1}{3}\sigma_{NN}^{in}$.

The model was later extended to describe A-A collisions also. For this purpose, the effective numbers of wounded quarks in the incident and target nuclei and the average numbers of encounters made by each of these quarks were estimated. For A-A collision, Eq. 1.3 may be written [21] as:

$$< n_s >_{AB} = N_q^{AB} \left[a + b \ln \frac{\sqrt{s_{AB}}}{N_q^{AB}} - c \ln^2 \frac{\sqrt{s_{AB}}}{N_q^{AB}}\right] \tag{1.4}$$

where $\sqrt{s_{AB}} = (\nu_q^{AB} S_a)^{1/2}$ and $\nu_q^{AB} = \nu_{qA}\nu_{qB} = \frac{A\sigma_{qN}^{in}}{\sigma_{qA}^{in}} \frac{B\sigma_{qN}^{in}}{\sigma_{qB}^{in}}$

while the mean number [25] of participant quarks in the target and projectile nuclei is

$$N_q^{AB} = \frac{1}{2}\left[\frac{N_B \sigma_{qA}^{in}}{\sigma_{AB}^{in}} + \frac{N_A \sigma_{qB}^{in}}{\sigma_{AB}^{in}}\right] \tag{1.5}$$

where N_A and N_B represent the numbers of valence quarks in nuclei A and B respectively.

The cross-section for A-A collisions may be parameterized [26] as:

$$\sigma_{AB}^{in} = \pi r^2 \left[A^{1/3} + b^{1/3} - \frac{C}{A^{1/3}+B^{1/3}}\right]^2 \tag{1.6}$$

This model predicts correctly the value of the mean multiplicity of relativistic charged particles for the central collisions. In such collisions all the quarks of the incident nucleus are envisaged to be wounded and thus for $N_q^{AB} = 3A$ [21], Eq. 1.4 would take the form:

$$< n_s >_{AB}^{central} = 3A\left[a + b \ln\left[\frac{\sqrt{\nu_q^{AB} S_a}}{3} - c \ln^2\left[\frac{\sqrt{\nu_q^{AB} S_a}}{3}\right]\right]\right] \tag{1.7}$$

Values of $< n_s >$ for p-p, p-A and A-A collisions at widely different incident energies are reported [21] to be quite compatible with their corresponding experimental values. The model, therefore, describes quite satisfactorily h-h, h-A and A-A interactions in terms of elementary quark-gluon interactions.

1.1.3 The Bjorken model

Bjorken model [27] is another simple model used to describe nucleus-nucleus collisions and it also permits estimation of the energy density reached in such collisions. According to this model, the two colliding nuclei are regarded as two thin discs as depicted in Fig. 1.1(a). The longitudinal thicknesses of the nuclei are neglected owing to extremely high energy so that the longitudinal coordinates of the two nuclei can be assumed to be almost the same. The two nuclei are visualized to proceed towards each other from the two extremes of z-axis, i.e. $z = -\infty$ and $z = +\infty$, with relativistic velocities. The collision is assumed to take place at the point $(z, t) = (0, 0)$ as shown in Fig. 1.1(b). The energy density in the region characterized by $z \sim 0$, can be in the form of quarks and gluons or hadrons. The space-time development of the collision as envisaged in this model is exhibited in Fig. 1.2. Soon after the occurrence of the collision at a very high energy at $(z, t) = (0, 0)$, the energy density in the region may be quite sufficient to produce quark-gluon plasma. To estimate the energy density, a longitudinal length Δz around $z = 0$, where the matter is at rest, is taken into consideration. The volume formed by Δz and A is $A\Delta z$.

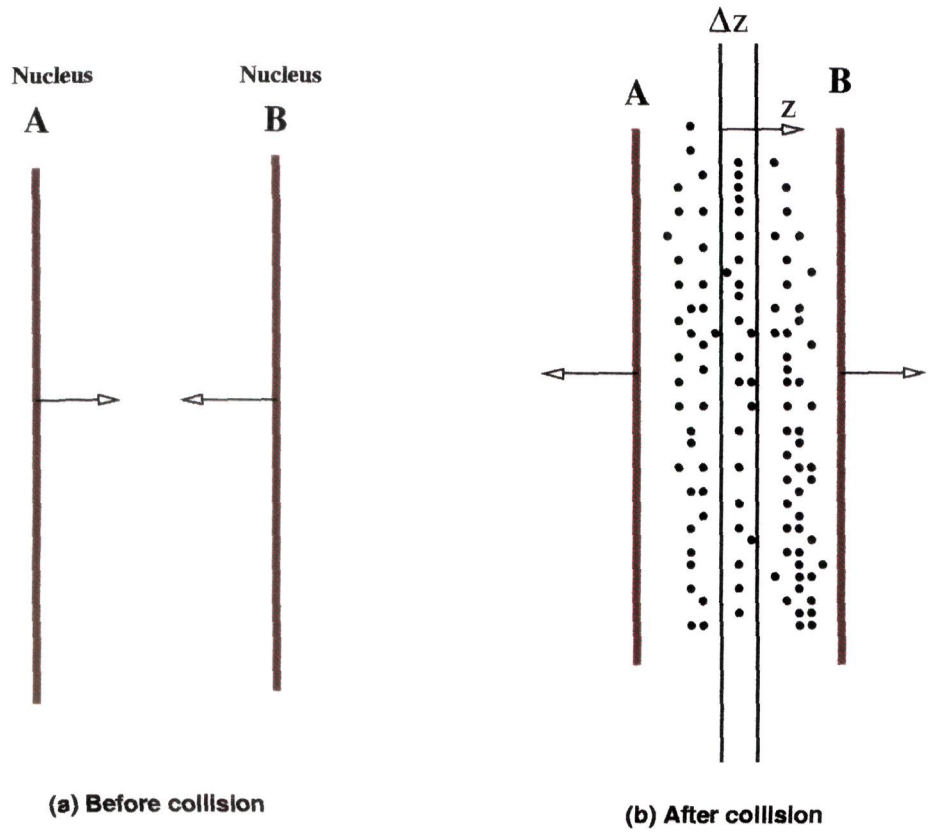

Fig. 1.1 The configurations of two colliding nuclei before and after collision

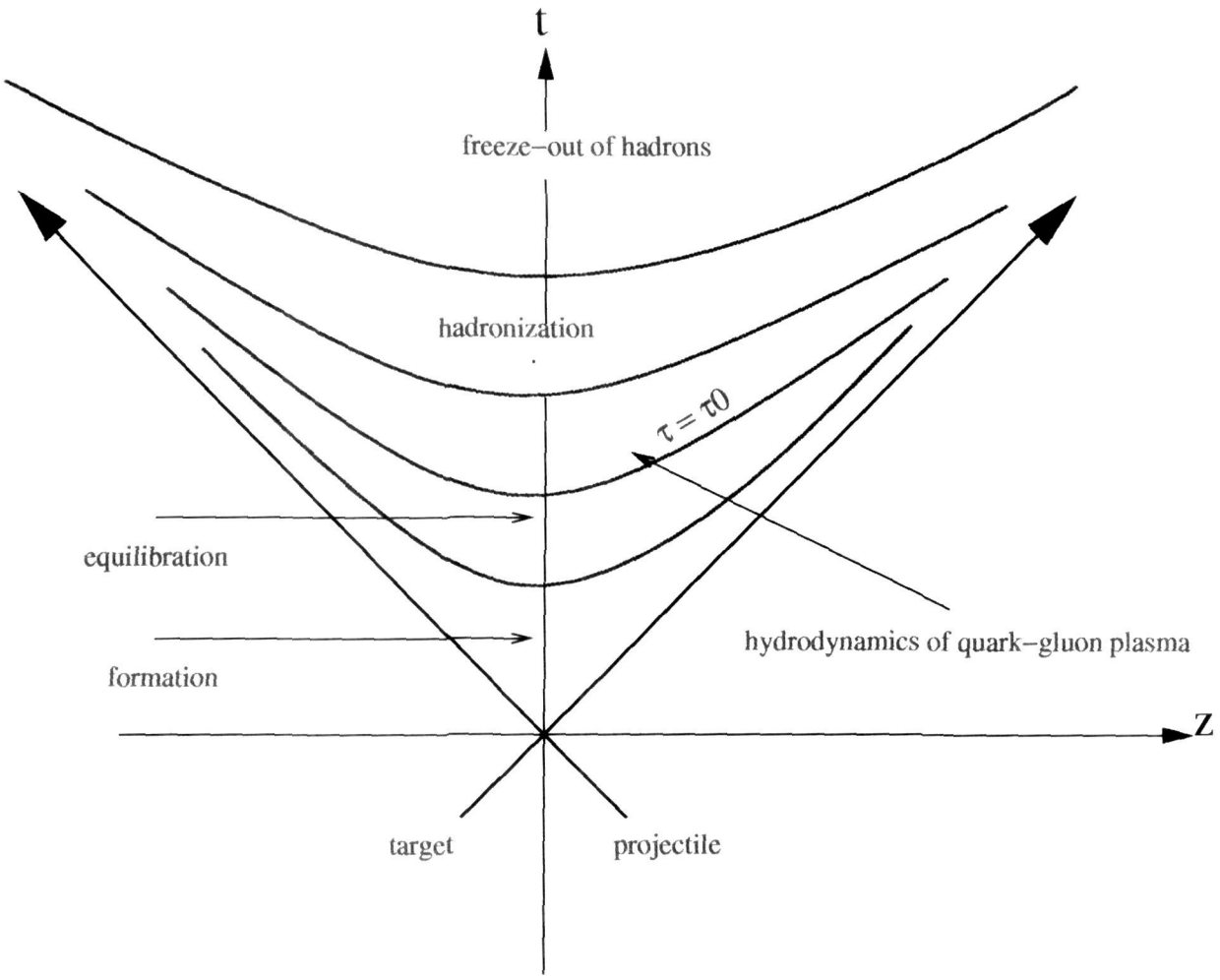

Fig. 1.2 Space–time evolution in a nucleus–nucleus collision

Thus, the number density in this volume at $z = 0$ and at proper time τ_0 is

$$\frac{\Delta N}{A\Delta z} = \frac{1}{A}\frac{dN}{dy}\frac{dy}{dz}\Big|_{y=0} \tag{1.8}$$

where ΔN represents the number of particles present in the volume AΔz and y is the rapidity of a particle. The proper time τ_0 is the time during which quark-gluon plasma may have been formed and equilibrated. If $E_T = m_T \cosh y$ is the transverse energy of a particle in this region, then the total energy contained in the collision region is:

$$E = N \frac{dE_\perp}{dy}\Delta y \tag{1.9}$$

The initial energy density averaged over the transverse area A at the proper time τ_0 is, therefore, given by:

$$\epsilon_0 = \frac{m_\perp}{\tau_0 A}\frac{dN}{dy}\Big|_{y=0} \tag{1.10}$$

In terms of the transverse energy, the above expression may be written as:

$$\epsilon_0 = \frac{1}{\tau_0 A}\frac{dE_\perp}{dy} \tag{1.11}$$

This model predicts $\epsilon_0 \approx 1.3$ GeV/fm^3 at AGS energy, for which $dE/d\eta = 200$ GeV for the central Au-Au collisions and $\epsilon_0 \approx 3$ GeV/fm^3 at the SPS energy having $dE/d\eta = 450$ GeV for Pb-Pb collisions [7].

1.1.4 FRITIOF of the Lund model

FRITIOF of the Lund model [28] is one of the most famous Monte Carlo simulation based models. The important ingredients of this model are the

string formation and its fragmentation. It is interesting to mention that a string refers to a longitudinally oriented object formed when the nucleons of the projectile come closer than some minimum distance, d $< (\sigma_{NN}/\pi)^{1/2}$. According to FRITIOF, a string is formed as a result of momentum exchange, that is, longitudinal excitation, as displayed in Fig. 1.3. This essentially means that the interaction of two hadrons with large momenta results in two longitudinally excited objects, called strings. Transverse momenta and masses are assigned to the string pieces at string fragmentation according to LUND formalism [29] of the fragmentation.

The FRITIOF Code

The FRITIOF code is written in FORTRAN 77. The various variables in the main programme, such as atomic numbers and mass numbers of the projectile and target nuclei, projectile energy and the number of events to be generated can be set by the user depending upon the requirements. The events are administered by various subroutines within the code. For instance, the subroutine JETSET in the FRITIOF code takes care of the hadronization and decay of particles.

1.2 Accelerators and heavy-ion colliders

Accelerators

Alternating Gradient Synchrotron (AGS) at Brookhaven National Laboratory (BNL) and the Super Proton Synchrotron (SPS) at CERN are the two

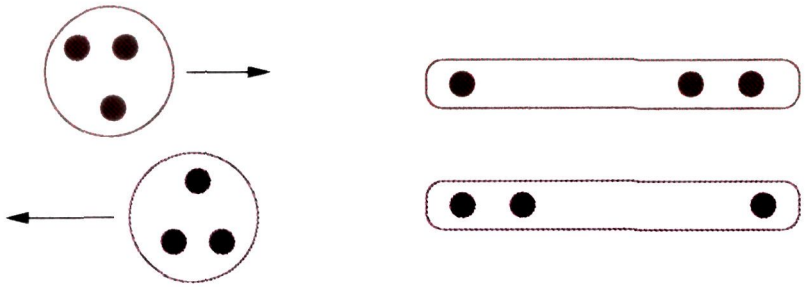

Fig. 1.3 String formation due to longitudinal excitation.

All partons in a string originate from one baryon.

major research facilities for relativistic heavy-ion experiments for examining the properties of dense hadronic matter and the signals of quark-gluon plasma formation. Both the machines are in operation since 1986; AGS provides beams ranging from proton to gold nuclei with momenta upto 14.6A GeV/c, whereas SPS produces beams ranging from proton to lead nuclei with momenta upto 200A GeV/c.

Heavy-ion colliders

Amongst the most important heavy-ion colliders are the Relativistic Heavy-Ion Collider (RHIC) at Brookhaven and the Large Hadron Collider (LHC) to be constructed at CERN: RHIC became operational in June, 2000 and the LHC is scheduled to start functioning in 2005. RHIC is envisaged to produce the deconfined state of quarks and gluons believed to have existed just millionth of a second after the Big Bang. The collisions at RHIC energies are planned to be studied by four major experiments, STAR, PHENIX, BRAHMS and PHOBOS.

The LHC at CERN will bring protons and ions into head-on collisions at energies never reached before. The collisions of heavy nuclei at LHC energies would recreate the condition which is believed to have existed in the early Universe. The LHC can collide proton beams with 7-on-7 TeV energy and allow lead-lead collisions to take place at about 1262 TeV centre-of-mass energy.

The energy regimes of various accelerators and heavy-ion colliders involving different projectiles are listed in Table 1.1.

Table1.1 Resume of heavy-ion accelerators and colliders.

Machine	Location	Projectile beam	Energy per nucleon (GeV)	Commencement year
AGS	BNL, USA	^{28}Si	14.5	1986
SPS	CERN	^{32}S	200	1986
AGS	BNL, USA	^{197}Au	11.5	1992
SPS	CERN	^{208}Pb	160	1994
SPS	CERN	^{208}Pb	158	1996
RHIC	BNL, USA	^{197}Au	100	2000
LHC	CERN	^{208}Pb	2700	2005*

* *Likely to become operational in 2005*

1.3 Signals of quark-gluon plasma

Quark-gluon plasma is the state of matter in which, contrary to hadronic matter, quarks and gluons are no longer confined in the interior of hadrons having radial dimension of about a fermi. It may be noted that deconfinement essentially refers to the freedom of quarks and gluons to move nearly freely to a greater region of space outside the radial domain which is usually associated with a hadron [30] with the constraint that these still remain confined within the region of strongly interacting matter. Lattice QCD predicts a phase transition to take place from hadronic phase to quark-gluon plasma phase around a critical temperature, $T_c \approx$ 150-200 MeV, which corresponds to an energy density of $\sim$ 1-3 GeV/fm^3 and baryon density of the order of 5 to 10 times

the normal nuclear matter density [31]. Furthermore, for investigating the characteristics of quark-gluon plasma experimentally, it is worthwhile to identify some parameters for studying the formation and characteristics of QGP. However, the small size of the plasma and its very short survival time pose serious problems in its experimental identification. Despite these difficulties, however, the past decade witnessed a great spurt of interest in the study of the properties and signals of the short lived quark-gluon plasma. Some of the most promising signals of quark-gluon plasma formation are briefly described below.

1.3.1 Dileptons

Lepton pairs are considered [32-40] as an interesting probe of quark-gluon plasma production. Lepton pairs are produced in QGP due to an interaction between a quark and an antiquark forming a virtual photon, γ^*, which subsequently decays into a lepton, l^-, and an antilepton, l^+, through the reaction, $q + \bar{q} \longrightarrow \gamma^* \longrightarrow l^- + l^+$. The produced l^- and l^+ pair is referred to as a lepton pair or a dilepton.

Since the dileptons produced in QGP medium interact electromagnetically only with the intervening hadronic medium, they leave the hot and dense reaction zone essentially unaffected. Thus, the lepton pairs provide direct information about the thermodynamic state of matter at the time of its creation. However, quark-gluon plasma may not be the only source of dilepton produc-

tion in high energy heavy-ion collisions. There are other processes as well which contribute to dilepton production. One of the other main sources of dilepton production is Drell-Yan process [41,42] in which a quark of a nucleon of one of the colliding nuclei can interact with a sea of antiquark of a nucleon of the other colliding nuclei to form a virtual photon which would subsequently decay into a l^-l^+ pair. Furthermore, the interaction of charged hadrons with their antiparticles, like $\pi^+ + \pi^- \longrightarrow l^+ + l^-$ and the decay of hadron resonances such as ρ, ω, ϕ and J/ψ would contribute to dilepton production.

It is worthmentioning that lepton pairs originating from quark-gluon plasma are identifiable only for the invariant masses above 1-1.5 GeV [43-46].

1.3.2 Direct photons

In addition to various other particles, quark-gluon plasma may also emit photons which result mainly from the electromagnetic interaction between the constituents of the plasma. The direct photons are regarded as relatively clean probe for studying QGP formation as these photons are hardly affected by the intervening hadronic medium. The most prominent process producing direct photons in the quark-gluon phase is the quark-antiquark annihilation, $q + \overline{q} \longrightarrow \gamma + g$ and QCD Compton scattering [47, 48]: (i) $q + g \longrightarrow \gamma + q$ and (ii) $\overline{q} + g \longrightarrow \overline{q} + \gamma$. However, there are other processes as well which result in the production of photons. These include pion annihilation, $\pi + \pi^- \longrightarrow \gamma + \rho$ and $\pi + \rho \longrightarrow \gamma + \pi$ reaction. It is worthmentioning that the photons other

than those coming from the mesonic decays are referred to as direct photons.

1.3.3 J/ψ suppression

J/ψ is a tiny bound state made up of a pair of heavy charm quark (c) and anticharm quark ($\bar{c}$). In free space, c and $\bar{c}$ interact through a linear confining potential and colour-Coulomb interaction. In high energy heavy-ion collisions, J/ψ may be produced in one of the many nucleon-nucleon collisions. The suppression of J/ψ production in QGP is regarded [49] as one of the most significant signatures of deconfinement of quarks at high temperatures. It is interesting to note that on account of high temperature in QGP phase, c and $\bar{c}$ forming J/ψ, are deconfined and thus the linear confining potential between c and $\bar{c}$ is lost. Furthermore, when the temperature rises above the critical temperature, there will be no bound state between c and $\bar{c}$ as each of the two would drift away from each other. Thus, c and $\bar{c}$ will find themselves so far apart that they hardly can form a bound state. This results in the suppression [50] of J/ψ production.

1.3.4 Strangeness enhancement

Enhanced production of strange particles in comparison to the production of light quark flavours, up (u) and down (d) quarks, has been suggested [51,52] as a signal of QGP formation in ultra-relativistic heavy-ion collisions. The basis of such an idea is the requirement of a large gluon density and a low energy threshold for the occurrence of the dominant QCD processes of $s\bar{s}$ production,

which make the production and equilibration of strangeness very significant [53].

Within a deconfined quark-gluon phase, $s\bar{s}$ pair production is described [54,55] reasonably well by the two lowest order QCD processes. Firstly, a gluon pair in the plasma phase annihilates to create a $s\bar{s}$ pair through the reaction: $g + g \longrightarrow s + \bar{s}$. Secondly, strange quarks and antiquarks may be produced in the collisions of light quark and antiquark through the reactions, $u + \bar{u} \longrightarrow s + \bar{s}$ and $d + \bar{d} \longrightarrow s + \bar{s}$.

1.3.5 Fluctuations as a probe for quark-gluon plasma

A general characteristic of any physical quantity to be measured experimentally is that it should exhibit fluctuations; the fluctuations depend on the properties of the system and, thus, in the case of relativistic heavy-ion collisions, fluctuations may carry information about the intervening medium created in the collisions.

Study of fluctuations in high energy nuclear collisions has, thus, become an important tool for exploring the underlying dynamics governing relativistic heavy-ion collisions [56-61]. Fluctuations in the multiparticle final state of heavy-ion collisions may be broadly divided into two categories: (i) statistical fluctuations, which arise due to difference in the impact parameters of the collisions from which the different produced particles originate and fluctuations in the number of primary collisions and (ii) non-statistical fluctuations,

which may arise due to some physical processes taking place in the collisions. Thus, the study of non-statistical fluctuations becomes significant only when one tries to explore the state of the matter formed in relativistic heavy-ion collisions, especially for looking at the after effects of the formation of quark-gluon plasma in these collisions [62].

1.4 Motivation behind the present work

As already stated, one of the possible approaches for investigating the dynamics of multiparticle production in relativistic heavy-ion collisions is to investigate the occurrence of fluctuations in particle density distribution of the particles produced in these collisions. This is due to the fact that fluctuations, apart from those arising due to statistical reasons, may point towards the occurrence of an uneven phenomenon during the collision. For instance, it is believed that fluctuations in multiplicity distribution of hadrons produced in heavy-ion collisions at high energies may be used to examine whether the quark-gluon system has undergone a phase transition [63, 64]. In the present work, for studying non-statistical fluctuations in relativistic nuclear collisions, the approach as adopted by Bialas and Peschanski [65] is used. In this approach, data are analyzed in terms of the scaled factorial moments as a function of decreasing rapidity bin sizes. For a non-statistical origin of the fluctuations, scaled factorial moments are predicted [65] to exhibit power law behaviour with decreasing bin width, referred to as "intermittency". Various aspects

of intermittency in 4.5A and 14.5A GeV/c ^{28}Si-nucleus collisions are studied thoroughly and systematically.

Intermittency is predicted [66] to be a typical feature of fractals, which in the case of heavy-ion collisions, refer to inelastic collisions with fractal dimensions A most complete description of the scaling behaviour of a fractal is given in terms of the fractal dimensions. This aspect is studied using the method of multifractal moments, first proposed by Hwa and others [67, 68]. These workers have suggested a power law behaviour similar to that of scaled factorial moments as an indication of underlying dynamics. Various important aspects of multifractal moments are thoroughly investigated and the results on this aspect are presented in Chapter IV.

Particles produced in relativistic nuclear collisions are envisaged [69] to be correlated. It may be interesting to note that correlations may be a manifestation of the formation of exotic state of nuclear matter, quark -gluon plasma [9,10]. Recently [12, 13, 69], short-range correlations amongst the relativistic charged particles produced in high energy nuclear interactions have been interpreted as a manifestation of the occurrence of intermittent pattern. An attempt is, therefore, made to investigate correlations and fluctuations in relativistic heavy-ion collisions. The results on the study relating to these important features of nuclear collisions are discussed in Chapter V.

Based on the systematic and well focussed observations of the present study, summary and concluding remarks are presented in Chapter VI.

References

1. E. Witten, *Phys. Rev.*, **D 36**, (1984) 272.
2. I. Bombaci, *Astronomy and Astrophysics*, **305**, (1996) 871.
3. H. Liu and G. L. Shaw, *Phys. Rev.*, **D 30**, (1984) 1137.
4. C. Griener, H. Stocker, *Phys. Rev. Lett.*, **58**, (1987) 1109.
5. C. Griener, H. Stocker, *Phys. Rev.*, **D 44**, (1991) 3527.
6. H. J. Crawford, M. S. Desai and G. L. Shaw, *Phys. Rev.*, **D 45**, (1992) 857.
7. J. P. Blaizot, *Nuc. Phys.*, **A 661**, (1999) 3c.
8. S. Abatzis et al (WA85 Collaboration), *Phys. Lett.*, **B 316**, (1993) 615: *Nucl. Phys.*, **A 556**, (1994) 225c.
9. J. Barke et al., (NA35 Collaboration), *Z. Phys.*, **C 48**, (1990) 191.
10. J. Schukraft et al., (NA34 Collaboration), *Nuc. Phys.*, **A 566**, (1989) 77c.
11. G. Baym, G. Friedman and I. Sarcevic, *Phys. Lett.*, **B 219**, (1989) 205.
12. E. A. De Wolf, I. M. Dremin and W. Kittel, *Phys. Rep.* **270** (1996) 1.
13. P. Bozek, M. Ploszajczak and R. Botet, *Phys. Rep.* **252** (1995) 101.
14. A. Bialas and M. Bleszynski and W. Czyz, *Nucl. Phys.*, **B 111**, (1976) 461.
15. P. Deines-Jones et al., *Phys. Rev.* , **C 62**, (2000) 014903.
16. H. Sumiyoshi, *Phys. Lett.*, **131**, (1983) 241.
17. H. Pi, *Comput. Phys. Commun.*, **71**, (1992) 173; L. Ding and E. Stenlund, *Lund Report*, **LP TP-87-6**, (1987)
18. A. Dabrowska et al., *Phys. Rev.*, **D 47**, (1993) 1751.
19. O. E. Pruet, *Ph. D. thesis*, **Louisiana State University**, (1990).
20. M. Shyam, C. P. Singh and S. K. Tuli, *Phys. Lett.*, **B 164**, (1985) 189.
21. C. P. Singh, M. Shyam and S. K. Tuli, *Phys. Rev.*, **C 40**, (1989) 1716.

22. V. V. Anisovich abd V. M. Shektar, *Nucl. Phys.*, **B 55**, (1973) 455: A. Bialas et al., *Acta. Phys. Pol.*, **B 8**, (1977) 585.

23. Yu. Shabelsky and V. M. Shektar,*Acta. Phys. Pol.*, **B 11**, (1980) 317.

24. A. Z. Patashinskii, *JETP Lett.*, **19**, (1974) 338.

25. T. W. Atwater and P. S. Frier, *Phys. Rev. Lett.*, **56**, (1986) 1350.

26. T. F. Huang et al., *Z. Phys.*, **C 29**, (1985) 611.

27. J. Bjorken, *Phys. Rev.*, **D 27**, (1983) 140.

28. B. Andersen, G. Gustafson and B. Nielsson-Almqvist, *Nucl. Phys.*, **B 281**, (1987) 289

29. B. Andersen, G. Gustafson, G. Ingelman and T. Sjostrand, *Phys. Rep.*, **97**, (1983) 31.

30. Cheuk-Yin Wong: **ORNL-CTP-9704** and **hep-ph/9712332**

31. J. Schukraft: *Proc. Int. Conf. Phys. and Astrophys. of Quark Gluon Plasma*, March 1997, Jaipur, India.

32. E. L. Feinberg, *Nuovo. Cim.*. **34**, (1976) 391.

33. E. V. Shuryak, *Phys. Lett.*,**B 78**, (1978) 150.

34. G. Domokos and J. J. Goldman, *Phys. Rev.*, **D 23**, (1981) 203.

35. K. Kajantie and H. I. Miettinen, *Z. Phys.*.**C 9**, (1981) 341; *Z. Phys.*.**C 14**, (1982) 357.

36. S. A. Chin, *Phys. Lett.*,**B 119**, (1982) 51.

37. G. Domokos, *Phys. Rev.*, **D 28**, (1983) 123.

38. L. McLerran and T. Toimela, *Phys. Rev.*, **D 31**, (1985) 545.

39. J. Cleymans, J. Feinberg and K. Redlich, *Phys. Rev.*, **D 35**, (1987) 2153.

40. J. Cleymans and J. Feinberg, *Phys. Lett.*, **B 168**, (1986) 405.

41. S. D. Drell and T. M. Yan, *Phys. Rev. Lett.*, **25**, (1987) 316.

42. C. Speiless et al, *Eur. Phys. J.*,**5**, (1998) 349.

43. K. Kajantie, M. Kataja, L. McLerran,*Phys. Rev.*, **D 34**, (1988) 811.

44. K. Kajantie,*Nucl. Phys.*, **A 461**, (1987) 225c.

45. K. Kajantie, J. Kapusta, L. McLerran and A. Mekjian, *Phys. Rev.*, **D 34**, (1986) R2746.

46. P. V. Ruuskanen, *Nucl. Phys.*, **A 525**, (1991) 255c; *Nucl. Phys.*, **A 544**, (1992) 169c.

47. C. Song, *Phys. Rev.*, **C 47**, (1993) 2861.

48. L. Xiong, E. V. Shuryak and G. E. Brown, *Phys. Rev.*, **D 46**, (1992) 3798.

49. T. Matsui and H. Satz, *Phys. Lett.* **B 178**, (1986) 416; T. Matsui, *Zeit. Phys.* **C38**, (1988) 245.

50. G. Domokos and J. J. Goldman, *Phys. Rev.*, **D 23**, (1981) 203.

51. P. Koch, B. Müller and J. Rafelski, *Phys. Rep.*, **142**, (1986) 167: J. rafelski, *Phys. Lett.*,**B 262**, (1991) 333.

52. J. Letessier and J. Rafelski,*Int. J. Mod. Phys.*, **E 9**, (2000) 107.

53. Kryzysztof Redlich and Ahmad Tounsi, *hep-ph/0105201* (2001) and references therein.

54. T. Biro and J. Zimyani, *Phys. Lett.*, **B 113**, (1982) 6; *Nucl. Phys.*, **A 395**, (1983) 525.

55. T. Matsui, B. Svetitsky and L. McLerran, *Phys. Rev.*, **D 34**, (1986) 783;

56. M. Gazdzicki and S. Mrowczynski, *Z. Phys.* **C 54** (1992) 127.

57. S. Mrowczynski, *Phys. Lett* **B 439** (1998) 6.

58. S. Mrowezski, *Phys. Lett.*, **B 430**, (1998) 9.

59 G. Roland et al. (NA49 Collaboration), *Nucl. Phys.* **A 638** (1998) 91c.

60 L. Stodolksy, *Phys. Rev. Lett* , **75**, (1995) 1044.

61. E. V. Shuryak, *Phys. Lett.*, **B 423**, (1998) 9.

62. Stephanov M. Rajagopal K. and Shuryak E.,*Phys. Rev. Lett.* **81** (1998) 4816.

63. A. Bialas and R. C. Hwa, *Phys. Lett.*, **B 253** , (1991) 436.

64. R. C. Hwa and M. T. Nazirove, *Phys. Rev. Lett.*, **69**, (1992) 741.

65. A. Bialas and R. Peschanski *Nucl. Phys.*, **B273** (1986) 703;

66. C. B. Chiu and R. C. Hwa,*Phys. Rev.*, **D 43**, (1991) 100. *Nucl. Phys.*, **B 308** (1988) 857.

67. R. C. Hwa, *Phys. Rev.*, **D 41** (1990) 1456.

68. R. C. Hwa and J. C. Pan, *Phys. Rev.*, **D 45**, (1992) 1476.

69. A. Shakeel, W. Bari et al., *J. Phys. Soc. Jpn.*, **71**, (2002) 1059.

CHAPTER II

EXPERIMENTAL TECHNIQUES AND GENERAL CHARACTERISTICS

2.1 Introduction

Detection and identification of charged particles produced in the collision of two high energy particles or nuclei requires measurement of a number of parameters in order to disentangle necessary information about the collision. This essentially includes the space localisation of the charged particle trajectories, measurements of the charges and momenta of the particles. Momenta may be determined by measuring the curvatures in the trajectories of charged particles in magnetic fields and mass of a particle is estimated by simultaneously measuring momentum and energy or momentum and velocity of the particle. As for as the neutral particles are concerned, one measures the energy and direction of emission of these particles with respect to the primary. It is worthmentioning that whatever method one uses, the basic principle is the interaction of the particle which takes place with the detector medium to create some observable signals. Measurement of these observables using distinct methods of measurements is what detection means, in general. The various detection methods are divided [1] into two categories: (i) the non-destructive methods in which various parameters relating to a particle are measured as in this procedure the identity of the particle to be detected does not change

and (ii) the destructive methods in which the identity of the particle changes during its detection. The latter method is mostly used for the detection of neutral particles which hardly interact with the detector medium. The non-destructive methods are mainly used for detecting charged particles. Using these basic concepts of particle detection, many approaches of particle detection and the detectors required for this are now in use. Particle detectors being used presently for investigating the particles produced in relativistic heavy-ion collisions are of high spatial accuracy in the micron range. These detectors are classified into two groups: (i) visual detectors and (ii) detectors with electronic read out. Bubble chamber, nuclear emulsion, etc., fall in the first category of detectors. These detectors provide 4π angular coverage that is suitable for studying general characteristics of interactions such as particle multiplicities, cross-sections, etc. The second category of detectors provide full and uniform angular coverage These are more suitable for investigating specific characteristics such as single particle spectra, two-particle correlation, etc. Such detectors include multiwire proportional chambers (MWPC), photon multiplicity detector (PMD), electromagnetic and hadron calorimeters, etc.

Among the visual detectors, nuclear emulsion is a detector having high spatial resolution capability, applicable to all ionizing particles of all charges. In nuclear emulsion each interaction is scanned and various measurements are carried out using microscope of high magnifying power.

2.2 Constituents of nuclear emulsion

The major constituents of nuclear emulsions as discussed by M. I. Adamovich et al [2] are hydrogen (22.4%), carbon (17.2%), nitrogen(4.1%), oxygen (12.6%), bromine (20.6%) and silver (22.7%). Besides these elements, there is a very low percentage ($< 1\%$) of sulphur and iodine. The constituents of nuclear emulsion are broadly classified [3,4] into two groups.

1. *Silver halide group:* Major component of this group is silver bromide with a small admixture of iodine.

2. *Gelatine:* This is composed of carbon, nitrogen, oxygen and hydrogen with some quantity of plasticiser and glycerine.

Gelatine in nuclear emulsion serves as a suspension matrix in which silver halide crystals are embedded. On the other hand, glycerine helps to reduce the brittleness of the emulsion.

In addition to all these elements, emulsion also contains some water content which helps in keeping it moist.

2.3 Tracks formation in nuclear emulsion and their classifications

Detection of charged particles using nuclear emulsion technique is based on energy loss suffered by the particles through ionization process while passing through it The energy loss, $-\frac{dE}{dx}$, which mainly depends on the charge and velocity of the particle, is given by [5]:

$$-\frac{dE}{dx} = (\frac{4\pi NZz^2e^4}{mv^2A})[\ln(\frac{2mv^2}{I(1-\beta^2)}) - \beta^2]$$

where m is the electron mass, z and v are the charge and velocity of the particle, $\beta = v/c$, N is Avogadro's number, Z and A are the atomic and mass numbers of the atoms of the medium and x is the path length in the medium, which is measured in g cm^{-2} or Kg m^{-2}, corresponding to the amount of matter traversed.

Energy lost by a charged particle is transferred to the atomic electrons. If energy gained by an electron is greater than the ionization potential, the electron is liberated and the atom is ionized. The ionization of the atoms produces some halide grains in such a way that when they are immersed in a developer, they get converted into silver grains which are easily distinguishable because of their black colour. Thus, as a charged particle advances through emulsion, it leaves behind a trail of black grains called track. By investigating the characteristics of these tracks, ionization produced may be determined and information about their charges and velocities can be obtained. The tracks in an interaction appear to come out from a single vertex. The recorded interaction in emulsion is thus called a star due to its characteristic appearance. The tracks formed by charged particles in nuclear emulsions are classified into three groups, namely, black, grey and shower tracks.

Black tracks are the tracks formed by singly or multiply charged particles having ranges < 3 mm. These are mainly low energy protons, deuterons, tritons and helium nuclei and some fraction of multiply charged fragments. These particles have relative velocities $\beta < 0.3$. The number of black tracks produced

in an interaction is denoted by n_b. Grey tracks are produced by particles having ranges $\geq$ 3 mm and relative velocities lying in the interval: $0.3 \leq \beta \leq 0.7$. These tracks are mainly produced by knock-out protons from the target and a very low percentage of slow pions. The number of grey tracks in an interaction is represented by n_g. Shower tracks are produced by charged particles having relative velocities $\beta > 0.7$. Most of these particles are pions with an admixture of kaons and protons. Shower tracks are produced by weakly ionizing particles. The number of shower tracks produced in an interaction is represented by n_s.

2.4 Scanning Procedure

The process of locating interactions in emulsion is known as scanning of the events In general, two different approaches are used for scanning emulsion stacks. These are:

1. *Line scanning:* In this method of scanning, each beam track is followed in a systematic manner from the entrance edge in order not to miss any single interaction. This procedure is useful when the beam has a low flux and is spread out over the entrance edge.

2 *Area scanning:* In area scanning, interaction points are searched volume wise, i.e., full depth of the pellicle is examined by using the z-motion of the microscope. This is also known as volume scanning. This method allows searching the interactions in the full depth of a certain area before the pellicle is shifted along the x-motion of the microscope.

In the present study a stack of ILFORD G5 emulsion, exposed to 14.5A GeV/c ^{28}Si nuclei from the AGS (BNL), has been used. A random sample comprising of 283 interactions with $n_h \geq 0$, where n_h represents the number of charged particles produced in an interaction with relative velocity $\beta \leq 0.7$, is analyzed. In order to examine the dependence of various parameters of multiparticle production on beam energy, the data involving 530 interactions, with the same description, produced by 4.5A GeV/c ^{28}Si nuclei from Synchrophasotron (Dubna), available in our laboratory are also analyzed.

2.5 Methods of measurements

2.5.1 Ionization measurements

Ionization caused by charged particles may be determined using the following methods

1. *Grain-density:* Grain density, g, of a track is defined as number of grains formed per unit length of the medium. Grain density is measured by counting the number of grains over a fixed length of a shower track.

The value of specific ionization, g*, in terms of the grain density is determined using:

$$g^* = \frac{g}{g_0}$$

where g_0 represents the grain density of a primary track.

2. *Delta-ray density:* As already stated, a charged particle while traversing through emulsion ionizes the atoms of the medium. If an electron liberated

during this process possesses an energy $\sim$ 2 KeV, it produces recognizable track of its own branching out of the main track which is referred to as a δ-ray. The density of δ-rays in nuclear emulsion is calculated from [6]:

$$n_\delta = (2.78 * 10^{-3})(\frac{Z^2}{\beta^2})(\frac{1}{E_{min}} - \frac{1}{E_{max}}) \text{ per } 100\ \mu m$$

where E_{min} and E_{max} represent respectively the minimum and maximum energies of δ-rays.

The δ-ray density is a function of charge and velocity of the particle and thus can give an additional information about the identity of the particle.

2.5.2 Angular measurements

Angular measurement refers to the determination of the space angle of a track. For this purpose, two angles, projected angle of the track in x-y plane and the dip-angle in y-z plane are measured in the following manner.

a. *Projected angle*

A goniometer having a least count of 0.25^o has been used to measure the projected angle. The vertex of a collision is focussed at the center of the goniometer and the track of the primary beam is aligned with one of the reference lines of the goniometer. The tracks of secondary charged particles are then aligned one by one with other reference lines of the goniometer and the goniometer scale readings are noted for measuring the projected angle with respect to the mean direction of the projectile beam. Projected angle is then calculated from:

$$\theta_p = \tan^{-1}(\frac{dy}{dx})$$

where dy and dx are respectively the differences of the two y- and x- coordinates at the two chosen reference points.

b. *Dip angle*

The dip angle of a track in the processed emulsion is determined by measuring the z-coordinates of the two points on the track separated by a known distance using the relation

$$\theta_d = \tan^{-1}(\frac{dz}{dx})$$

For the unprocessed emulsion, the formula is modified as

$$\theta_d = \tan^{-1}(\frac{SF*dz}{dx})$$

where SF represents the shrinkage factor of the emulsion.

Once dip and projected angles of a track are measured, the space angle, θ_s, can be estimated using the following expression:

$$\theta_s = \cos^{-1}[\cos\theta_p * \cos\theta_d]$$

Or, $\theta_s = \cos^{-1}[\cos(\tan^{-1}(\frac{dy}{dx})) * \cos(\tan^{-1}(\frac{SF*dz}{dx}))]$

2.6 General characteristics of 4.5A and 14.5A GeV/c ^{28}Si-nucleus interactions.

2.6.1 Mean multiplicity

Mean multiplicities of various types of charged secondaries produced in 4.5A and 14.5A GeV/c ^{28}Si-nucleus interactions are presented in Table 2 1. It is interesting to note from the table that the value of $< n_g >$, within the error

limits, is independent of projectile energy. On the other hand, mean multiplicity of relativistic charged particles, $< n_s >$, strongly depends on the projectile energy and target mass, whereas $< n_b >$ does not exhibit such trend.

Table 2.1 Mean multiplicities of black, grey and shower particles produced in the interactions of 4.5A and 14.5A GeV/c ^{28}Si nuclei with various targets.

4.5A GeV/c			
Type of interaction	$< n_b >$	$< n_g >$	$< n_s >$
Si-Em	6.22±0.22	8.43±0.15	10.20±0.22
Si-CNO	2.93±0.07	1.53±0.06	7.84±0.35
Si-AgBr	13.31±0.30	7.38±0.30	17.09±0.58
14.5A GeV/c			
Si-Em	5.65±0.31	8.24±0.21	15.07±0.62
Si-CNO	2.60±0.14	1.67±0.11	11.99±0.71
Si-AgBr	10.72±0.39	5.94±0.35	19.37±1.02

2.6.2 Multiplicity distribution

Study of multiplicity distributions of various charged particles produced in relativistic nuclear collisions is considered to be quite useful due to the fact that the behaviour of the distributions may help test the predictions of various phenomenological and theoretical models put forward to explain the mechanism of multiparticle production in these collisions. It was, therefore,

considered worthwhile to study some important characteristics of multiplicity distributions of the particles produced in ^{28}Si-nucleus interactions at the two projectile energies.

a. n_b distribution

Multiplicity distributions of the black tracks are shown in Fig. 2.1. It may be noticed from the figure that percentage of interactions having n_b values in the interval $4 \leq n_b \leq 14$ tends to increase with increasing projectile energy. However, for the interactions characterized by $n_b > 14$ it decreases.

In order to investigate whether the distribution is sensitive to the target mass, n_b distributions for the interactions due to CNO and AgBr targets for both the energies are displayed in Fig. 2.2. It is observed that the interactions due to lighter targets have higher probability of interactions with lower n_b values. However, the interactions due to AgBr targets appear to have higher probability for the interactions having higher values of n_b.

b. n_g distribution

n_g distributions for the two beam energies are shown in Fig. 2.3. The distribution is observed to be essentially insensitive to the projectile energy except a slight enrichment of the events having lower values of n_g occurring in the case of higher incident energy.

Multiplicity distributions of grey particles produced in the interactions due to CNO and AgBr targets are exhibited in Fig. 2.4. The distribution for the interactions due to heavier targets is observed to be comparatively broader

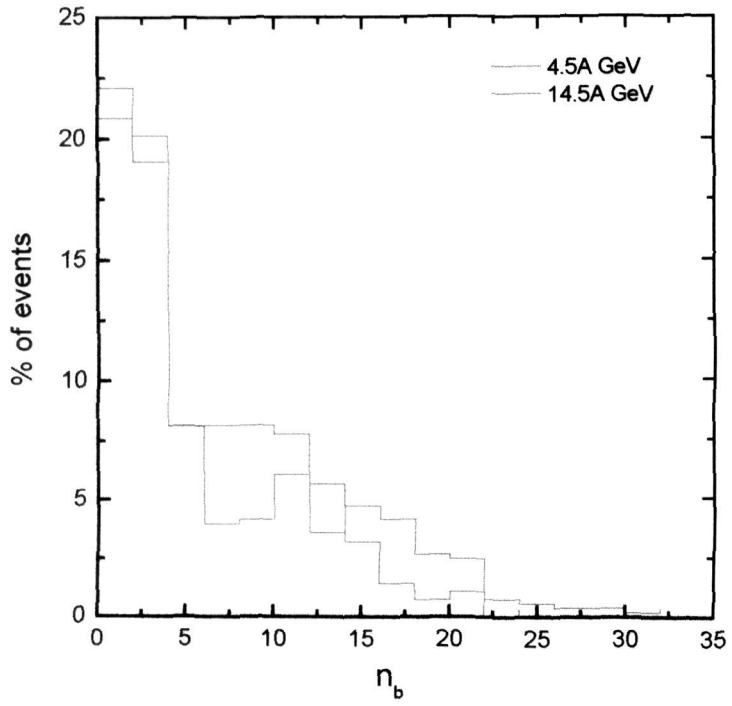

Fig. 2.1 n_b distributions for 4.5A and 14.5A GeV ^{28}Si-Em interactions.

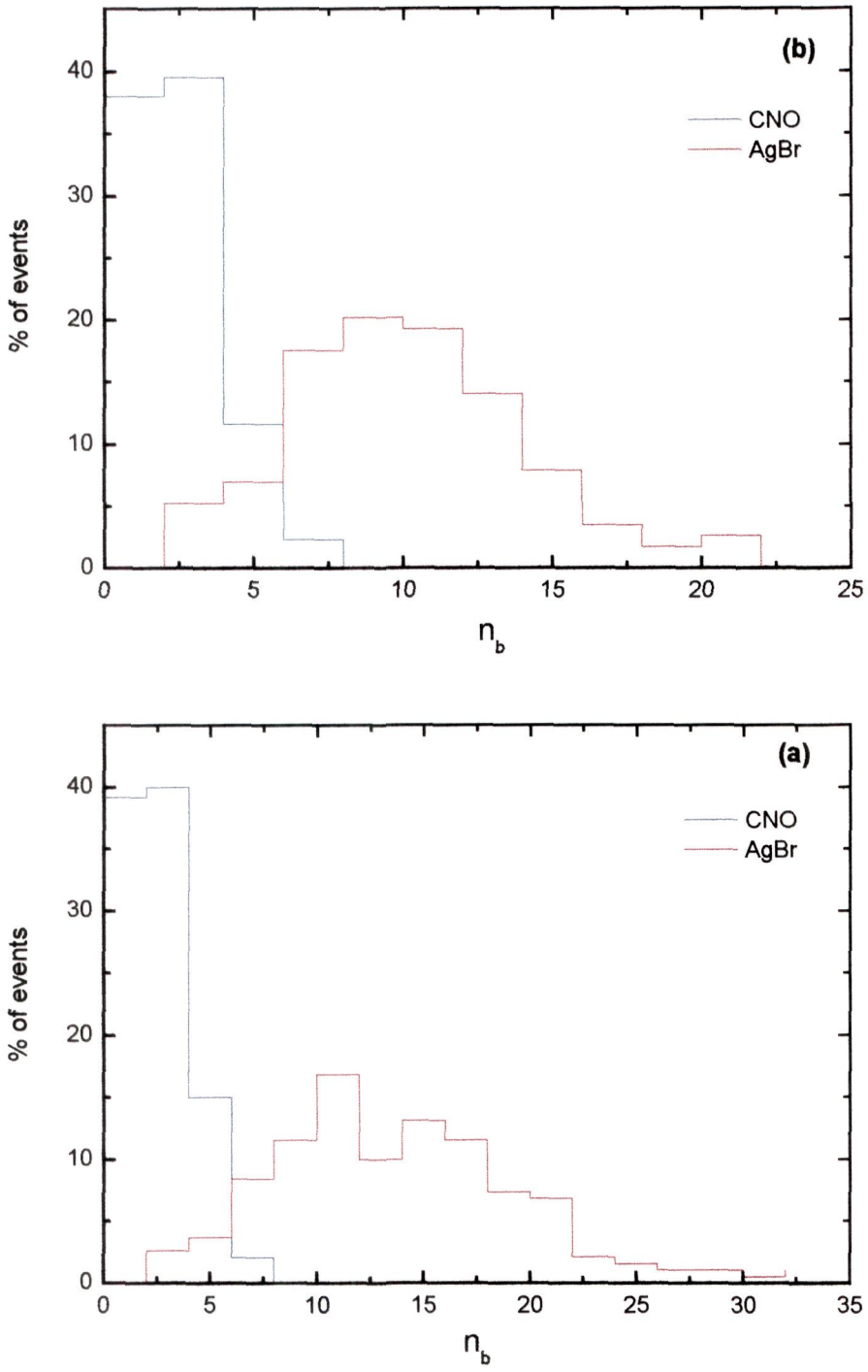

Fig. 2.2 n_b distributions for the interactions caused by ^{28}Si nuclei with CNO and AgBr targets at: (a) 4.5A and (b) 14.5A GeV

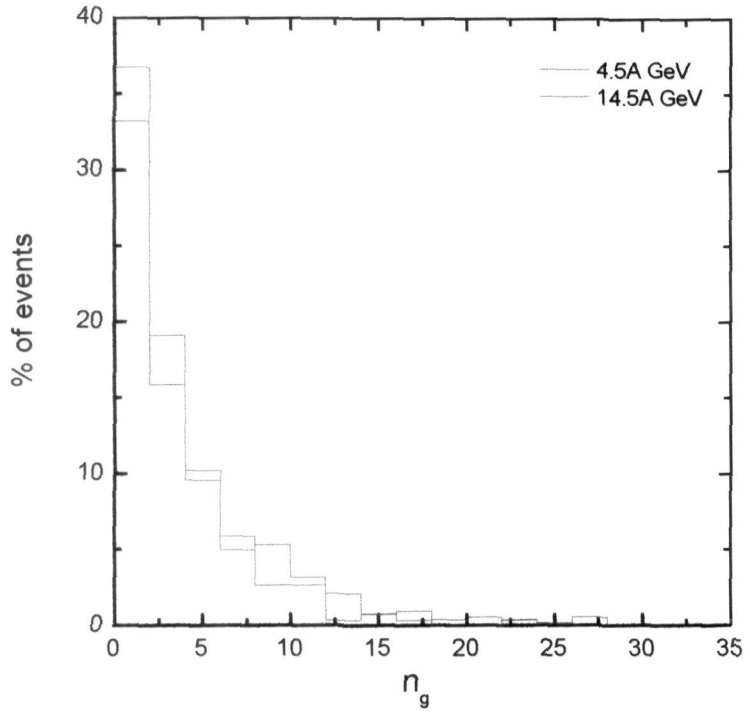

Fig. 2.3 n_g distributions for 4.5A and 14.5A GeV ^{28}Si-Em interactions.

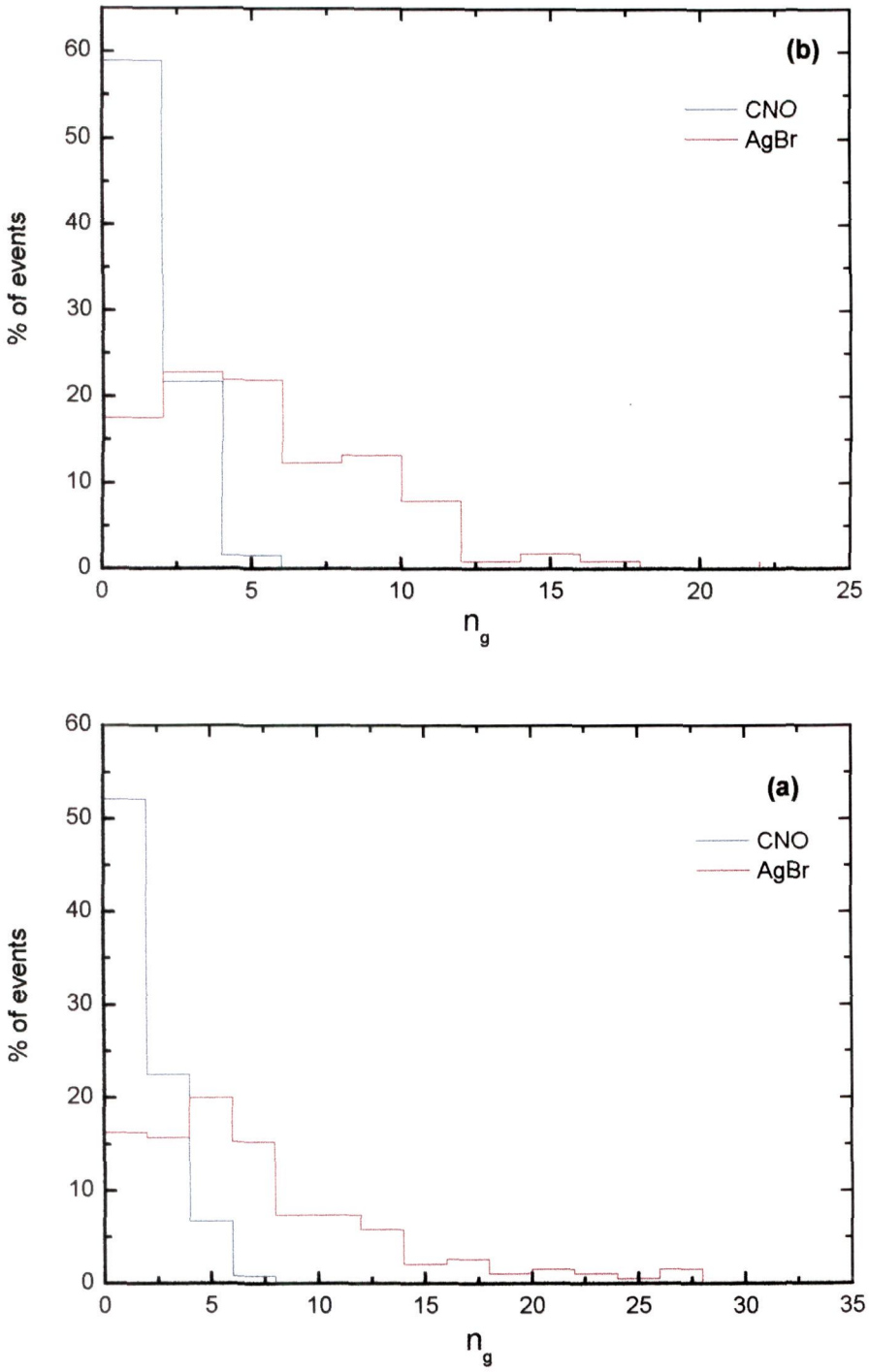

Fig. 2.4 n_g distributions for the interactions of (a) 4.5A and (b) 14.5A GeV ^{28}Si nuclei with CNO and AgBr targets.

than those for the interactions due to lighter targets.

c. n_s distribution

Multiplicity distributions of relativistic charged particles produced in 4.5A and 14.5A GeV/c ^{28}Si-nucleus collisions are displayed in Fig. 2.5. The distributions are found to be nicely reproduced by the negative binomial distribution [7] having the form:

$$p(n, \bar{n}, k) = k(k+1).....(k+n-1)\Big[\frac{\frac{\bar{n}}{k}}{1+\frac{\bar{n}}{k}}\Big]^{n}\Big[\frac{1+\frac{\bar{n}}{k}}{n!}\Big]^{k}$$

where n represents the multiplicity , $\bar{n}$ is the mean multiplicity and k is a number, which is calculated by using the relation:

$$\frac{1}{k}+\frac{1}{\bar{n}} = \frac{D^2(n)}{\bar{n}^2}$$

It may be mentioned that the result is in agreement with the values reported [8-10] earlier.

It is quite evident from Fig. 2.5 that the peaks of the distributions tend to shift towards higher values of n_s with increasing energy. Figs. 2.6 and 2.7 exhibit n_s distributions for the interactions caused by 4.5A and 14.5A GeV/c ^{28}Si nuclei with CNO and AgBr targets respectively. The distribution is observed to widen with increasing target mass.

The values of $\bar{n}$, k and χ^2/D.F. for the NBD fits to the experimental distributions, obtained using CERN standard program MINUIT, are listed in Table 2.2.

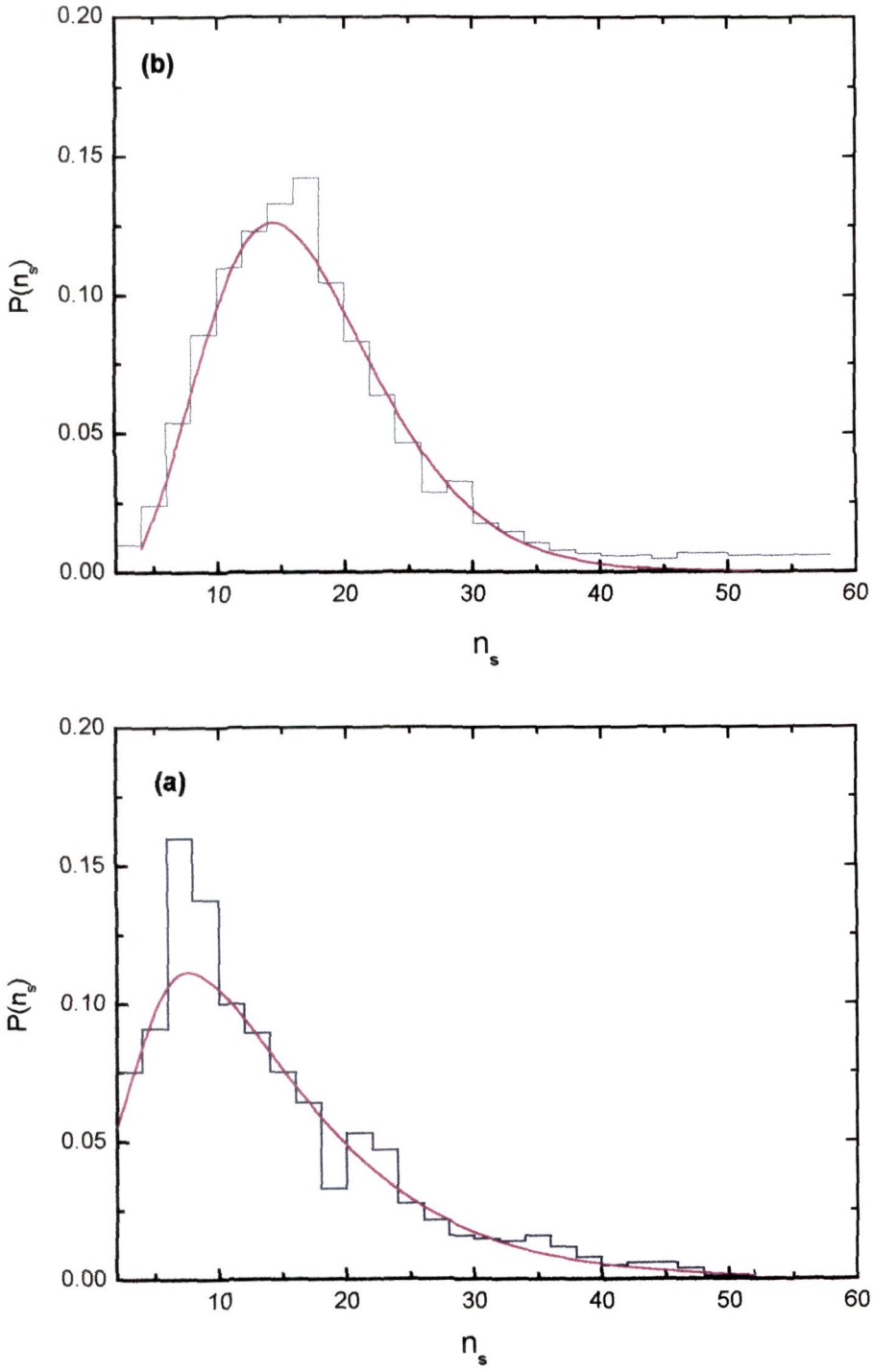

Fig. 2.5 n_s distributions for ^{28}Si-Em interactions at: (a) 4.5A and (b) 14.5A GeV. The curves represent the Gaussian fits to the data.

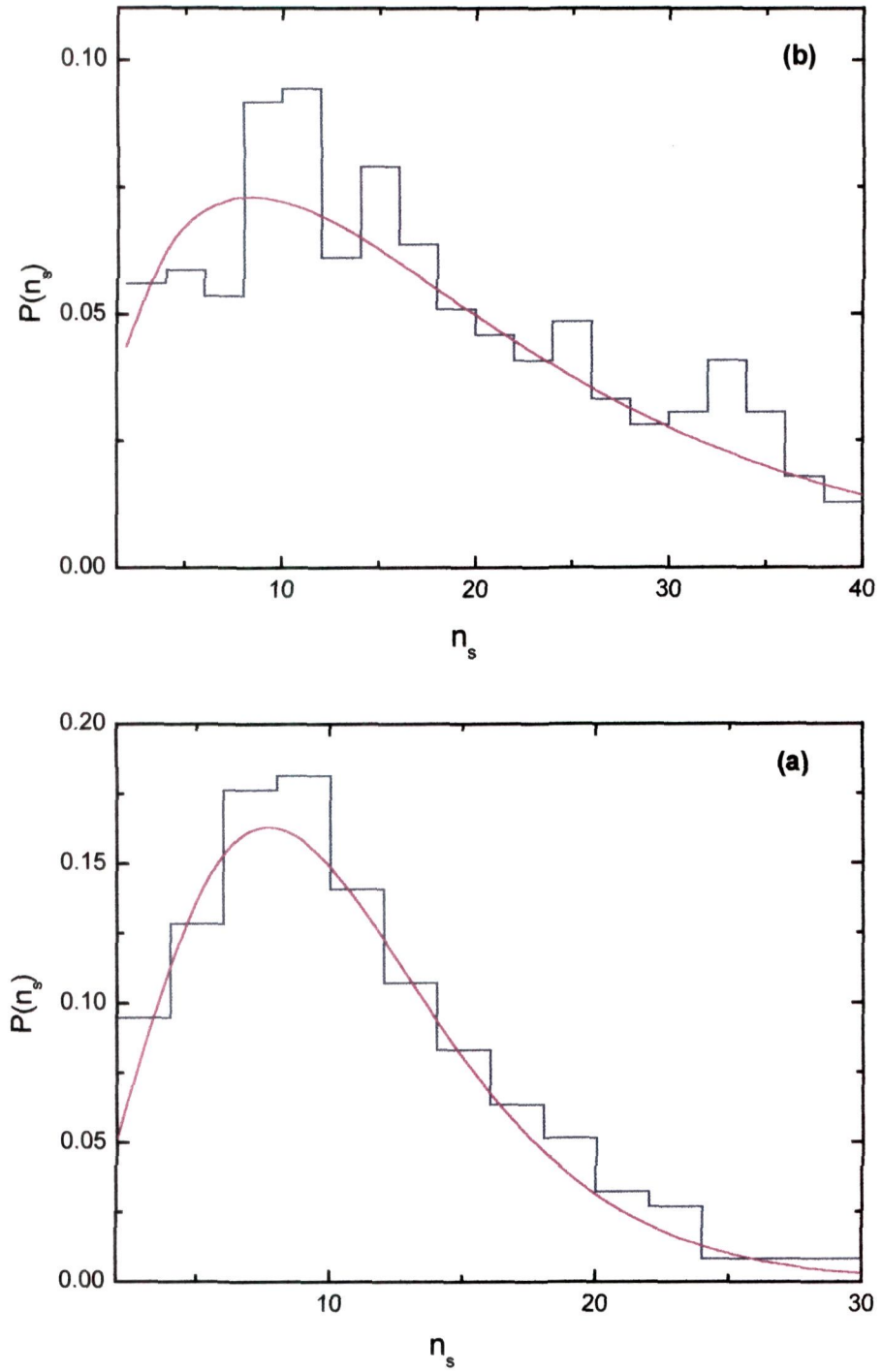

Fig. 2.6 n_s distributions for the interactions caused by 4.5A GeV ^{28}Si nuclei with: (a) CNO and (b) AgBr targets. The curves represent the Gaussian fits to the data.

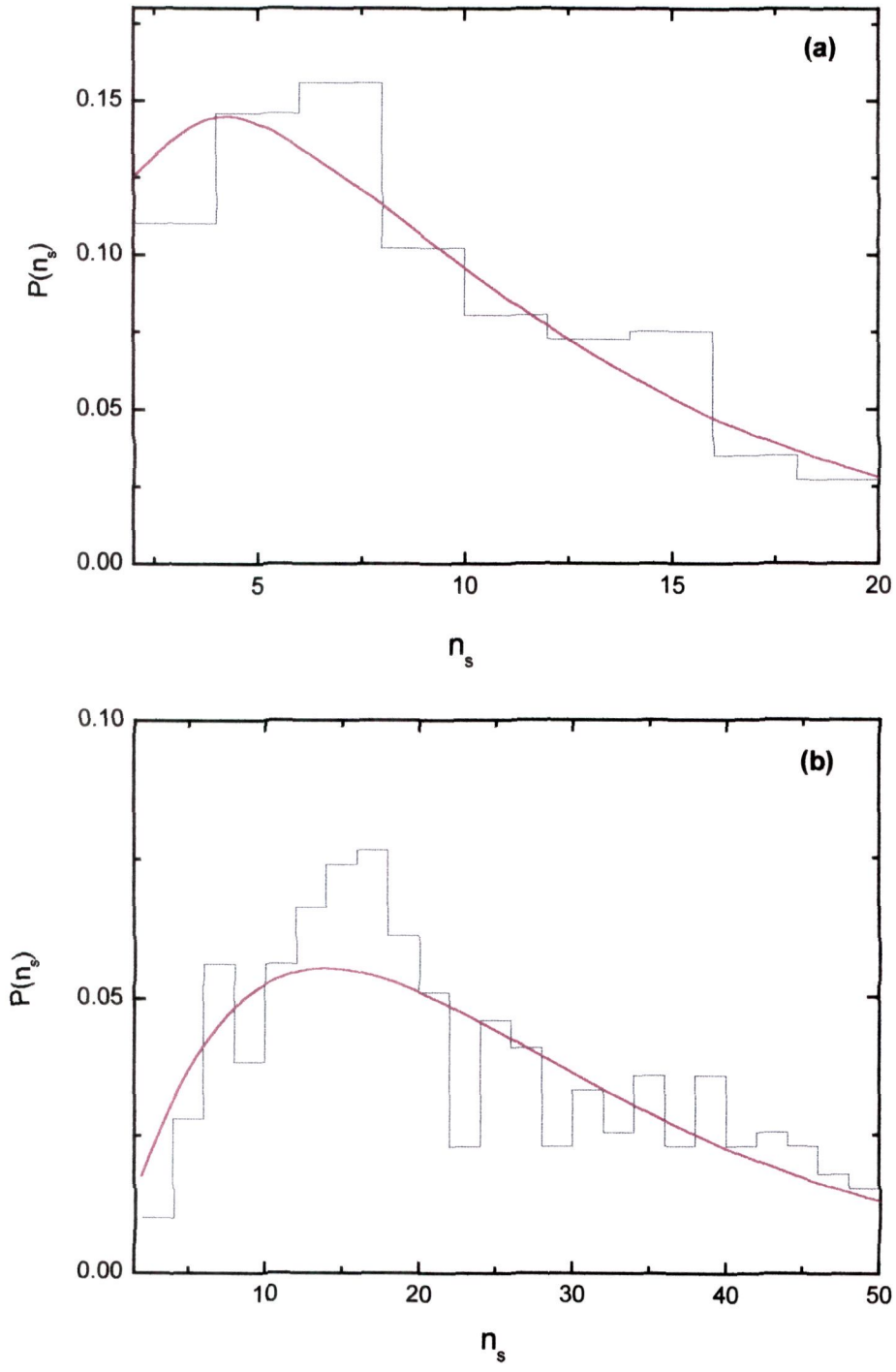

Fig. 2.7 n_s distributions for the interactions caused by 14.5A GeV ^{28}Si nuclei with: (a) CNO and (b) AgBr targets. The curves represent the Gaussian fits to the data.

Table 2.2 Values of $\bar{n}$, k and the χ^2/D.F. for NBD fits to n_s distributions.

Interaction type	$< n_s >$ (Experimental)	$\bar{n}$ (NBD)	k	χ^2/D.F.
4.5A GeV/c				
^{28}Si-CNO	7.84±0.35	7.64±1.77	1.22±0.43	0.98
^{28}Si-Em	10.20±0.22	11.87±0.71	1.78±0.71	1.00
^{28}Si-AgBr	17.09±0.58	18.93±0.47	1.78±0.78	0.76
14.5A GeV/c				
^{28}Si-CNO	11.99±0.71	11.71±0.51	2.71±0.12	0.95
^{28}Si-Em	15.07±0.62	15.83±0.43	2.21±0.13	0.57
^{28}Si-AgBr	19.37±1.02	19.41±0.54	1.00±0.06	1.51

2.6.3 Pseudorapidity distributions

The distributions of pseudorapidity, η, defined as $\eta = -\ln \tan(\theta/2)$, where θ is the emission angle with respect to the mean direction of the incident beam, of relativistic charged particles produced in high energy nuclear collisions is one of the most interesting experimental aspects to investigate the mechanism of multiparticle production in these collisions. The normalized pseudorapidity distributions, $(\frac{1}{N_{ev}}\frac{dn}{d\eta})$ of the relativistic charged particles produced in 4.5A and 14.5A GeV/c ^{28}Si-emulsion interactions are displayed in Fig. 2.8, where N_{ev} represents the total number of events. The curves in the figure are due to the Gaussian distribution which, incidentally, reproduce the shapes of the experimental distributions reasonably well.

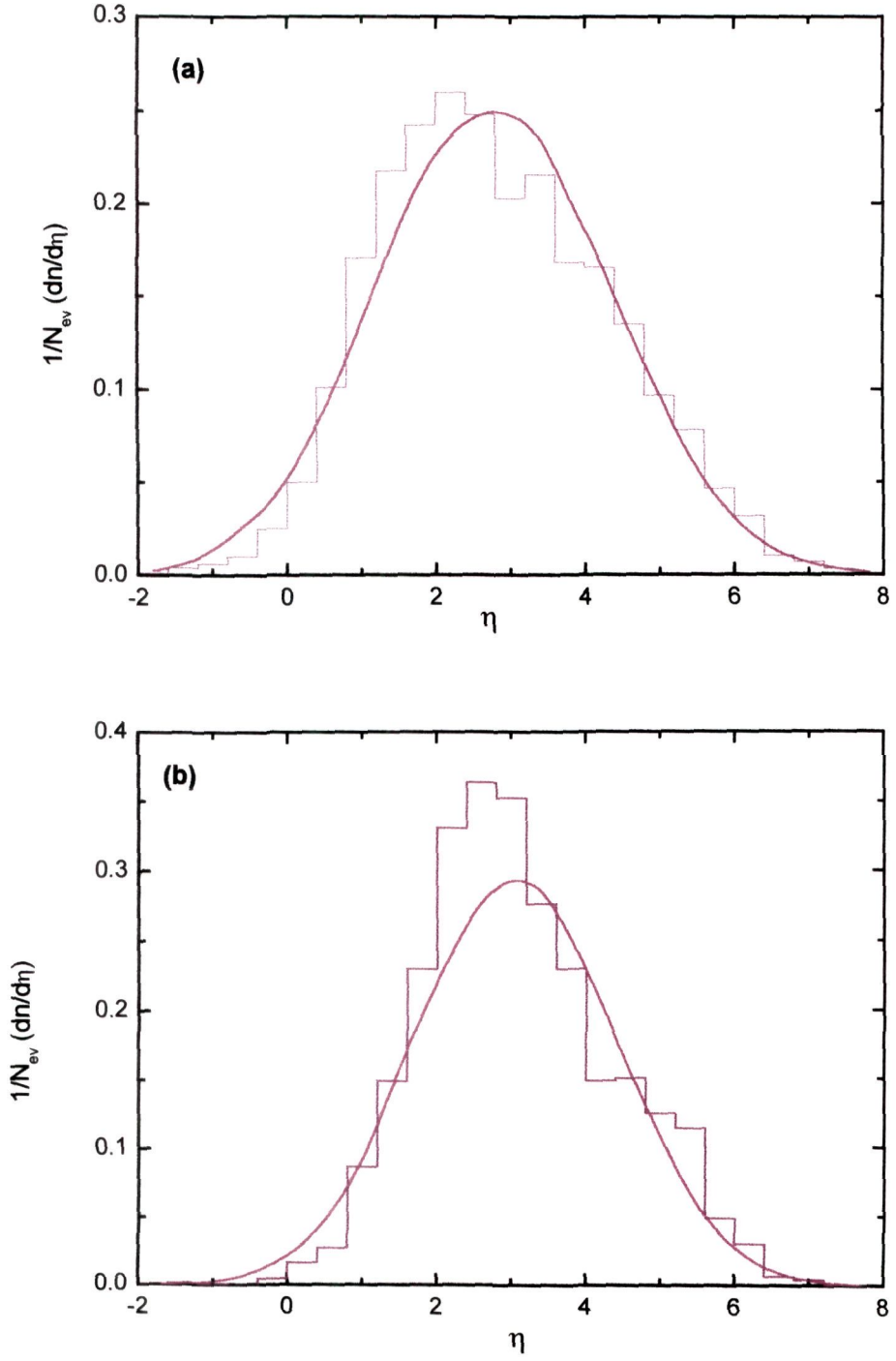

Fig. 2.8 η distributions for ^{28}Si-Em interactions at: (a) 4.5A and (b) 14.5A GeV.

References

1. C. W. Fabjan and H. G. Fischer: *Rep. Prog. Phys.* **43** (1980) 1003.
2. M. I Adamovich et al: (EMU01 collaboration) *Nucl. Phys.* **A 593** (1995) 535.
3. C. F. Powell, P. H. Fowler and D. H. Perkins : *The study of elementary particles by photographic method*, Pergamon Press, London (1959)
4. Mustafa Abdussalam Nasr, *Ph.D. Thesis*, submitted to the Aligarh Muslim University, 1995
5. D. H. Perkins, *Introduction to High Energy Physics* , 4^{th} ed. Cambridge University Press, UK, (2000)
6. D. H. Perkins et al, *Phill Mag.* (1955) 857
7. G. J. Alner et al, (UA5 Collaboration), *Phys. Lett.*, **B 160**, (1985) 199.
8. G. Baroni et al, *Nucl. Phys.*, **A531** (1991) 191
9. Alma-Ata-Dubna-Dushanbe-Erevan-Kosice-Leinngard-Moscow-Rezez-Sofia-Tbilsi Collaboration, *Sov. J. Nucl. Phys.*, **51, No.4**, (1987) 669
10. D. Ghosh, A. Mukhopadhyay, A. Ghosh and J. Roy, *Nuov. Cim.*, **104A, No. 5**, (1991) 683
11. A. Mukhopadhyay et al, *Nuov Cim.*, **A 106**, (1993) 967

CHAPTER III

INTERMITTENCY IN RELATIVISTIC HEAVY-ION COLLISION

3.1 Introduction

Study of non-statistical fluctuations in relativistic nuclear collisions has recently attracted a great deal of attention due to the possibility of disentangling important information about the mechanism of multiparticle production in such collisions. Although fluctuation studies have a long history dating back to the investigation of the fluctuations occurring in turbulent flow [1-3], the non-linear phenomenon generated considerable interest in the field of high energy physics only after the observation of unexpectedly large local fluctuations in a very high multiplicity event recorded by JACEE Collaboration [4]. Similar ideas have been applied to various other fields including astrophysics, magnetohydrodynamics [5], etc. In the special case of ultra-relativistic heavy-ion collisions, the idea of fluctuations was introduced by Bialas and Peschanski [6-7]. Study of fluctuations in multiplicity distributions of the particles produced in heavy-ion collisions is envisaged [8-10] to be a very sensitive tool for examining the dynamics of multiparticle production, particularly its role in looking at some of the fascinating features of quark-gluon plasma [11]. Several attempts [6,7,12,13] have been made recently to understand the underlying physics of the origin of non-statistical fluctuations. Amongst these, the method

of scaled factorial moments (SFM) proposed by Bialas and Peschanski [6,7] is considered to be one of the most significant diagnostic tools for extracting the dynamical contribution to the fluctuations in multiplicity distributions in high energy collisions. These authors have suggested a power law growth for the scaled factorial moments with decreasing phase space bins, which is referred to as "intermittency", indicating thereby the presence of fluctuations.

Intermittency pattern has been observed in electron-positron annihilation [14,15], hadron-hadron [16,17], hadron-nucleus [18-20] and nucleus-nucleus [21-26] collisions at high energies. More recently, NA49 Collaboration [27] presented an event-by-event analysis of fluctuations in central Pb-Pb collisions at 158 GeV per nucleon energy. In addition to the progress made in experimental studies on non-statistical fluctuations, many milestones have been achieved on theoretical front as well. Many studies focussing especially on various aspects relating to the occurrence of fluctuations as an evidence for thermalization and critical fluctuations at QGP phase transition have been undertaken [28-30].

In the beginning of this chapter, mathematical formalism relating to the study of intermittency in relativistic heavy-ion collisions is presented. Thereafter, some of the most useful and important models describing the intermittent behaviour and the occurrence of phase transition are discussed. Finally, results on various aspects of intermittency observed in 4.5A and 14.5A GeV/c ^{28}Si-nucleus collisions using scaled factorial moments and the Ginzburg-Landau description are presented.

3.2 Mathematical formalism

The observations of the spike events first observed in cosmic ray interactions [4] and later in the laboratory [31] have resulted in great spurt of interest in studying intermittent behaviour in high energy collisions. Bialas and Peschanski [6,7] have done pioneering work in this field by formulating the characteristics of intermittency theoretically. Under this, a pseudorapidity interval $\Delta\eta$ is divided into M bins of equal size, $\delta\eta = \Delta\eta/M$. If n_m is the number of particles in the m^{th} bin, where m takes on the values from 1 to M, then depending on the type of averaging, two types of cell averaged moments are defined as described in the following section.

3.2.1 Horizontal scaled factorial moments

The q^{th} order scaled factorial moment for a large multiplicity single event is defined [6,7] as:

$$F_q = M^{q-1} \sum_{m=1}^{M} \frac{n_m(n_m-1).....(n_m+q-1)}{N(N-1).....(N-q+1)} \tag{3.1}$$

where N represents the total number of particles in the event in the pseudorapidity interval $\Delta\eta$.

For a sample of events, having different multiplicities, the above expression changes to [32]:

$$F_q = M^{q-1} \sum_{m=1}^{M} \frac{n_m(n_m-1).... ..(n_m+q-1)}{<N>^q} \tag{3.2}$$

where $< N >$ represents the mean multiplicity of the data sample in the interval $\Delta\eta$.

On averaging over the number of events in the data sample, one gets:

$$< F_q > = \frac{M^{q-1}}{N_{evt}} \sum_{N_{evt}} \sum_{m=1}^{M} \frac{n_m(n_m-1) \ldots (n_m+q-1)}{<N>^q} \tag{3.3}$$

It has been shown [6,7] that for smooth rapidity distributions, i.e., rapidity distributions not exhibiting any fluctuations other than the statistical ones, $< F_q >$ is essentially independent of the resolution $\delta\eta$ in the limit $\delta\eta \rightarrow 0$. However, if there exists any dynamical contribution to these fluctuations, the scaled factorial moments should obey [6,7] the following power law:

$$< F_q > = \left[\frac{\Delta\eta}{\delta\eta}\right]^{\phi_q}, \qquad \text{for} \quad \delta\eta \rightarrow 0 \tag{3.4}$$

For a situation, where the above power law holds, the spectrum is said to be intermittent

The positive constants, ϕ_q, referred to as the intermittency indices, characterize the strength of the intermittency effect. The power law predicts a characteristic linear rise of $\ln< F_q >$ as a function of $\ln \delta\eta$ for comparatively smaller bin widths.

The intermittent indices can be obtained from the asymptotic behaviour represented by:

$$\phi_q = -\frac{\Delta \ln < F_q >}{\Delta \ln \delta\eta} \tag{3.5}$$

The power law behaviour of the scaled factorial moments is envisaged [31,32] to be due to the fractal nature of the particle emission source. This aspect is studied through the behaviour of anomalous fractal dimensions, d_q, which are obtained directly from the slopes ϕ_q using:

$$d_q = \frac{\phi_q}{q-1} \tag{3.6}$$

The scaled factorial moments are sensitive to the shape of the pseudorapidity distribution. Thus for a non-flat distribution, varying within a finite bin of width $\delta\eta$, an extra M dependent correction factor, R_q is introduced [35] in the following fashion:

$$R_q = M^{q-1} \sum_m \frac{<n_m>^q}{<n>^q} \tag{3.7}$$

$$\text{where} \quad < n_m > = \frac{1}{N_{evt}} \sum_{i=1}^{N} \frac{<n_{m,i}>^q}{<N>^q} \tag{3.8}$$

Thus, the corrected scaled factorial moments are calculated from:

$$< F_q >^{corr} = \frac{<F_q>}{R_q} \tag{3.9}$$

The correction factor, however, becomes insignificant in the case of flat distributions

3.2.2 Vertical scaled factorial moments

The vertical scaled factorial moments are defined as:

$$F_q^v = \frac{1}{M} \sum_{m=1}^{M} \frac{n_m(n_m-1) \quad (n_m+q-1)}{<n'_m>^q} \tag{3.10}$$

and on averaging over all the events $< F_q^v >$ would become:

$$< F_q^v > = \frac{1}{M} \sum_{m=1}^{M} \frac{1}{N_{evt}} \sum_{i=1}^{N_{evt}} \frac{n_{m,i}(n_{m,i}-1) \quad (n_{m,i}+q-1)}{<n'_m>^q} \tag{3.11}$$

$$\text{where} \quad < n'_m > = \frac{1}{N_{evt}} \sum_{i=1}^{N_{evt}} n_{m,i} \tag{3.12}$$

is the average multiplicity of the m^{th} bin over the whole data sample comprising of the number of events, N_{evt}.

3.3 Random cascade model

The power law behaviour and the existence of fractal dimensions are well understood concepts in fluid turbulence [3,4]. However, an important issue to be addressed is whether an analogous approach could be used while dealing with the intermittency phenomenon in relativistic nuclear collisions. It is worthmentioning that, intermittency in turbulence was first demonstrated in terms of Cascade Models [36]. However, a modified form of these models [6,7], put forward by Bialas and Peschanski, are being mostly applied in studying multiparticle production processes in relativistic nuclear collisions. In such models, the phase space, which in relativistic collisions, is represented by the pseudorapidity variable, η, or the azimuthal angle, ϕ, is partitioned in a series of self-similar steps. If M denotes the number of bins obtained by breaking up the total phase space into λ parts at each step of the μ iterations of the self-similar cascade then:

$$M = \lambda^{\mu} = \frac{\Delta\eta}{\delta\eta} \tag{3.13}$$

for a total rapidity range $\Delta\eta$ divided into bins of width $\delta\eta$.

The partition of the phase space can be visualized in terms of the Cayley tree shown in Fig. 3.1 or the phase space partition box diagram shown in Fig. 3.2 for the simplest case of $\lambda = 2$. In cascade models, one multiparticle event

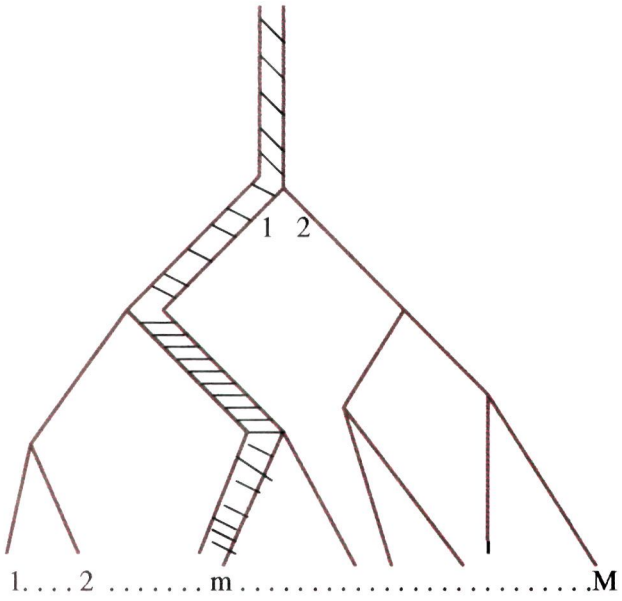

Fig. 3.1 Cayley tree representation of intermittency.

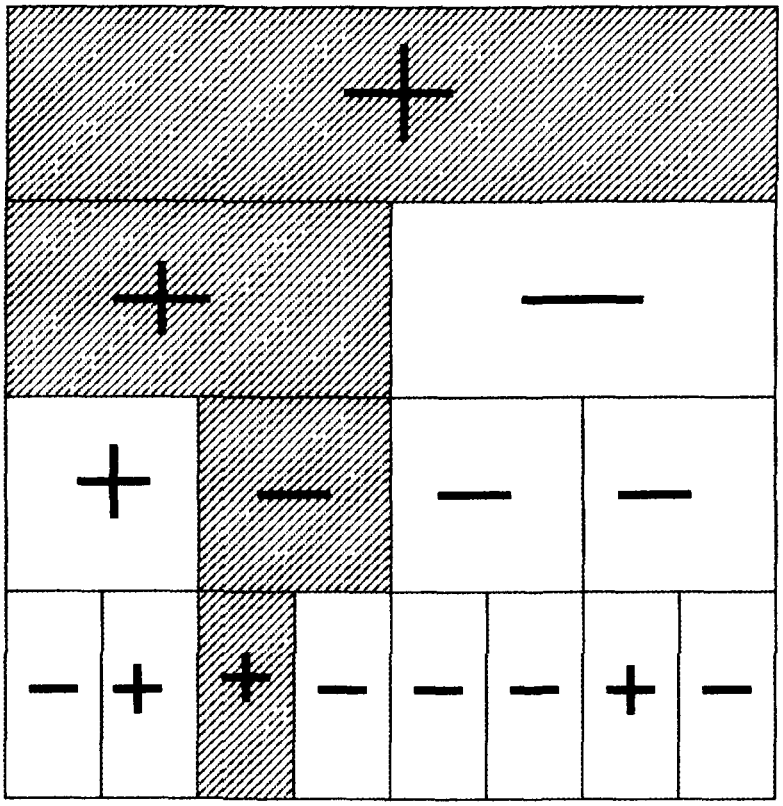

Fig. 3.2. Box diagram of intermittency. The initial phase space is divided into boxes following the Cayley tree scheme of Fig. 3.1

is defined by a set of randomly chosen numbers, W's, one for each link of the Cayley tree or equivalently for each box of the phase space partition diagram. The random numbers are considered to be independent random realizations of a random function following an arbitrary probability distribution r(W) with the constraints:

$$< W^q > = \int W^q \, r(W) dW \quad \text{and} \tag{3.14}$$

$$< W > = 1 \tag{3.15}$$

The density P_m in the m^{th} bin is given by the product:

$$P_m = \frac{1}{M} \prod_{n=1}^{\mu} W_n \tag{3.16}$$

$$\text{or,} \quad P_m = \frac{1}{M} \frac{\rho(m)}{<\rho(m)>} \tag{3.17}$$

where $\rho(m)$ is the particle density in the m^{th} bin for which the path is defined through a sequence of indices n.

It may be mentioned that for the second event, the Random Cascade Models assume a new set of random choices for all W's in the tree structure. This essentially means that W's are independent of the scale at which they operate.

The intermittent behaviour in this model is represented as:

$$F_q = < (MP_m)^q > \tag{3.18}$$

$$\text{or,} \quad F_q = < \prod_{n=1}^{\mu} W_n^q > \tag{3.19}$$

$$\text{or,} \quad F_q = \left(\frac{\Delta\eta}{\delta\eta}\right)^{\ln<W^q>/\ln\lambda} \tag{3.20}$$

The intermittency indices are expressed as:

$$\phi_q = \ln < W^q > / \ln\lambda \tag{3.21}$$

which implies that the random cascade model indices possess multifractal spectrum [37]. Random cascade models for the simplest case of $\lambda = 2$ are referred to as the α-models [2,3], in which the distribution r(W) is expressed by two level probability distribution:

$$r(W) = p\ \delta(W - W_-) + (1 - p)\ \delta(W - W_+) \tag{3.22}$$

where $0 \leq W_- < W_+$ and the normalization condition requires:

$$p\ W_- + (1 - p)\ W_+ = 1 \tag{3.23}$$

Here $W_+(> 1)$ represents the density enhancement and occurs with a probability p at each step of the cascade and $W_-(< 1)$ denotes the density depletion with probability (1 p).

The enhancement and the depletion create respectively "spikes" and "holes" in the rapidity distribution. The intermittency indices in this case are expressed as:

$$\phi_q = \ln\ [p\ W_-^q + (1 - p)\ W_+^q] / \ln 2 \tag{3.24}$$

3.4 Phase transition and Ginzburg-Landau model

The importance of ultra-relativistic heavy-ion collisions for providing an opportunity to study the vacuum properties of QCD has already been stated in Chapter I. In such collisions, kinetic energies of the colliding nuclei are

converted into thermal ones and a hot and dense state of matter, quark-gluon plasma, is envisaged to be formed. The system will cool with its subsequent expansion and will undergo a phase transition from deconfined QGP to confined hadrons. Since the only experimental observables are the final state particles, one, therefore, searches for the signals of such a phase transition by studying the characteristics of these particles. In addition to many other signals, non-statistical fluctuations in the final state of particle production are visualized to be the experimental tool to diagnostically confirm the elusive quark-hadron phase transition [38-42]. Theoretical study of the fluctuations in quark-hadron phase transition is being carried out [40,43] for the last several years. Amongst many phenomenological models, the Ginzburg-Landau Model has been used to make useful predictions which can be compared with the experimental results [44,45]. This model has been extensively used in describing the scaling behaviour such as the scaled factorial moments in both the first-order [46-50] and the second-order [46] phase transitions, the multiplicity difference correlators [47] and multiplicity distribution in the phase transitions [48-50].

In the Ginzburg-Landau description, the scaled factorial moments are expressed [46] as:

$$F_q = f_q / f_1^q \tag{3.25}$$

$$\text{where } f_q = \frac{1}{Z} \int D\phi \left(\int_\delta dZ |\phi|^2\right)^q \exp(-F[\phi]) \tag{3.26}$$

$$\text{and } Z = \int D\phi \exp(-F[\phi]) \tag{3.27}$$

where F is the free energy function given by:

$$F(\phi) = \int dZ\ [a|\phi|^2 + b|\phi|^4 + c|\nabla\phi|^2] \tag{3.28}$$

Here $a \propto (T - T_c)$ represents the deviation from the critical point. It may be noted that b and c appearing in Eq. 3.28 are greater than zero and $|\phi|^2$ is associated with the multiplicity density of the system.

3.5 Results and discussion

3.5.1 Variation of $\ln < F_q >$ with $-\ln \delta\eta$

Figs. 3.3-3.5 exhibit $\ln < F_q >$ versus $-\ln \delta\eta$ plots for the interactions of 4.5A and 14.5A GeV/c ^{28}Si nuclei with emulsion, CNO and AgBr targets. The solid lines in the plots represent the least squares fits to the experimental data.

For all the three categories of interactions at both the energies, the SFM are observed to increase linearly with decreasing bin widths $\delta\eta$ indicating thereby the presence of intermittent behaviour in all these interactions.

At a particular incident energy, the SFM are found to have higher values for the interactions due to CNO than those due to AgBr targets. This effect may be a projection of lower multiplicity in the events resulting from the interactions due to CNO than those from AgBr targets [19].

No significant change in the scaled factorial moments is observed when the incident energy is increased threefold.

3.5.2 Variation of intermittency indices, ϕ_q, with q

The intermittency indices, ϕ_q, which characterize the strength of intermit-

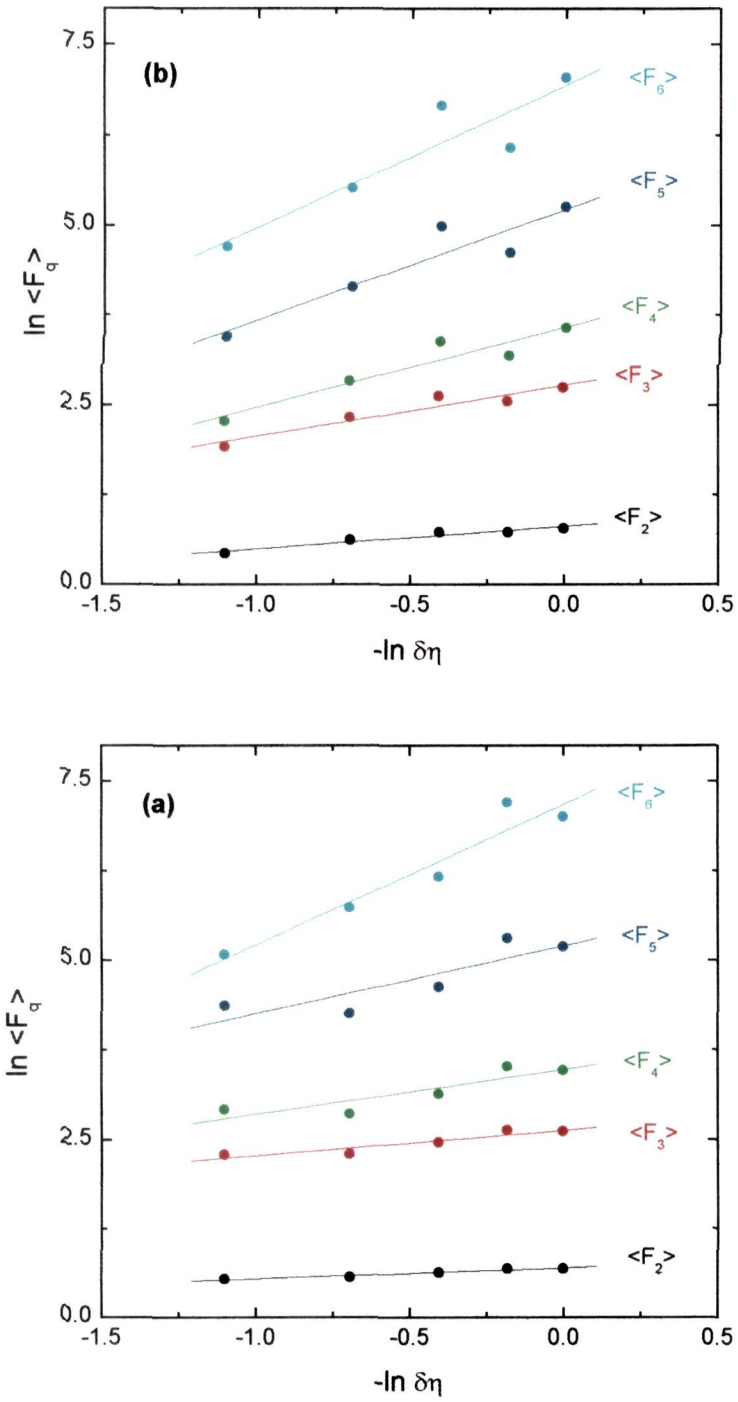

Fig. 3.3 Variations of ln $\langle F_q \rangle$ with -ln $\delta\eta$ for ^{28}Si-Em interactions at: (a) 4.5A and (b) 14.5A GeV/c.

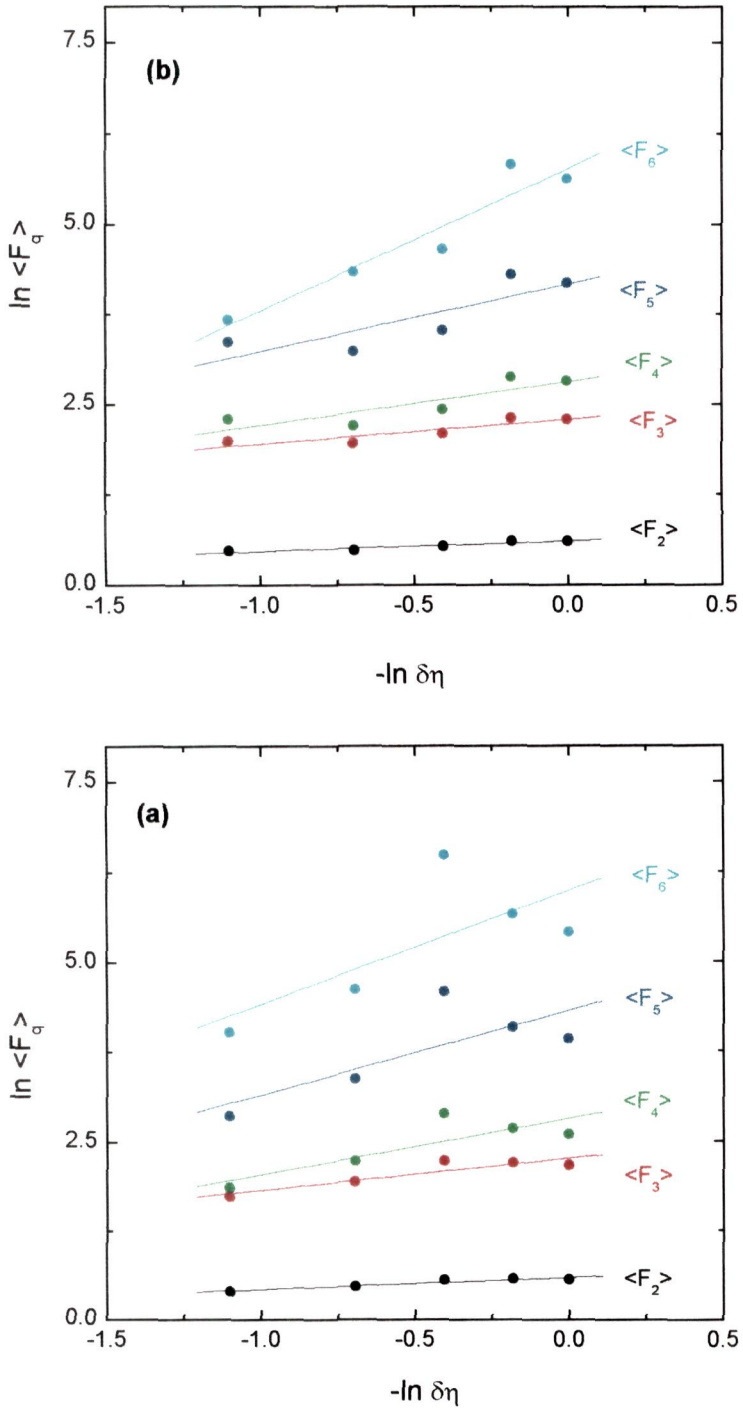

Fig. 3.4 Variations of ln $<F_q>$ with -ln δη for 4.5A GeV/c ^{28}Si nuclei interactions with: (a) CNO and (b) AgBr targets.

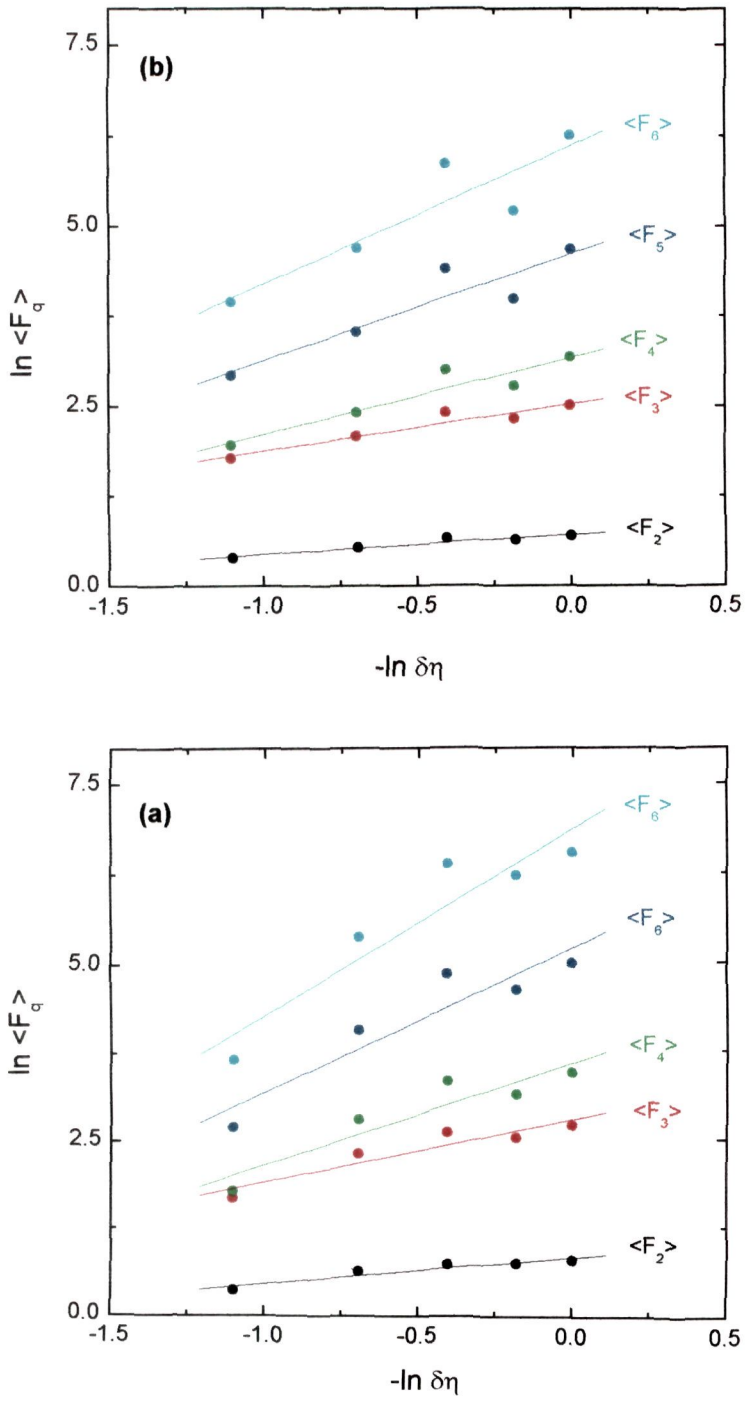

Fig. 3.5 Variations of ln $\langle F_q \rangle$ with -ln $\delta\eta$ for 14.5A GeV/c ^{28}Si nuclei interactions with: (a) CNO and (b) AgBr targets.

tency effect have been obtained from the linear dependence of ln $< F_q >$ on $-\ln \delta\eta$. The values of ϕ_q obtained for the interactions of 4.5A and 14.5A GeV/c ^{28}Si nuclei with various targets are listed in Tables 3.1 and 3.2 respectively. Figs. 3.6-3.8 display ϕ_q versus q plots for various interactions considered in the present study. The indicated errors in the plots are the statistical errors. The slopes are observed to increase with the order of the moment. This feature of the ϕ_q distribution would give an important clue to the underlying dynamics.

In Fig. 3.6 the slope parameters are observed to have higher values for the case of higher incident energy for each order of the moments. The intermittency indices for the interactions due to CNO are observed to be higher than those due to AgBr for each order of the moments. The difference is more pronounced for higher order moments.

3.5.3 Variation of anomalous dimensions, d_q, with q

The values of anomalous dimensions, d_q, are plotted as a function of the order of moment q in Figs. 3.9-3.11. The anomalous dimensions tend to increase with the order of the moment. Dependence of the anomalous dimensions on the energy of the projectile is clearly seen in Fig. 3.9; d_q values are found to be comparatively higher for the interactions caused by 14.5A GeV/c ^{28}Si nuclei as compared to the corresponding values for the interactions induced by 4.5A GeV/c ^{28}Si nuclei for each order of the moment.

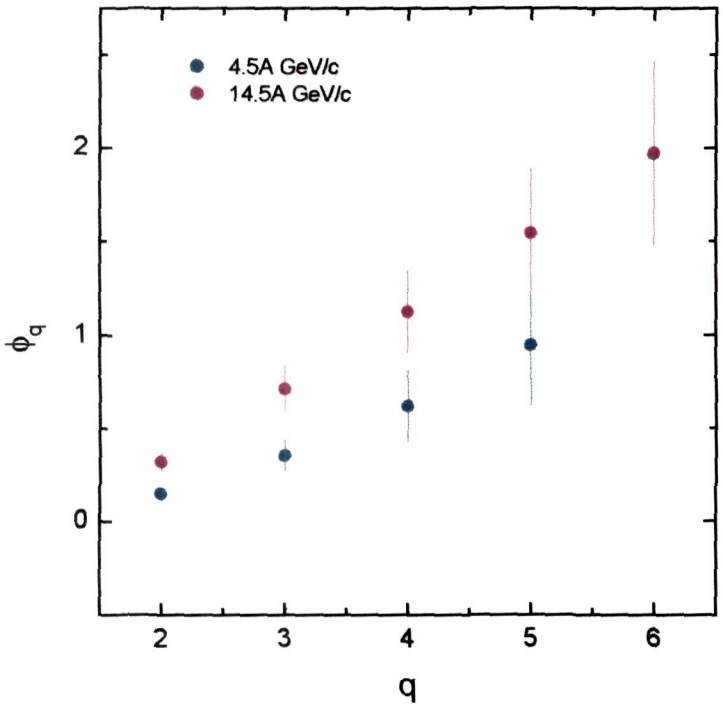

Fig. 3.6 Variations of ϕ_q with q for ^{28}Si-Em interactions at 4.5A and 14.5A GeV/c.

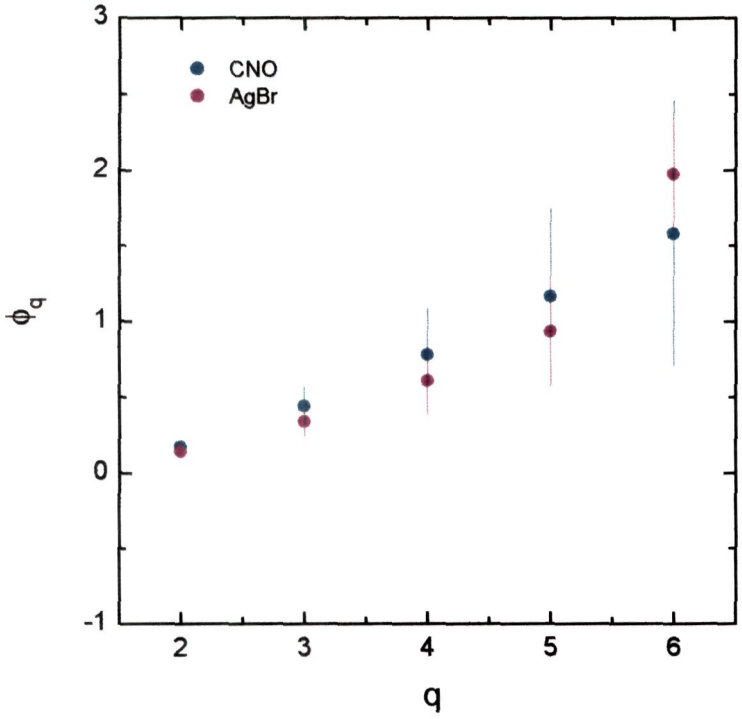

Fig. 3.7 Variations of ϕ_q with q for the interactions of ^{28}Si nuclei with CNO and AgBr at 4.5A GeV/c.

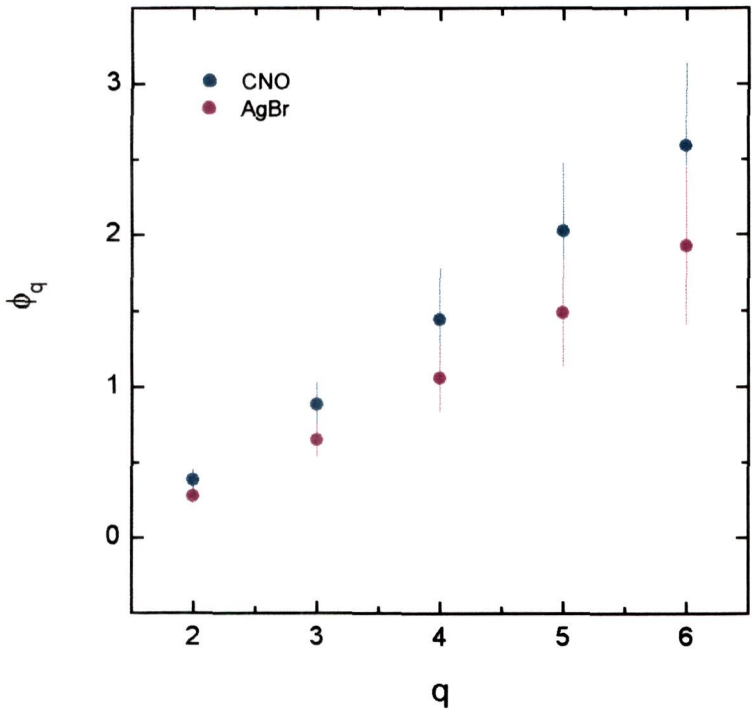

Fig. 3.8 Variations of ϕ_q with q for the interactions of ^{28}Si nuclei with CNO and AgBr at 14.5A GeV/c.

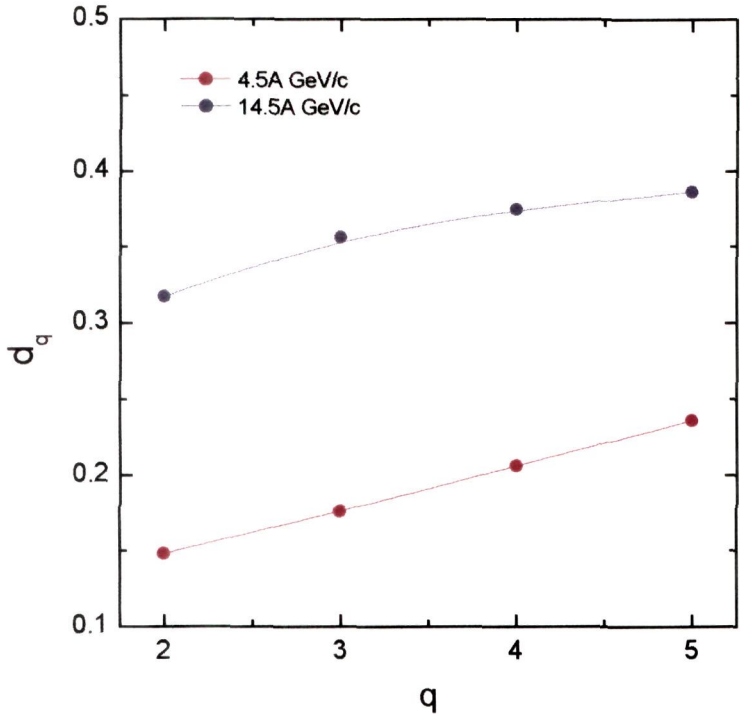

Fig. 3.9 Variations of d_q with q for ^{28}Si-Em interactions at 4.5A and 14.5A GeV/c.

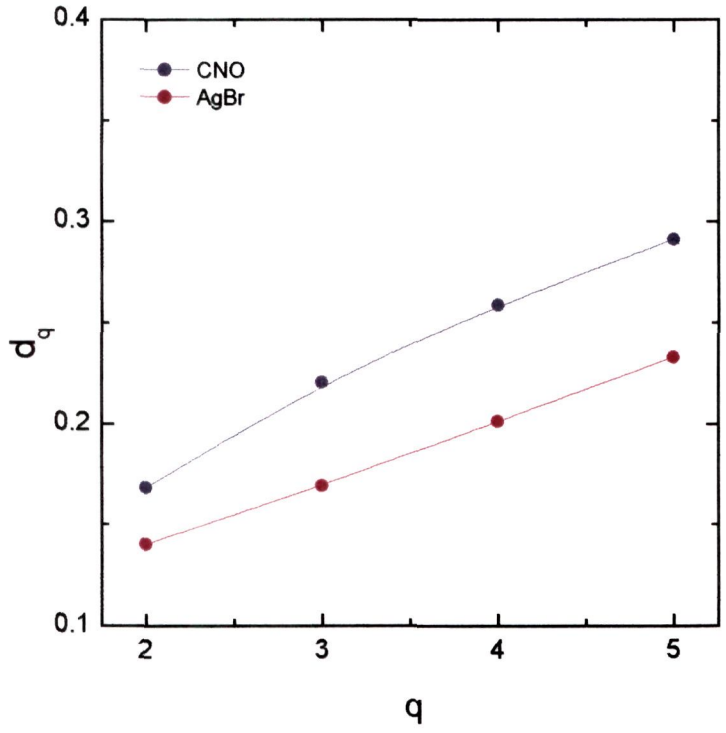

Fig. 3.10 Variations of d_q with q for the interactions of ^{28}Si nuclei with CNO and AgBr at 4.5A GeV/c.

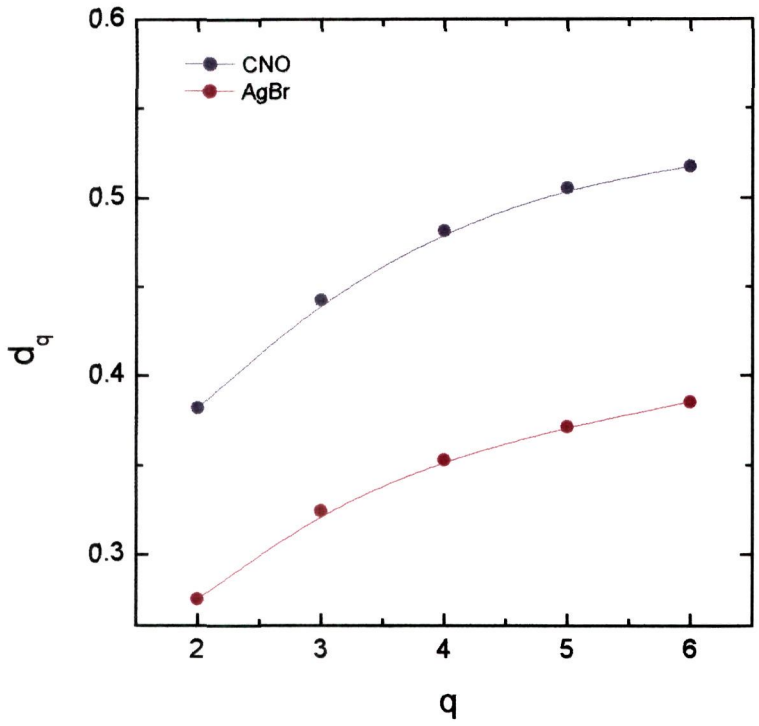

Fig. 3.11 Variations of d_q with q for the interactions of ^{28}Si nuclei with CNO and AgBr at 14.5A GeV/c.

Table 3.1. Values of the slope parameters ϕ_q for the collisions of 4.5A GeV/c ^{28}Si nuclei with Emulsion, CNO and AgBr targets.

Order of moment (q)	ϕ_q (Si-Em)	ϕ_q (Si-CNO)	ϕ_q (Si-AgBr)
2	0.15±0.02	0.17±0.03	0.14±0.03
3	0.35±0.08	0.44±0.12	0.34±0.01
4	0.62±0.19	1.77±0.31	0.60±0.22
5	0.94±0.32	1.16±0.56	0.93±0.36
6	1.96±0.33	1.56±0.87	1.97±0.36

Table 3.2. Values of the slope parameters ϕ_q for the interactions of 14.5A GeV/c ^{28}Si nuclei with Emulsion, CNO and AgBr targets.

Order of moment (q)	ϕ_q (Si-Em)	ϕ_q (Si-CNO)	ϕ_q (Si-AgBr)
2	0.32±0.05	0.38±0.07	0.27±0.04
3	0.71±0.12	0.88±0.19	0.65±0.11
4	1.12±0.22	1.44±0.33	1.06±0.22
5	1.54±0.33	2.02±0.45	1.48±0.34
6	1.97±0.49	2.58±0.55	1.93±0.52

The values of the anomalous dimensions for the interactions due to lighter targets (CNO) are observed to be relatively higher in comparison to the corre-

sponding values for the heavier targets (AgBr) for each order of the moment.

3.5.4 Non-thermal phase transition

It has been suggested [33] that intermittent behaviour in the final state of multiparticle production in a heavy-ion collision may be a projection of non-thermal phase transition believed to occur during the evolution of the collision which in turn would be responsible for the occurrence of anomalous events. A non-thermal phase transition in heavy-ion collisions is a type of transition in which the new phase need not be characterized by thermodynamical behaviour. If a phase transition of this nature takes place then the function:

$$\lambda_q = \frac{(\phi_q+1)}{q} \tag{3.29}$$

is predicted [33,34] to have a minimum at some value of $q = q_c$, where q_c need not necessarily be an integer. The region satisfying the condition $q < q_c$ is dominated by many small fluctuations, whereas the region $q > q_c$ contains rarely occurring large fluctuations.

Figs. 3.12 and 3.13 show λ_q vs q plots for 4.5A and 14.5A GeV/c ^{28}Si-Em interactions. It may be of interest to note that a distinct minimum at $q_c \sim 5$ for 4.5A GeV/c ^{28}Si-Em interactions is observed; the observed minimum in the variation of λ_q with q may be an indication for the occurrence of a phase transition [34].

3.5.5 Results on Ginzburg-Landau description

An important and interesting phenomenon in the context of Ginzburg-

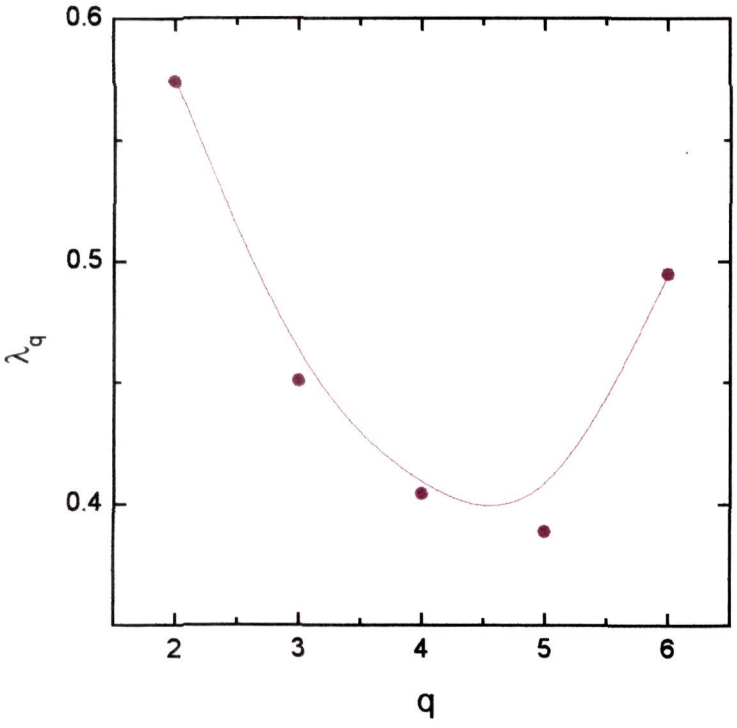

Fig. 3.12 Variation of λ_q with q for ^{28}Si-Em interactions at 4.5A GeV/c.

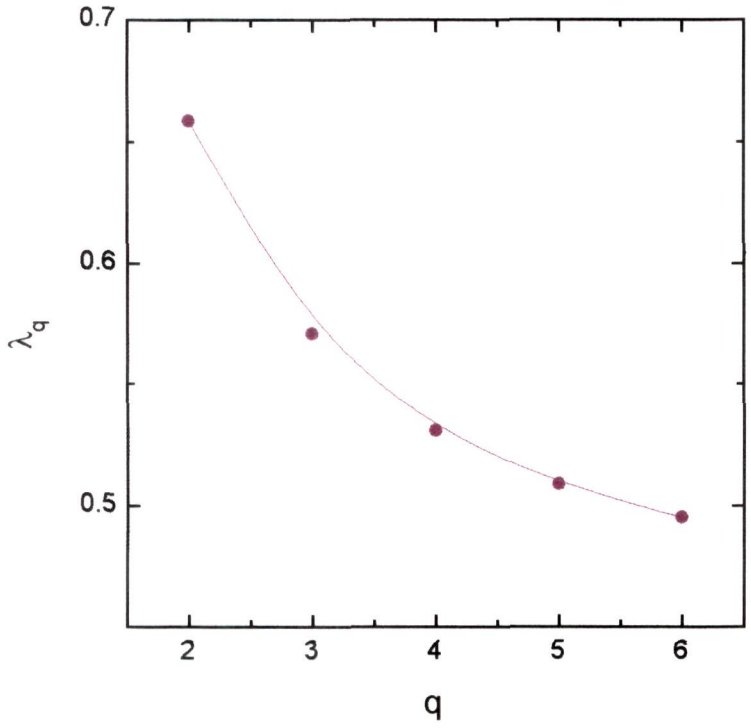

Fig. 3.13 Variation of λ_q with q for ^{28}Si-Em interactions at 14.5A GeV/c.

Landau description is the power law scaling behaviour between $< F_q >$ and $< F_2 >$ which is expressed as:

$$< F_q > = < F_2 >^{\beta_q} \tag{3.30}$$

The variations of ln $< F_q >$ as a function of ln $< F_2 >$ are shown in Figs. 3.14-3.16 for the various categories of interactions. The slopes β_q are obtained from the linear fits to the data exhibited in these figures.

It is worthmentioning that in the framework of Ginzburg-Landau model, the slope parameter, β_q, is predicted to follow the equation:

$$\beta_q = (q-1)^{\nu} \tag{3.31}$$

where ν is a quantity valid for all the systems described by the Ginzburg-Landau model, independent of the dimensions of the parameters of the model. Figs. 3.17-3.19 are the plots of ln β_q as a function of ln $(q-1)$.

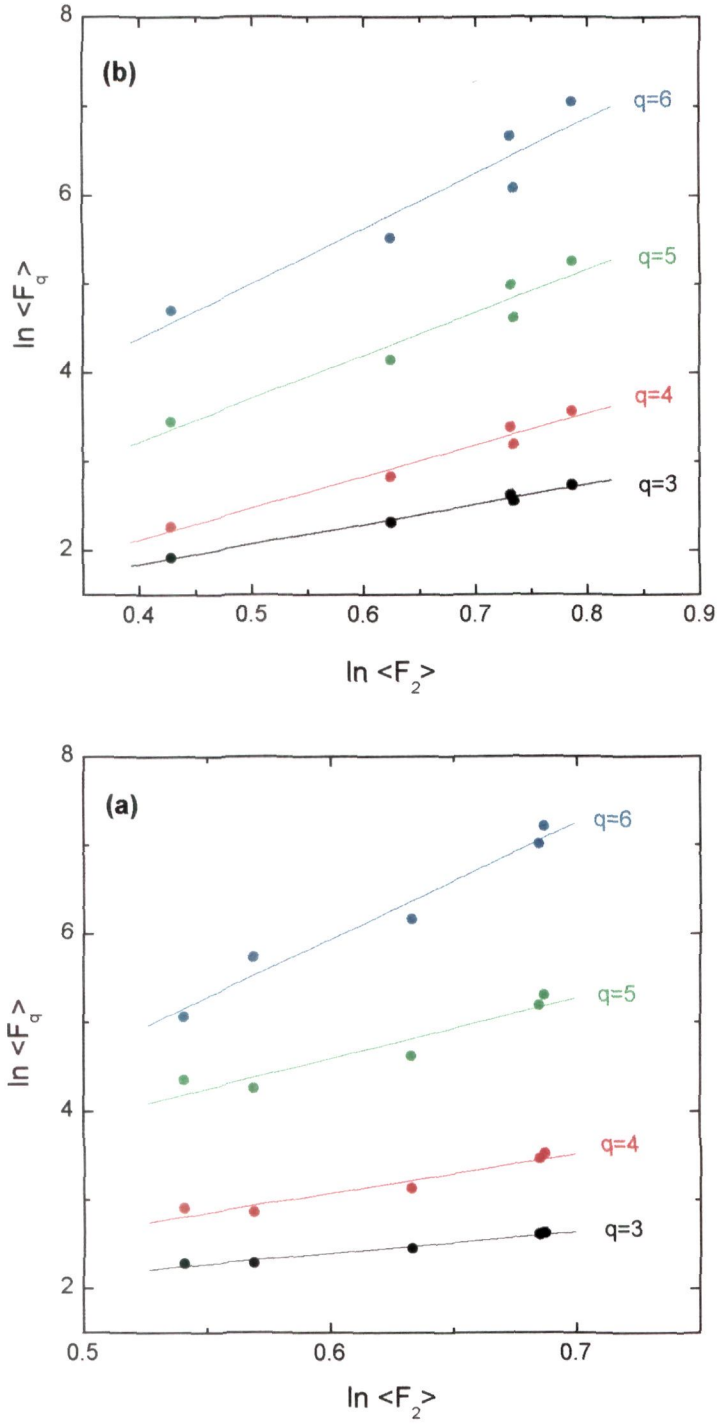

Fig. 3.14 Variations of ln $\langle F_q \rangle$ with ln $\langle F_2 \rangle$ for ^{28}Si-Em interactions at: (a) 4.5A and (b) 14.5A GeV/c.

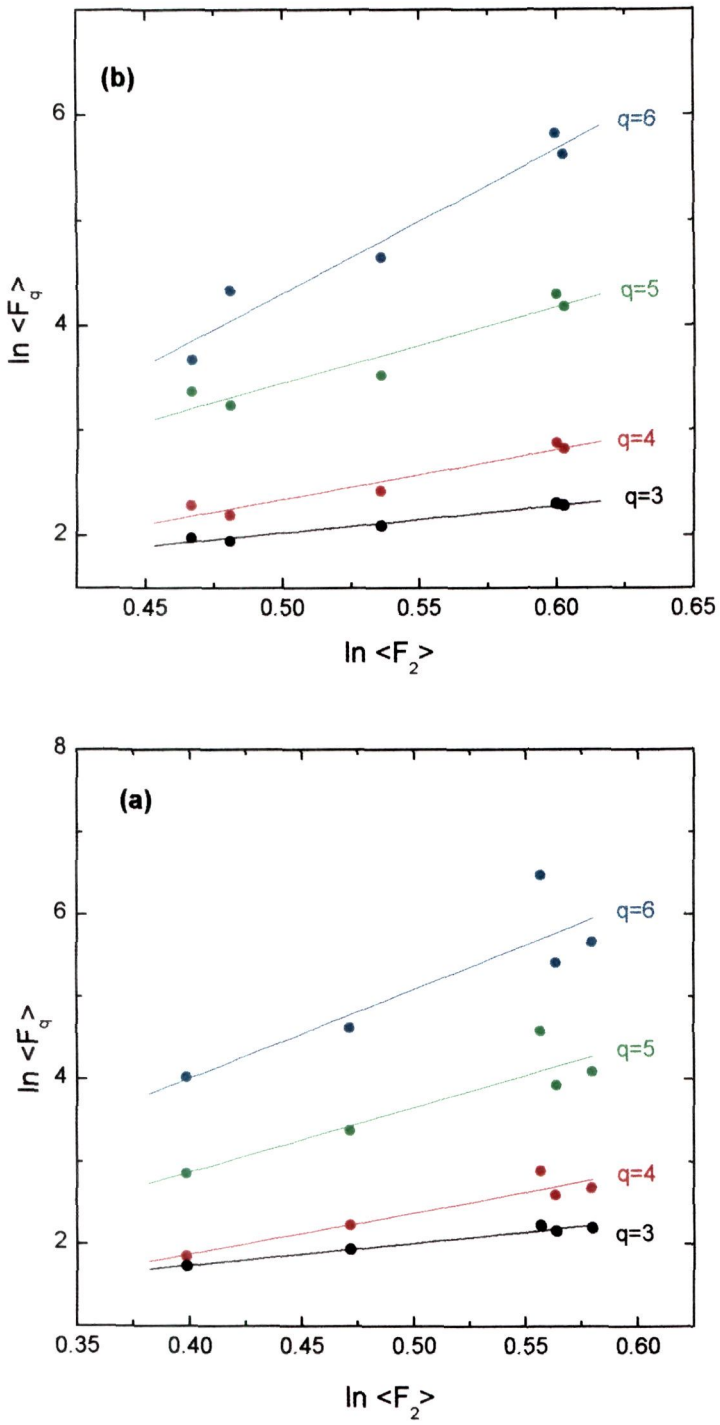

Fig. 3.15 Variations of ln $\langle F_q \rangle$ with ln $\langle F_2 \rangle$ for the interactions of 4.5A GeV/c ^{28}Si nuclei with: (a) CNO and (b) AgBr.

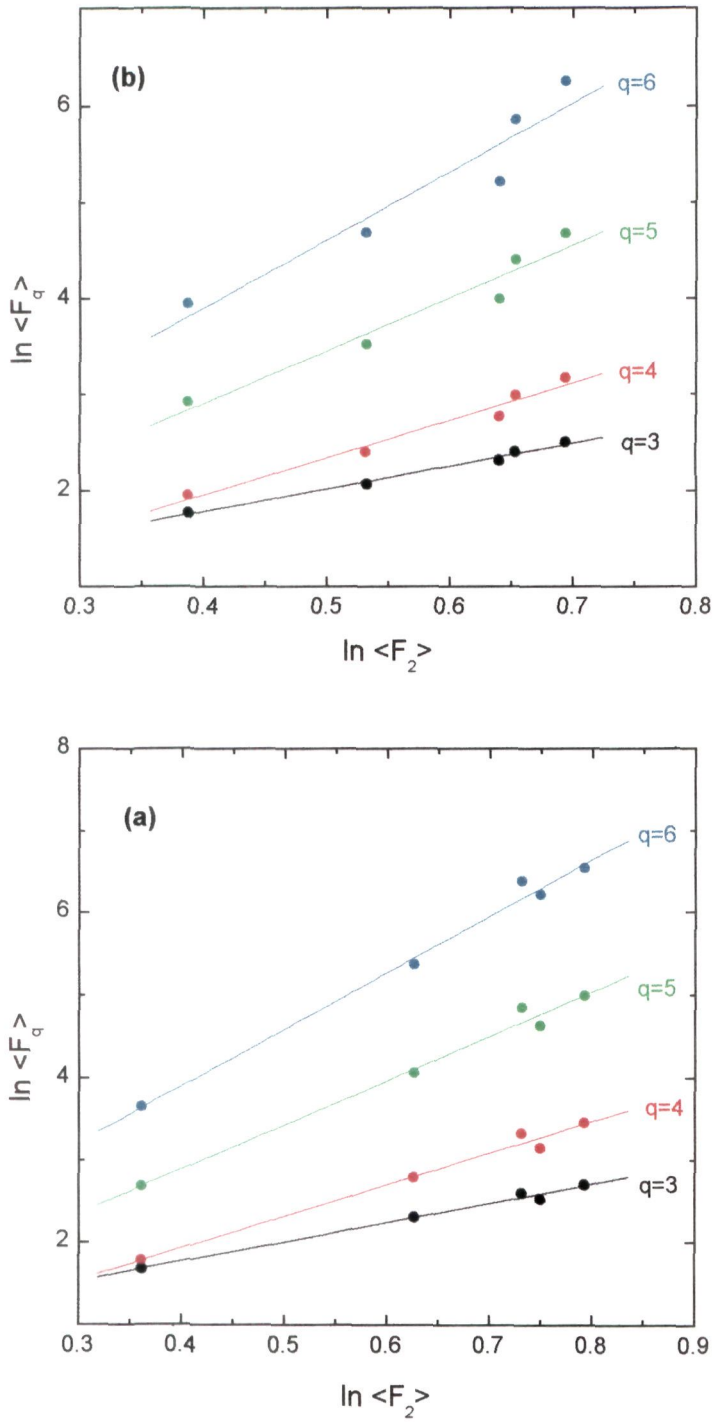

Fig. 3.16 Variations of ln $\langle F_q \rangle$ with ln $\langle F_2 \rangle$ for the interactions of 14.5A GeV/c ^{28}Si nuclei with: (a) CNO and (b) AgBr.

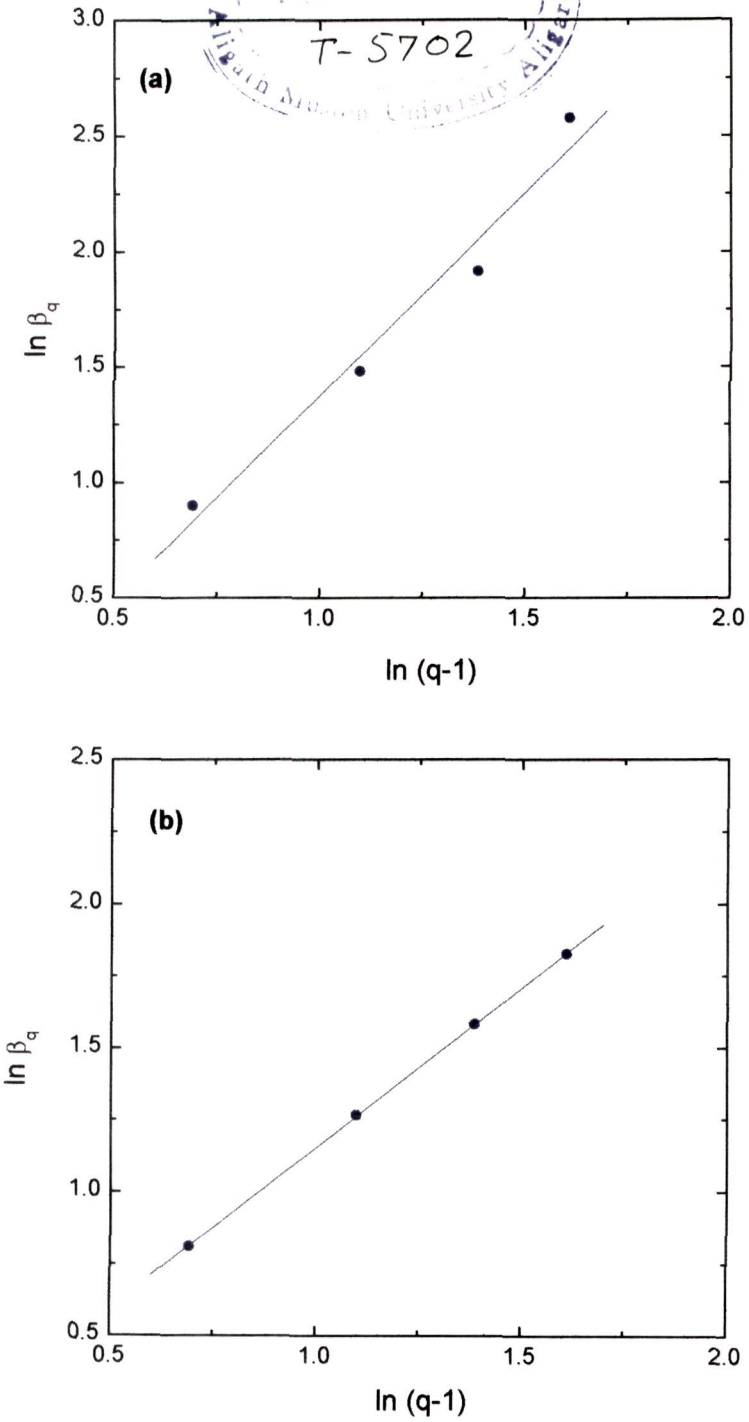

Fig. 3.17 Variations of ln β_q with ln (q-1) for ^{28}Si-Em interactions at: (a) 4.5A and (b) 14.5A Gev/c.

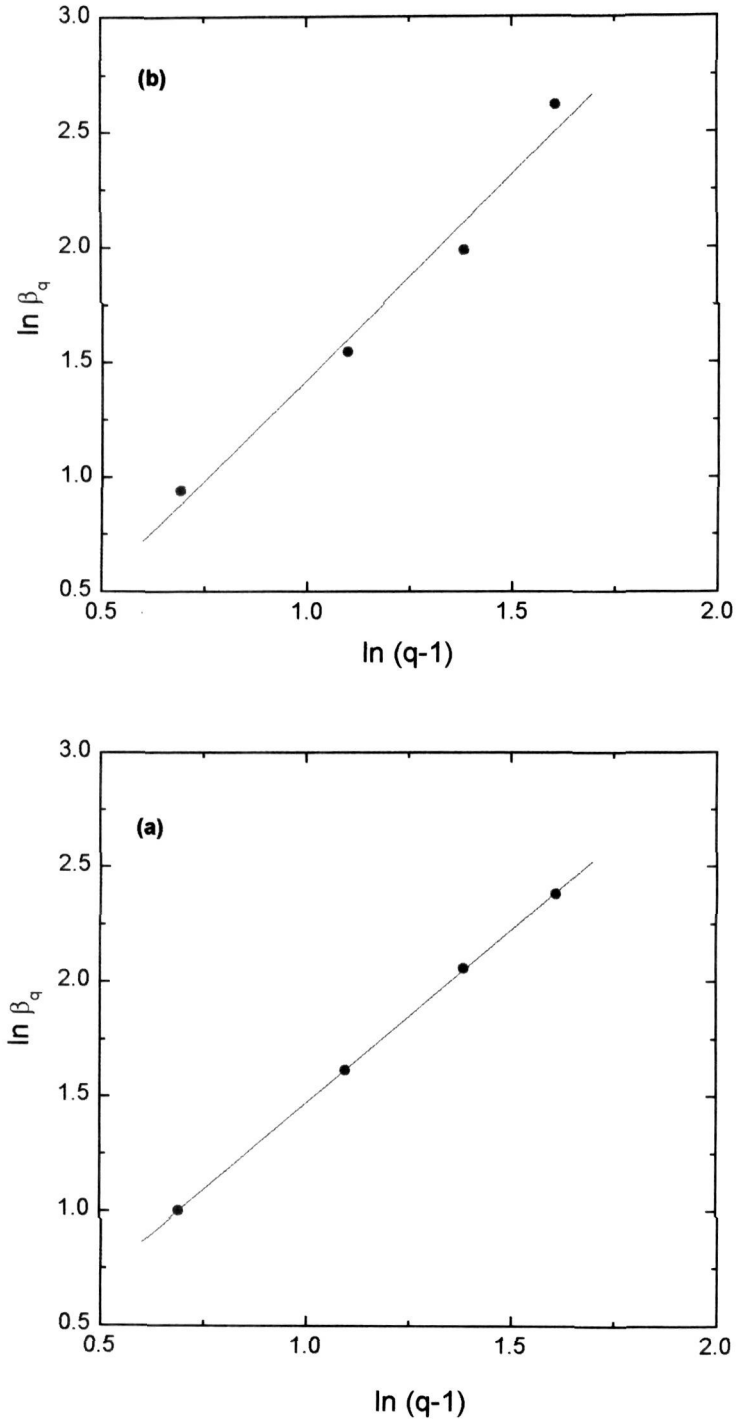

Fig. 3.18 Variations of ln β_q with ln (q-1) for the interactions of 4.5A GeV/c ^{28}Si nuclei with: (a) CNO and (b) AgBr.

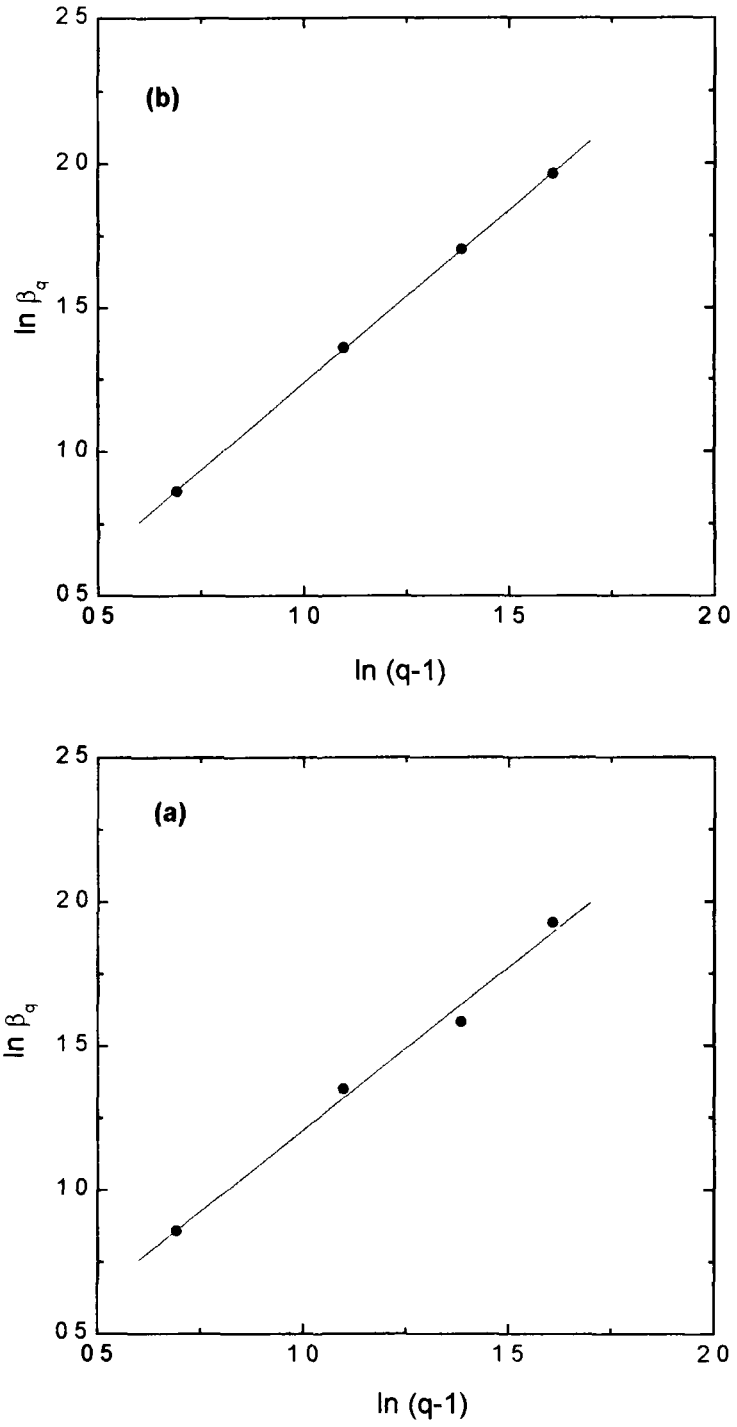

Fig. 3.19 Variations of ln β_q with ln (q-1) for the interactions of 14.5A GeV/c ^{28}Si nuclei with: (a) CNO and (b) AgBr.

References

1. B. Mandelbrot, *J. Fluid. Mech.*, **62**, (1974) 331.
2. U. Frisch, P. Sulem and M. Melkin, *J. Fluid. Mech.*, **87**, (1978) 719.
3. S. Lovejoy and D. Schertzer, *Proc. Conf. on Turbulent Shear Flows*, **4**, Ed. L. J. S. Bradbury et al, (Springer, Berlin 148)
4. T. H. Burnett et al., (JACEE Collaboration), *Phys. Rev. Lett.* **50** (1983) 2062.
5. Y. B. Zeldiovich et al., *Usp. Fiz.*, **Nauk**, (1987) 3.
6. A. Bialas and R. Peschanski, *Nucl. Phys.*, **B 273** (1986) 703.
7. A. Bialas and R. Peschanski, *Nucl. Phys.*, **B 308** (1988) 857.
8. Stodolksy, *Phys. Rev. Lett.*, **75**, (1995) 1044.
9. S. Mrowezski, *Phys. Lett.*, **B 430**, (1998) 9.
10. E. V. Shuryak, *Phys. Lett.*, **B 423**, (1998) 9.
11. Stephanov M. Rajagopal K. and Shuryak E., *Phys. Rev. Lett.*, **81** (1998) 4816; *Phys. Rev.*, **D 60** (1990) 114028; preprint *hep-ph*/**9903292** (1990).
12. R. C. Hwa, *Phys. Rev.*, **D 41** (1990) 1456.
13. R. C. Hwa and J. C. Pan, *Phys. Rev.*, **D 45** (1992) 1476.
14. P. Abreu et al (DELPHI Collaboration), *Phys. Lett.*, **B 247** (1990) 137.
15. W. Braunschweig et al (TASSO Collaboration), *Phys. Lett.*, **B 231** (1989) 548.
16. W. Shaoshun, Z. Jie, Y. Yunxiu, X, Chinguo and Z. Yu, *Phys. Rev.*, **D 49** (1994) 5785.
17. C. Albajar et al (UA1 Collaboration), *Nucl. Phys.*, **B 345** (1990) 1.
18. R. Holynski et al (KLM Collaboration), *Phys. Rev.*, **C 40** (1989) R2449.
19. D. Ghosh et al, *Phys. Rev.*, **D 49** (1994) 3113.
20. R. K. Shivpuri and V. K. Verma, *Phys. Rev.*, **D 47** (1993) 123.
21. M. I. Adamovich et al. (EMU01 Collaboration), *Phys. Rev. Lett.*, **65** (1990) 412; *Z. Phys.*, **C 49** (1991) 395.

22. T. Akensson et al. (HELIOS Collaboration), *Phys. Lett.*, **B 25** (1990) 303.

23. K. Sengupta, P. L. Jain, G. Singh and S. N. Kim, *Phys. Lett.*, **B 236** (1990) 219.

24. P. L. Jain and G. Singh, *Mod. Phys. Lett.* **A 7** (1992) 93.

25. R. Hassan, M. Zafar, M. S. Ahmad and A. Tufail, *Int. J. Mod. Phys.*, **A 14** (1999) 3451.

26. M. M. Aggarwal, *Proceedings on* 3rd *International Conference on Physics and Astrophysics of Quark Gluon Plasma*, editors B.C. Sinha, D. K. Srivastava and Y. P. Vyogi (Narosa Publishing House) (1998).

27. G. Roland et al. (NA49 Collaboration), *Nucl. Phys.*, **A 638** (1998) 91c; H. Appelhauser et al. (NA49 Collaboration), preprint *hep-ex*/**9904014** (1999).

28. M. Gazdzicki and S. Mrowczynski, *Z. Phys.*, **C 54** (1992) 127.

29. S. Mrowczynski, *Phys. Lett*, **B 439** (1998) 6.

30. M. A. Halasz, A. D. Jackson, R. E. Shrock, M. A. Stephanov, J. J. M. Verbaarschot, *Phys. Rev.*, **D 58** (1998) 96007.

31. M. Adamus et al (NA22), *Phys. Lett.*, **B 185** (1987) 200.

32. A. Bialas and R. Peschanski, *Jagellonian Universıty Report* **JPJU/4/88**.

33. A. Bialas and K. Zalewski, *Phys. Lett.*, **B 238** (1990) 413; *Nucl Phys.*, **B 237** (1989) 65.

34. R. Peschanski, *Int. J. Mod. Phys.*, **A 6** (1991) 3681; *Nucl Phys.*, **B 327** (1989) 144.

35. K. Fialkowski, N. Wosick and J. Wosick, *Acta. Phys. Pol.*, **B 20** (1988) 639.

36. A. N. Kolmogorov, *Docl. Akad. Sci, USSR*, **30** (1941) 301; E. A. Novikov and R. W. Stewart, *Izv. Acad. Sci. USSR*, **SerGeofiz 3**, (1941) 408.

37. G. Paladin and A. Vulpiani, *Phys. Rep.*, **156** (1987) 117.

38. L. Van Hove, *Z. Phys.*, **C 21** (1983) 93.

39. M. Gyulassy et al, *Nucl. Phys.*, **B 237** (1984) 477; *Nucl. Phys.*, **A 418** (1984) 59c.

40. A. Bialas and R. C. Hwa, *Phys. Lett.*, **B 253** (199) 436.

41. R. C. Hwa, *Nucl. Phys.*, **A 525** (1991) 537c

42. G. Baym, H. Heiselberg, *Phys. Lett.*, **B 469** (1999) 7; M. A. Sakawa, U. Heinz, B. Muller, *Phys. Rev. Lett.*, **85** (2000) 2072.

43. R. C. Hwa and M. T. Nazirove, *Phys. Rev. Lett.*, **69** (1992) 74.

44. R. C. Hwa, *Quark Gluon Plasma*, **Vol. 2**, Ed. R. C. Hwa (World Scientific, Singapore)

45. R. C. Hwa, *Mod. Phys. Lett.*, **A 9** (1994) 863.

46. X. Cai, C B. Yang and Z. M. Zhou, *Phys. Rev.*, **C 54** (1996) 2775.

47. C. B. Yang, X. R. Wong and X. Cai, *Science in China*, **40** (1997) 1065.

48. R. C. Hwa, *Phys. Rev.*, **C 50** (1994) 383.

49. I. A. Lebedov and M. T. Nazirov, *Mod. Phys. Lett.*, **A 9** (1994) 2999.

50. A. K. Mohanty and S. K. Kataria, *Phys. Rev. Lett*, **730** (1994) 2672.

CHAPTER IV

MULTIFRACTALITY IN RELATIVISTIC HEAVY-ION COLLISION

4.1 Introduction

Study of high-energy nucleus-nucleus collisions may address several important issues concerning multiparticle production. Besides this, these collisions are envisaged to create conditions necessary for the production of quark-gluon plasma (QGP). Various studies [1-4] suggest the possibility of existence of a deconfined phase of matter comprising essentially of quarks and gluons at energy density $\sim$ 3 GeV/fm^3 with a subsequent phase transition to hadrons. Several important and fascinating signatures [5] for the production of QGP have been proposed. One of the various possible approaches is to investigate the fluctuations in particle densities. Such investigations are carried out with the realization that a phase transition may give rise to fluctuations in individual events which may manifest as clear peaks or spikes in the phase space domains [6-8]. In the case of hydrodynamic turbulence, this aspect is studied via scaling properties of the moments of the relevant distributions as functions of the bin sizes of the phase space [9].

An attempt to investigate some important characteristics of the mechanism involved in multiparticle production was made by Bialas and Peschanski [10], who have suggested a power law behaviour for the factorial moments as

function of successively decreasing phase space bins which is referred to as intermittency. The search for a link between intermittency and a phase transition, leads to a thermodynamic formulation of fractal dimensions of which intermittency is a special case [11-14]. A fractal or a self-similar object has the characteristic property of satisfying a power law scaling behaviour which reflects the underlying dynamics [15]. In this chapter, method of multifractal moments [15] is used to investigate the scaling properties of relativistic nucleus-nucleus collisions. In Section 4.2, some features of fractals and relevance of their studies for investigating the important characteristics of mechanism of multiparticle production has been briefly described. In Section 4.3, various mathematical formalisms used to study multifractality are presented. Experimental results on multifractal studies in relativistic nuclear collisions are presented in Section 4.4.

4.2 Multifractality

Fractals, in general, refer to the geometrical objects which do not possess any characteristic scale but instead are self-similar over many length scales [16]. As the study of self-similar properties of multiplicity fluctuations in high energy nuclear collisions is one of the main concerns, an attempt is, therefore, made to carry out fractal analysis which is closely connected with such studies [17]. However, it is of prime importance to know, while studying multiparticle production, which feature of high energy collisions has fractal nature.

The existence of fractal nature can be understood in terms of the presence of holes in a cantor set [16,18] as shown in Fig. 4.1. As an example, one may look at the rapidity distribution of the relativistic particles produced in a very-high-multiplicity event recorded by JACEE [6] Collaboration; the rapidity distribution of the event is displayed in Fig. 4.2. The distribution is a typical one as it has unusual several peaks and valleys.

The particle number density in each rapidity bin depends on whether the resolution of the binning is of the order of or better than the rapidity separation between neighbouring particles [17]. Empty bins in the distribution are analogous to the holes in the cantor set. If a distribution under study possesses fractal properties, then the set of non-empty bins would form fractal set [17]. Furthermore, if M represents the number of bins and $\delta\eta$ is the bin size in the rapidity space, then in the limit $\delta\eta \longrightarrow 0$, the fractal property of M suggests

$$M \propto (\delta\eta)^{-D_0} \tag{4.1}$$

where D_0 is the fractal dimension ($D_0 < 1$).

In addition to the set of non-empty bins, there is a possibility of many other subsets with different fractal properties. All such subsets collectively constitute the multifractal structure. In the present study, the standard method of multifractal analysis [9,19,21] is used. The rapidity space, $\Delta\eta = \eta_{max} - \eta_{min}$, in an event and the bin width, $\delta\eta$, are related as:

$$\delta\eta = \Delta\eta/M \tag{4.2}$$

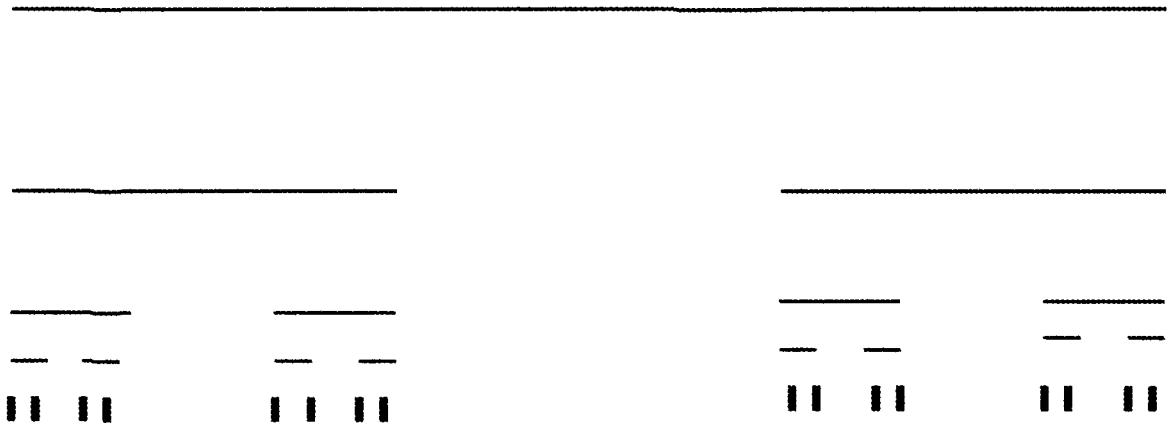

Fig. 4.1. Cantor Set (an example of fractal object). The set is constructed by removing the middle third of a unit interval and subsequent repetition of this action in each interval of previous step.

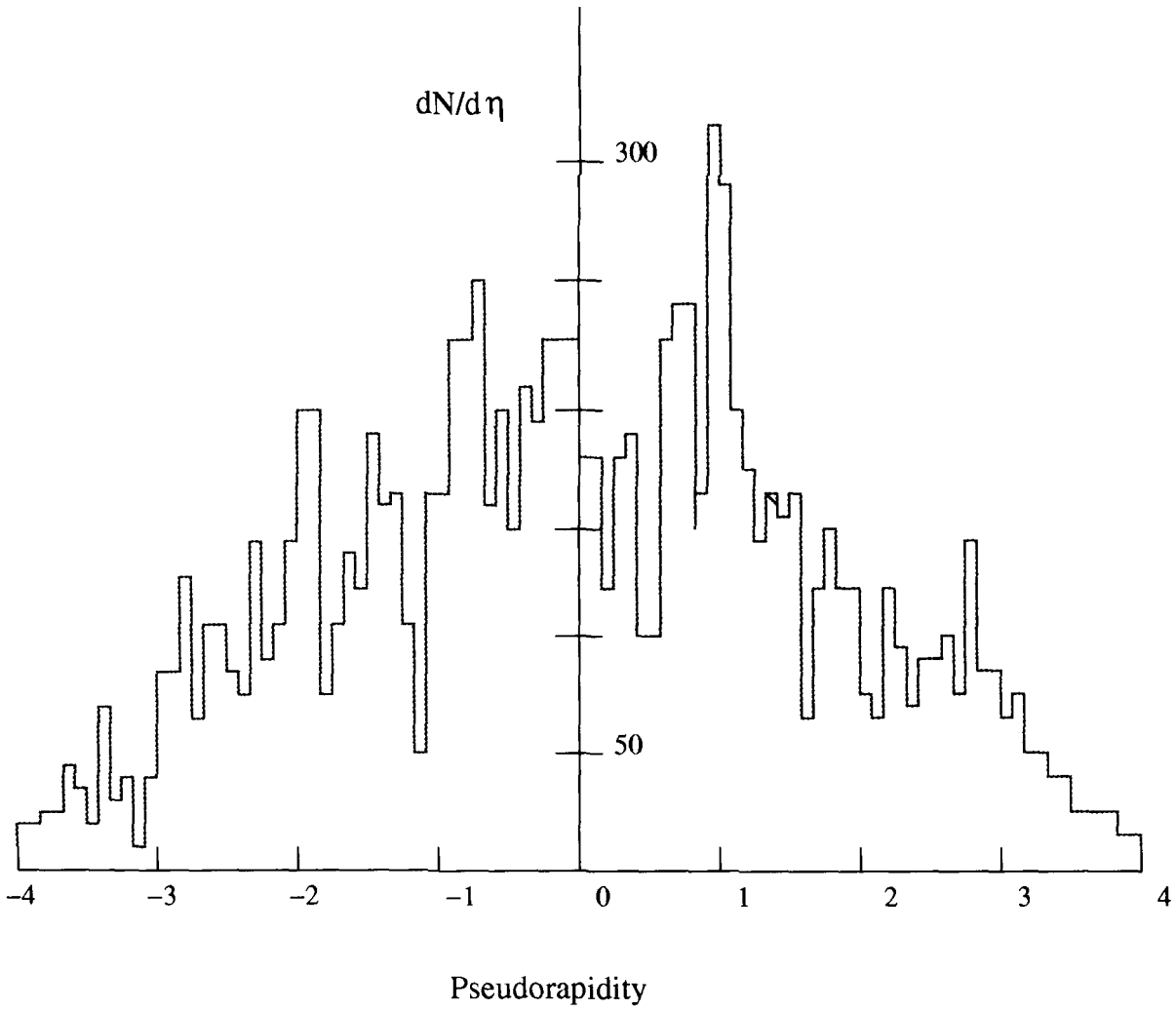

Fig. 4.2 JACEE event

If n_j denotes the number of particles in j^{th} bin, where j labels the bins and obviously if non-empty bins are also included, then j would run from 1 to M. The total number of particles in an event is estimated using the relation, $n = \sum_{j=1}^{M} n_j$ and the fraction of particles in the j^{th} bin is estimated from $p_j = n_j/n$. The quantity p_j is a small number when $\delta\eta$ is very small and fluctuates distinctly amongst the various bins. For a smooth but not necessarily flat rapidity distribution, p_j in the limit $\delta\eta \longrightarrow 0$, would have a first order linear dependence on $\delta\eta$, i.e., p_j will vary as $\delta\eta$. However, for a non-smooth rapidity distribution, that is, the distributions with apparent fluctuations, the dependence may be expressed in a more general form

$$p_j \propto (\delta\eta)^{\alpha} \tag{4.3}$$

where α is positive. It may be noted that the proportionality sign applies to non-empty bins only. The above relationship, which maps j to α through the binning resolution dependence, is a fundamental step for examining multifractality. It is quite clear that in an event different bins would have different α values. However, it is possible to map many bins to a small interval in α. For instance, if we consider a particular interval $d\alpha$ located at α_r i.e., $\alpha_r < \alpha < \alpha_r + d\alpha$, then all the bins that correspond to this interval constitute a fractal subset, S_r; the characteristics of the set depend on α_r. For the full range of α, the integration of α_r results in a fractal set which includes all the non-empty bins of the event. If M_r represents the number of elements in the

subset S_r, then the total number of non-empty bins in the event is:

$$M' = \sum_r M_r \tag{4.4}$$

where M' may obviously be different from M, because the non-empty bins only are being considered.

For small $\delta\eta$, the dependence of M_r on $\delta\eta$ is expressed as:

$$M_r \propto (\delta\eta)^{-f(\alpha_r)} \tag{4.5}$$

The exponent $f(\alpha_r)$ characterizes the fractal properties of all subsets, S_r. Thus $f(\alpha_r)$ is a function to which multiplicity fluctuations in the rapidity distributions are mapped. This spectral function is, therefore, of main interest in carrying out multifractal analysis.

In the next section, various mathematical descriptions relating to the determination of spectral function, $f(\alpha)$, for examining the multifractal nature are presented.

4.3 Mathematical formalism

As already mentioned, for studying multifractality, a given pseudorapidity range, $\Delta\eta = \eta_{max} - \eta_{min}$, is divided into M bins of width $\delta\eta = \Delta\eta/M$. If n_j denotes the particle multiplicity in the j^{th} bin, then a multifractal moment, G_q, is defined [15,22] as:

$$G_q = \sum_j (p_j)^q \tag{4.6}$$

where the summation is carried out over the non-empty bins only which constitute a fractal set. On averaging over all the events in a data sample consisting of N_{evt} events, $< G_q >$ is expressed as:

$$< G_q > = \frac{1}{N_{evt}} \sum_1^{N_{evt}} G_q \tag{4.7}$$

For the fractal nature of rapidity distribution, $< G_q >$ should exhibit a power law behaviour [23] over a range of small $\delta\eta$ in the following fashion:

$$< G_q > \propto (\delta\eta)^{\tau_q} \tag{4.8}$$

where τ_q are the mass exponents and may be determined from the observed linear dependence of $\ln < G_q >$ on $\ln\delta\eta$ using:

$$\tau_q = \lim_{\delta\eta \to 0} \frac{\Delta \ln < G_q >}{\Delta \ln \delta\eta} \tag{4.9}$$

The spectral function, $f(\alpha_q)$, which can be obtained [15] by Legendre transform using the standard procedure of multifractals [24] is calculated from:

$$f(\alpha_q) = q\alpha_q - \tau_q \tag{4.10}$$

where α_q defined as:

$$\alpha_q = \frac{d\tau_q}{dq} \tag{4.11}$$

are referred to as the Lipschitz-Holder exponents [23].

For a multifractal structure, the spectral function is a smooth function, concave downwards with its maximum at $\alpha_{q=0}$. The left $(q > 0)$ and right $(q < 0)$ wings of the plots of the function give a quantitative description of the

fluctuation density in the dense and sparse regions of a single particle pseudorapidity distribution [22].

Inhomogeneity of the pseudorapidity distribution is determined by the width of the distribution. The non-existence of a sharp peak in $f(\alpha_q)$ versus α_q plot at α_q corresponding to $q = 0$ reveals non-smooth nature of the pseudorapidity distribution in the phase space [26].

One of the most basic properties of the fractals which describes the scaling behaviour are the generalized dimensions; the generalized dimensions, D_q, are defined [27]as:

$$D_q = \frac{\tau_q}{q-1} \tag{4.12}$$

It may be of interest to note that if D_q decreases with increasing q, the pattern is known as multifractal and on the other hand, if D_q is constant, the pattern is referred to as monofractal [27,28]. For $q = 0$, $D_0 = f(\alpha_0)$ is known as fractal dimension whereas for $q = 0$, $G_0 = M$ and $M \propto (\delta\eta)^{\tau_q}$; M may be expressed as:

$$M \propto (\delta\eta)^{-D_0} \tag{4.13}$$

which, incidentally, is identical to Eq. 4.1; the dependence envisaged in Eq. 4.13 is the basic property of a fractal set. Hence D_0 is referred to as the fractal dimensions for describing multiparticle production process. For $q = 1$, we have the information dimension, D_1, related to α_1 and $f(\alpha_1)$ in the following fashion:

$$D_1 = \alpha_1 = f(\alpha_1)$$

Using the definition of G_q moments and the power law behaviour one would get:

$$D_1 = -\lim_{\delta\eta\to 0}\frac{S(\delta\eta)}{\ln\delta\eta}$$

where

$$S(\delta\eta) = -\sum_{j=1}^{M} p_j \ln p_j \tag{4.14}$$

is the definition of entropy in information theory [26]. For q = 2, Eq. 4.12 may be used to find the correlation dimension [29,30]. It may be mentioned that p_j^2 in Eq. 4.6 represents the probability of having two particles in the j^{th} bin. In terms of the spectral function, $f(\alpha)$, the correlation dimension is determined using the following expression:

$$D_2 = 2\alpha_2 - f(\alpha_2) \tag{4.15}$$

4.4. Results and discussion

4.4.1 Multifractal moments

4.4.1.1 Variation of $\ln < G_q >$ with $-\ln\delta\eta$

The values of $\ln < G_q >$ as a function of $-\ln\delta\eta$ for 4.5A and 14.5A GeV/c ^{28}Si-Em collisions are plotted in Fig. 4.3. The multifractal moments are observed to increase linearly with decreasing bin width, $\delta\eta$. Furthermore, the moments with positive values of q exhibit linearity over a relatively wider range of $-\ln\delta\eta$ than the moments with negative q values which tend to saturate with decreasing $\delta\eta$. This effect may be due to decrease in the particle

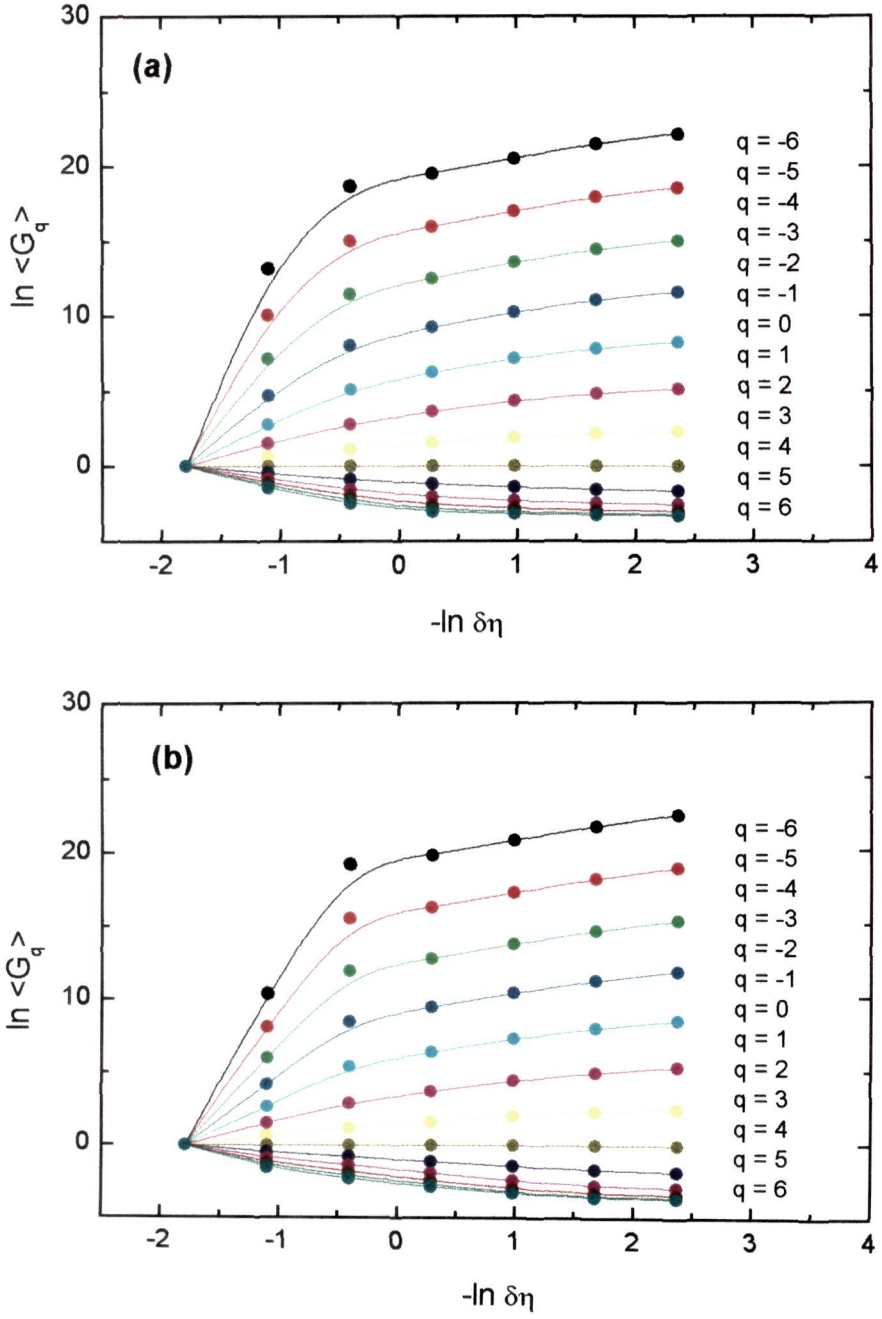

Fig. 4.3 *Variations of ln $\langle G_q \rangle$ with -ln δη for the experimental data on ^{28}Si-Em interactions at: (a) 4.5A and (b) 14.5A GeV/c.*

multiplicity in smaller bin widths [31]. The observed linear rise of multifractal moments in pseudorapidity phase space manifests self-similarity in the mechanism of particle production for the interactions considered in the present work.

In order to extract the dynamical component of the multifractal moments, experimental results are compared with those for the Monte Carlo generated data sets, MC-4.5 and MC-14.5 corresponding respectively to 4.5A and 14.5A GeV/c ^{28}Si-Em collisions. The Monte Carlo events are generated applying the following criteria:

* Multiplicity distribution of the particles should be similar to the corresponding experimental distribution.

* The emitted particles should not be correlated.

* For each event with multiplicity n, its multiplicity distribution should have a Gaussian shape with its mean value and dispersion comparable with the corresponding experimental values for the whole sample.

Figs. 4.4 and 4.5 are the plots of $\ln < G_q >$ versus $-\ln\delta\eta$ for the Monte Carlo generated data sample and the sample generated using FRITIOF. The plots for the generated data samples are found to be quite compatible with the corresponding experimental plots. It is interesting to note that similar trends have also been observed in relativistic hadron-nucleus [32] and nulceus-nucleus [33] collisions.

In order to examine the dependence of multifractal moments on target mass, the values of $\ln < G_q >$ are plotted as a function of $-\ln\delta\eta$ for the in-

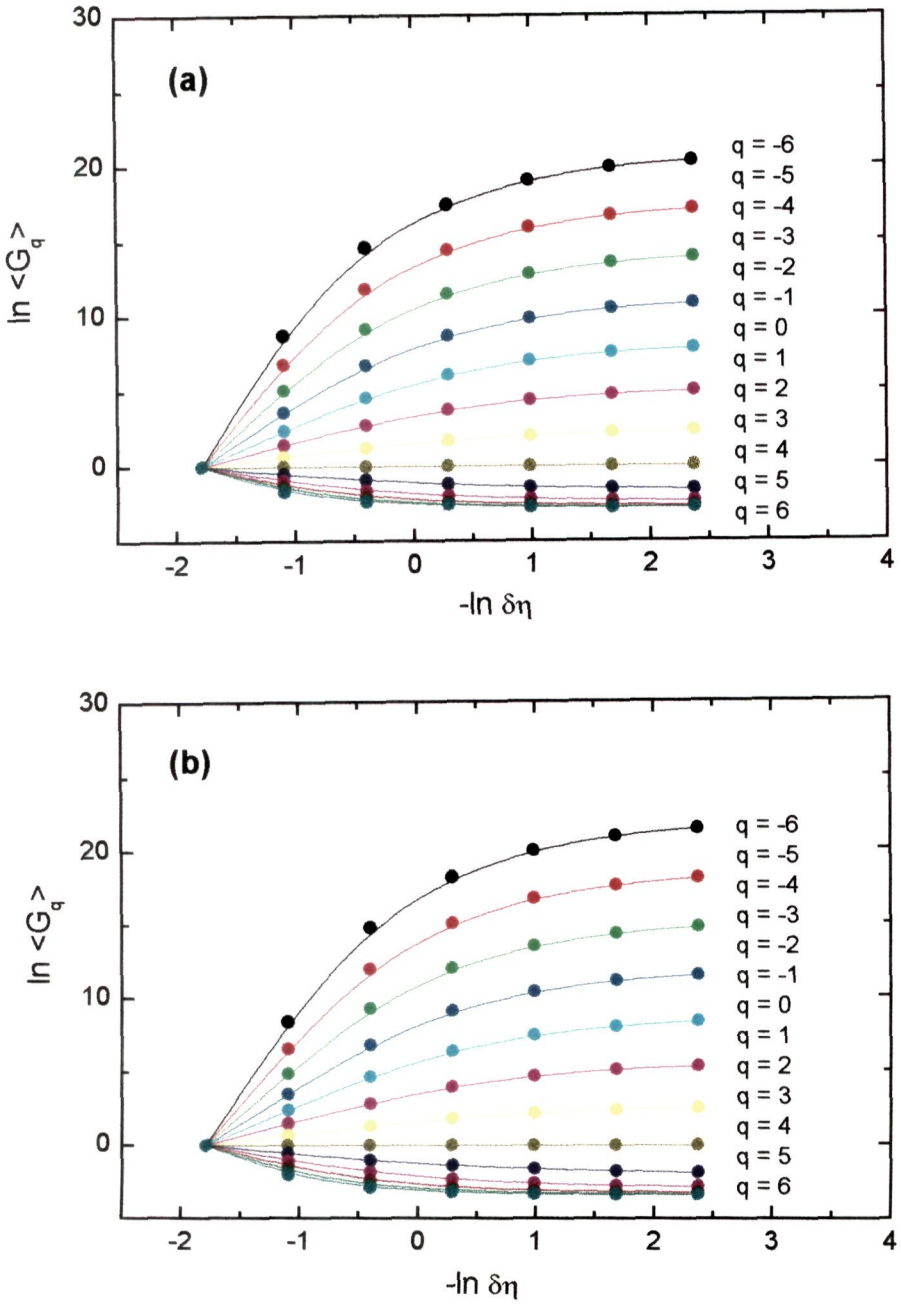

Fig. 4.4 Variations of ln $\langle G_q \rangle$ with -ln $\delta\eta$ for the Monte Carlo generated data on ^{28}Si-Em interactions at: (a) 4.5A and (b) 14.5A GeV/c.

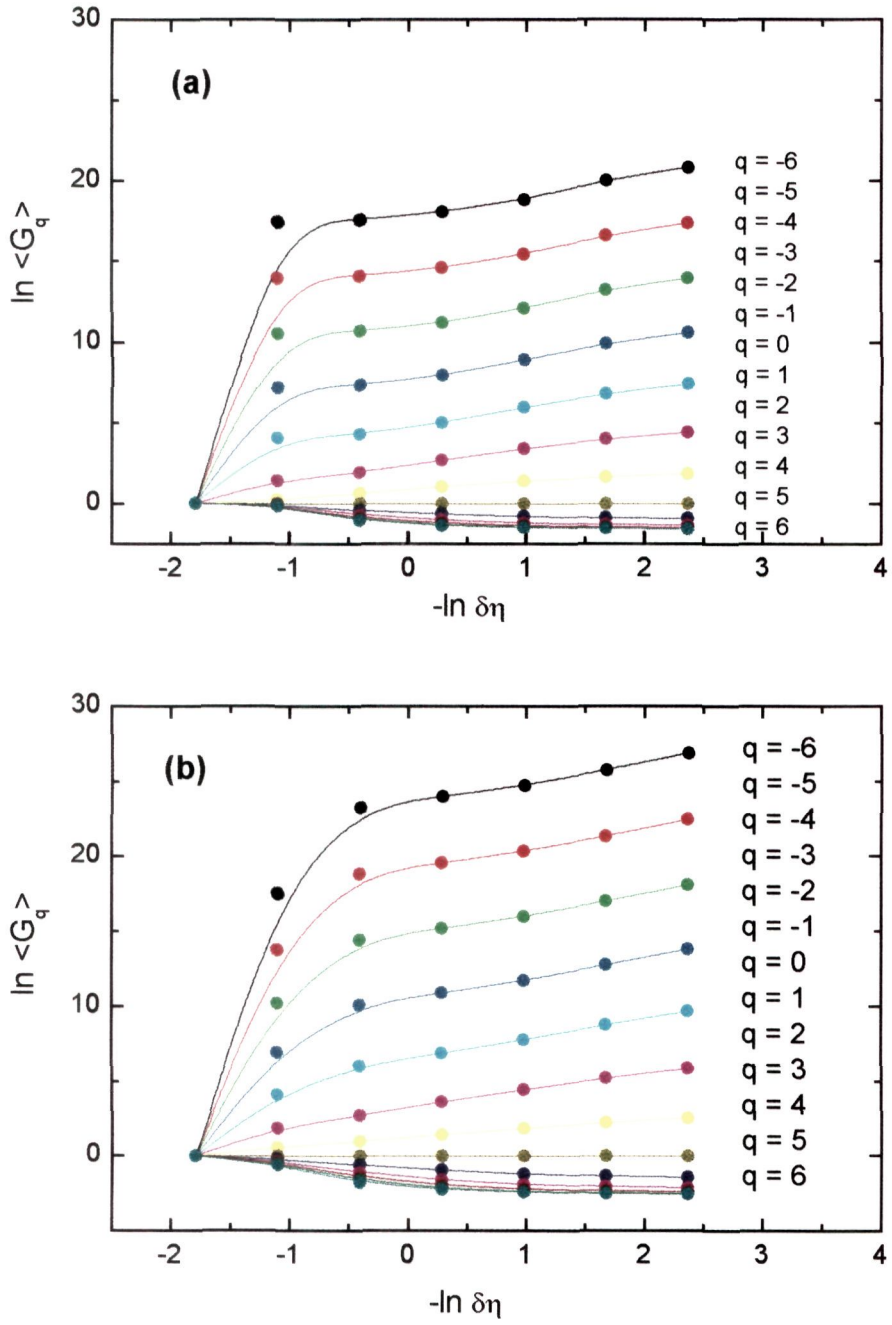

Fig. 4.5 Variations of ln $\langle G_q \rangle$ with -ln $\delta\eta$ for the FRITIOF generated data on ^{28}Si-Em interactions at: (a) 4.5A and (b) 14.5A GeV/c.

teractions of ^{28}Si nuclei with CNO and AgBr targets at 4.5A and 14.5A GeV energies which are displayed in Figs. 4.6 and 4.7 respectively. The multifractal moments for the interactions due to CNO targets tend to saturate earlier than those for the collisions due to AgBr targets. This behaviour may be attributed to lower multiplicity values in the interactions due to lighter targets as compared to those with the heavier targets [31].

4.4.1.2 Mass exponents

The mass exponents, τ_q, are obtained from the linear dependence of ln $< G_q >$ on $-\ln\delta\eta$. For carrying out fittings, only the portions of the curves showing linear behaviour are considered. The values of the mass exponents for the interactions of 4.5A and 14.5A GeV/c ^{28}Si nuclei with various targets are respectively listed in Tables 4.1 and 4.2.

Variations of τ_q, τ_q^{stat} and τ_q^{dyn} with the order of the moment q are shown in Fig. 4.8; τ_q^{stat} represents the slopes for the Monte Carlo generated data sets and τ_q^{dyn} represents the dynamical component of the parameter which is calculated using the relation:

$$\tau_q^{dyn} = \tau_q - \tau_q^{stat} + q - 1 \tag{4.16}$$

In Fig 4.8, it is seen that τ_q increases with q. However, the rate of the increase in the regions corresponding to positive and negative values of q are quite different. In the region characterized by $q < 0$, the increase in τ_q with q is relatively more rapid in comparison to that for the region where $q > 0$.

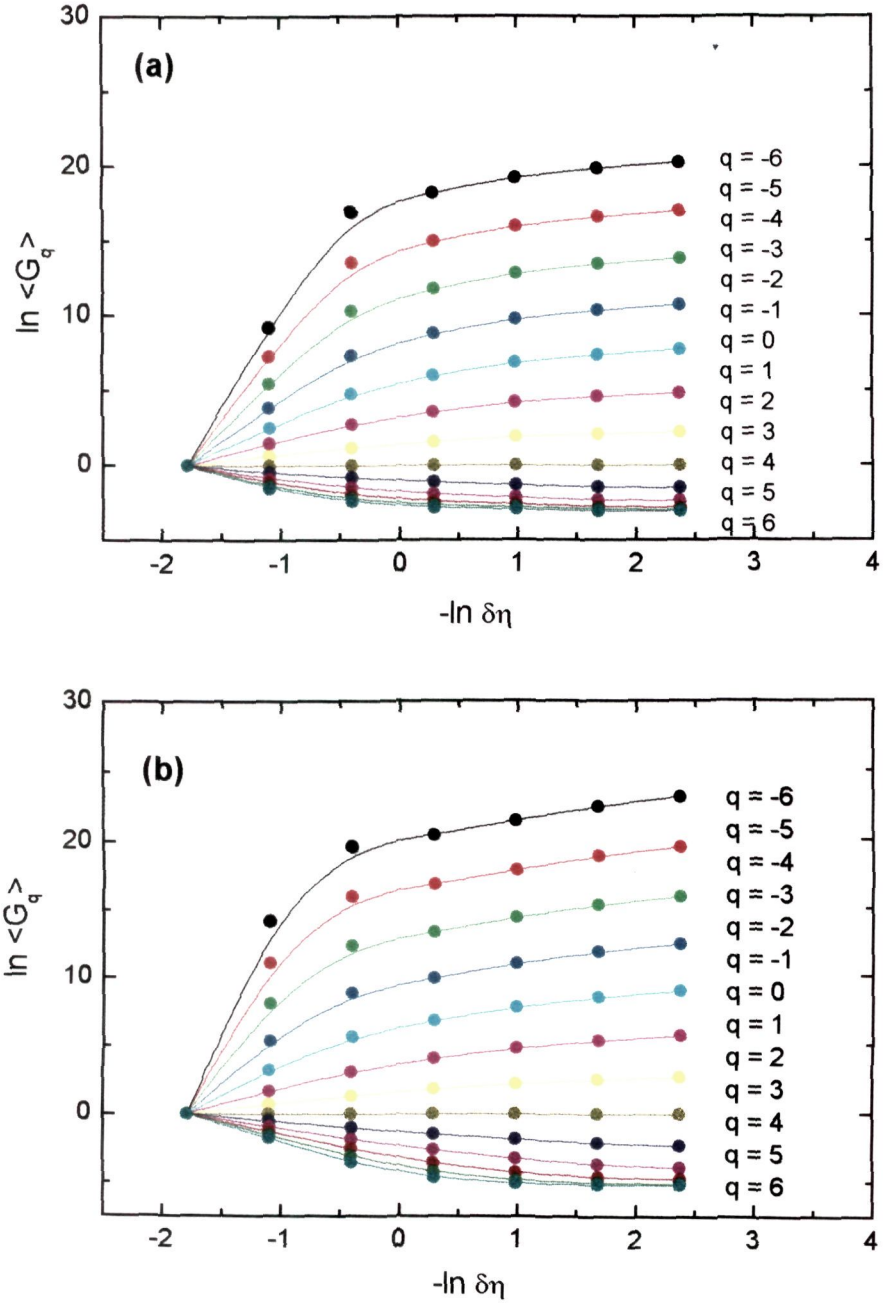

Fig. 4.6 Variations of ln $\langle G_q \rangle$ with -ln $\delta\eta$ for the interactions of 4.5A GeV/c ^{28}Si nuclei with: (a) CNO and (b) AgBr.

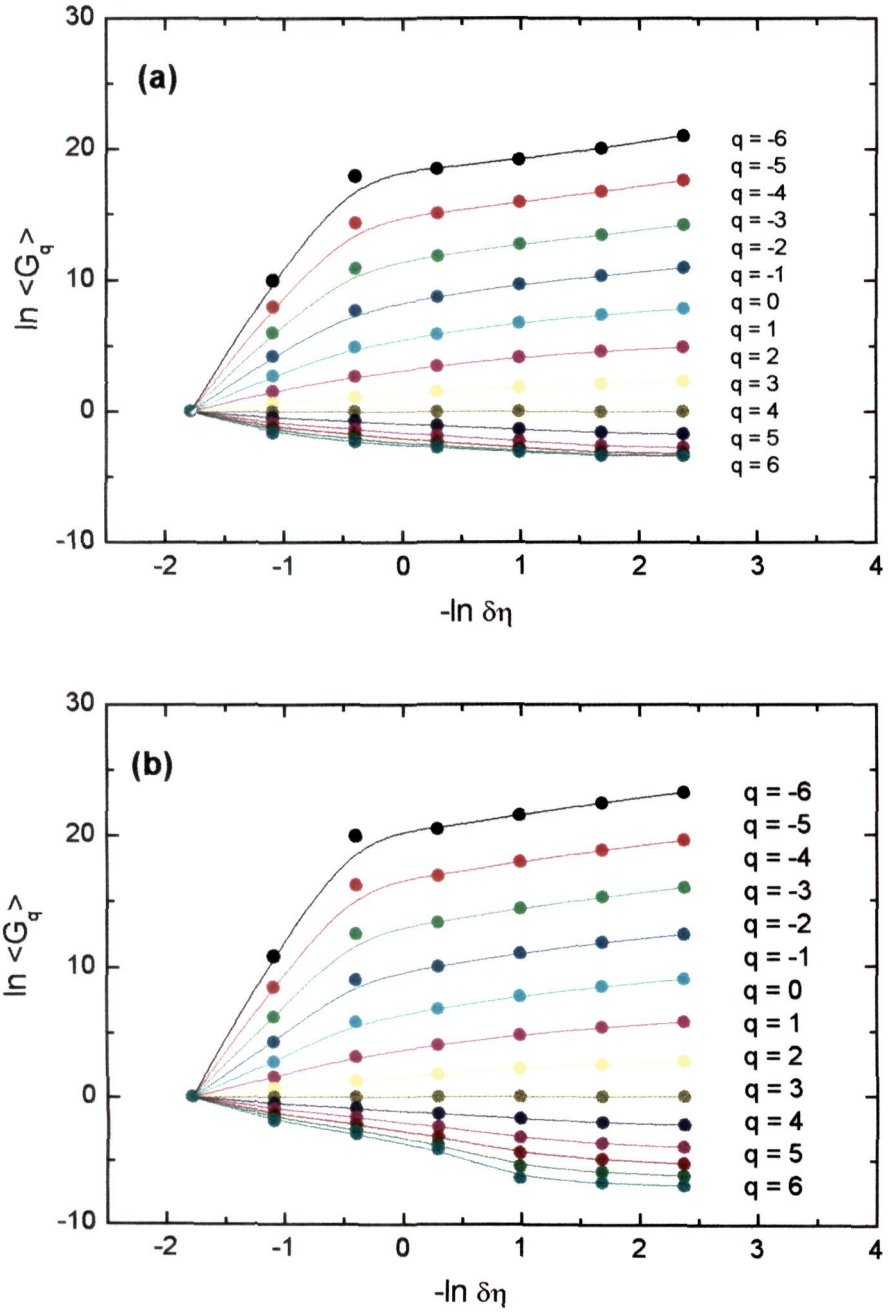

Fig. 4.7 Variations of ln $\langle G_q \rangle$ with -ln $\delta\eta$ for the interactions of 14.5A GeV/c ^{28}Si nuclei with: (a) CNO and (b) AgBr.

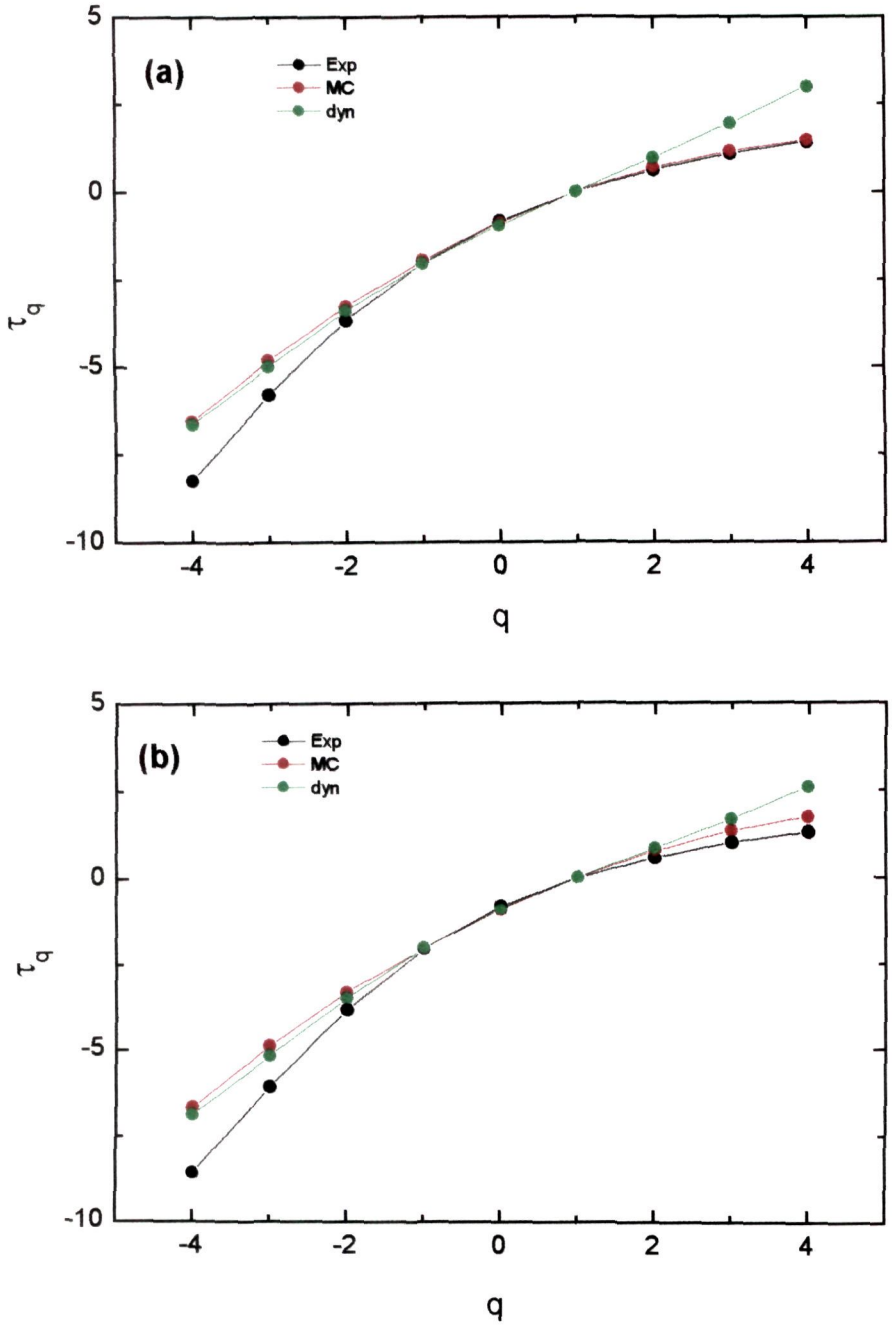

Fig. 4.8 Variations of τ_q with q for ^{28}Si-Em interactions at: (a) 4.5A and (b) 14.5A GeV/c.

Table 4.1. Values of the Mass exponents τ_q for the interactions of 4.5A GeV/c ^{28} Si nuclei with Emulsion, CNO and AgBr.

order of moment (q)	τ_q (Si-Em)	τ_q (Si-CNO)	τ_q (Si-AgBr)
-6	-13.45± 3.19	-12.20±0.62	-14.12±0.36
-5	-10.80± 2.11	-9.74±0.42	-11.46±2.58
-4	-8.23±1.21	-7.47±0.25	-8.85±1.59
-3	-5.79±0.55	-5.26±0.16	-6.35±0.79
-2	-3.65±0.23	-3.42±0.11	-4.06±0.32
-1	-2.00±0.10	-1.94±0.08	-2.24±0.12
0	-0.84±0.04	-0.83±0.05	-0.93±0.03
1	0	0	0
2	0.63±0.02	0.62±0.05	0.73±0.01
3	1.09±0.04	1.08±0.10	1.33±0.01
4	1.43±0.07	1.40±0.16	1.83±0.02
5	1.65±0.11	1.62±0.22	2.23±0.02
6	1.80±0.16	1.77±0.27	2.55±0.01

Incidentally, this observation is in agreement with the predictions of gluon model [32]. Furthermore, τ_q^{dyn} is different from τ_q, indicating the presence of dynamical contribution to the fluctuations. In Fig. 4.9, the observed slope parameters, τ_q, are found to be comparable with the corresponding FRITIOF values.

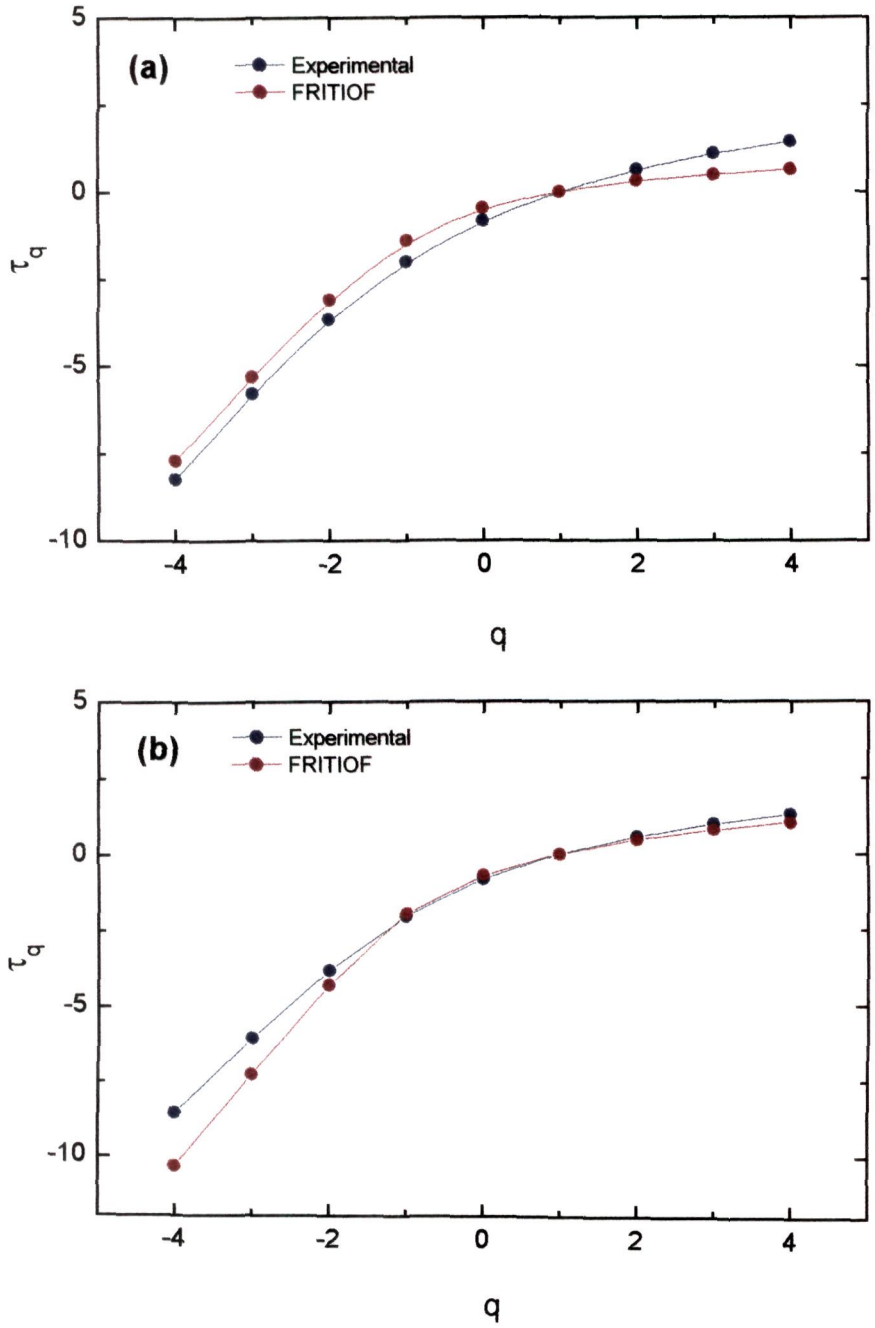

Fig. 4.9 Variations of experimental and FRITIOF values of τ_q with q for ^{28}Si-Em interactions at: (a) 4.5A and (b) 14.5A GeV/c.

Table 4.2. Values of the Mass exponents τ_q for the interactions of 14.5A GeV/c ^{28} Si nuclei with Emulsion, CNO and AgBr.

order of moment (q)	τ_q (Si-Em)	τ_q (Si-CNO)	τ_q (Si-AgBr)
-6	-13.84± 0.63	-12.92±0.86	-14.37±0.73
-5	-11.16± 0.27	-10.32±0.65	-11.67±0.28
-4	-8.55±0.03	-7.84±0.45	-9.03±0.05
-3	-6.07±0.07	-5.52±0.31	-6.48±0.21
-2	-3.84±0.03	-3.50±0.22	-4.16±0.15
-1	-2.05±0.06	-1.91±0.16	-2.24±0.01
0	-0.82±0.06	-0.77±0.09	-0.89±0.04
1	0	0	0
2	0.57±0.08	0.55±0.09	0.64±0.07
3	0.99±0.16	0.96±0.18	1.14±0.15
4	1.29±0.23	1.27±0.27	1.53±0.22
5	1.52±0.29	1.50±0.34	1.85±0.29
6	1.68±0.35	1.67±0.40	2.09±0.35

Fig. 4.10 exhibits τ_q vs q plots for ^{28}Si-Em interactions both at 4.5A and 14.5A GeV energies. It is worthmentioning that the values of τ_q for different q are slightly higher for the lower projectile energy in comparison to those for the higher energy. However, this result is in disagreement with those reported in earlier [31].

For investigating target dependence of the mass exponents, τ_q, its values for the interactions due to CNO and AgBr targets are plotted in Fig. 4.11. For

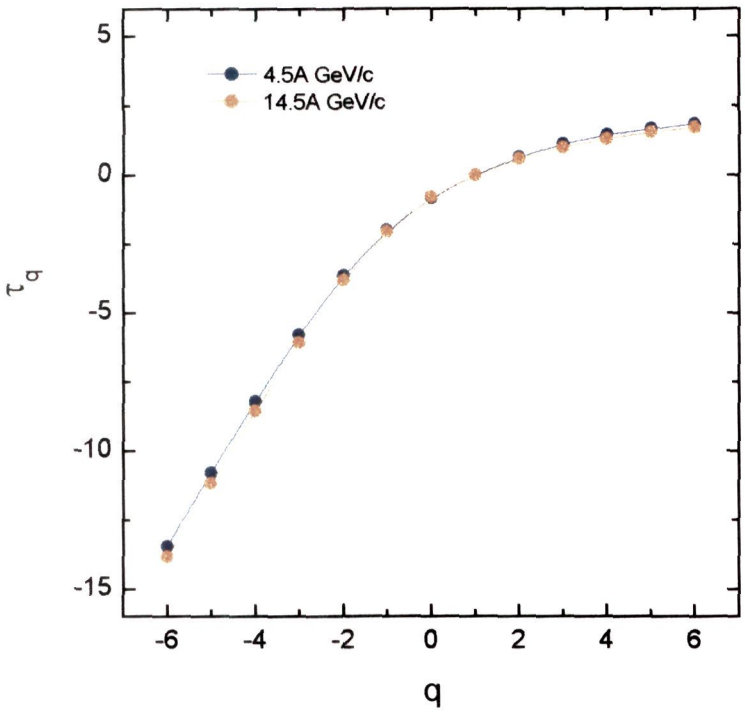

Fig. 4.10 Variations of τ_q with q for ^{28}Si-Em interactions at 4.5A and 14.5A GeV/c.

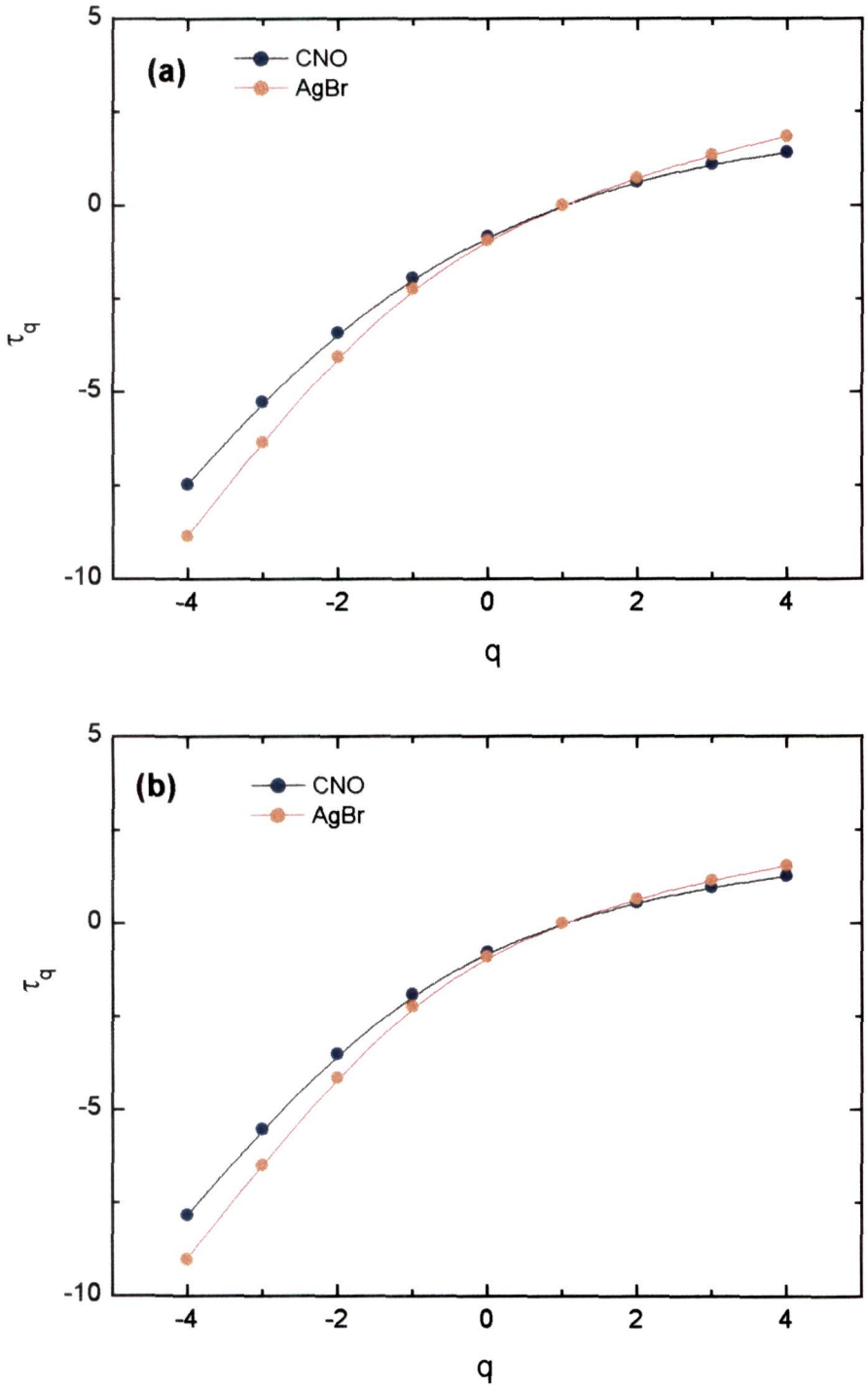

Fig. 4.11 Variations of τ_q with q for the interactions of ^{28}Si nuclei with CNO and AgBr at: (a) 4.5A and (b) 14.5A GeV/c.

$q < 1$, the mass exponents have relatively lower values for the interactions due to AgBr than those for CNO, whereas in the region corresponding to $q > 1$, the opposite trend is observed.

4.4.1.3 Dependence of generalized dimensions on q

Variations of the generalized dimensions, D_q, with the order of the moment, q, for ^{28}Si-Em interactions at the two incident energies are exhibited in Fig. 4.12. For both the energies, generalized dimensions satisfy the multifractality condition, namely, $D_q > D_{q'}$, where $q < q'$. The generalized dimensions are found to be positive for all the orders of the moments q and demonstrate a decreasing trend with increasing q. This behaviour is in excellent agreement with the predictions of multifractal cascade model [35]. It may be noted that D_q turns out to be more than unity for $q \leq -2$, a result in agreement with those reported [31] earlier for different projectiles over a wide range of beam energies It is also noticed in Fig. 4.12 that the generalized dimensions tend to attain lower values for higher projectile energy in the region characterized by $q < 0$, i.e., for negative order moments. However, in the region having $q > 0$, this trend seems to change, but not very significantly.

In order to examine whether there exists any dependence of the generalized dimensions corresponding to a certain order of moment on the target size, D_q vs q plots for the interactions of ^{28}Si nuclei with CNO and AgBr targets are plotted in Fig. 4.13. The generalized dimensions have higher values for the

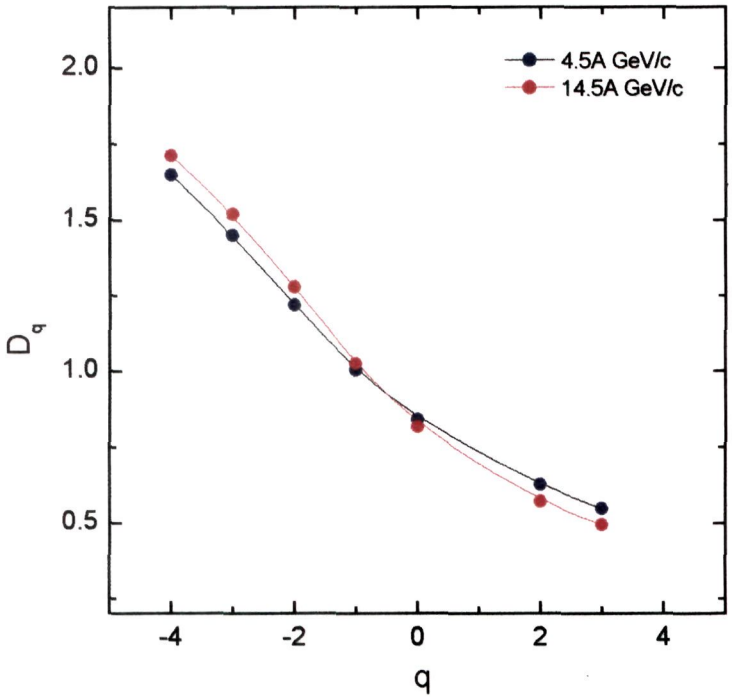

Fig. 4.12 Variations of D_q with q for ^{28}Si-Em interactions at 4.5A and 14.5A GeV/c.

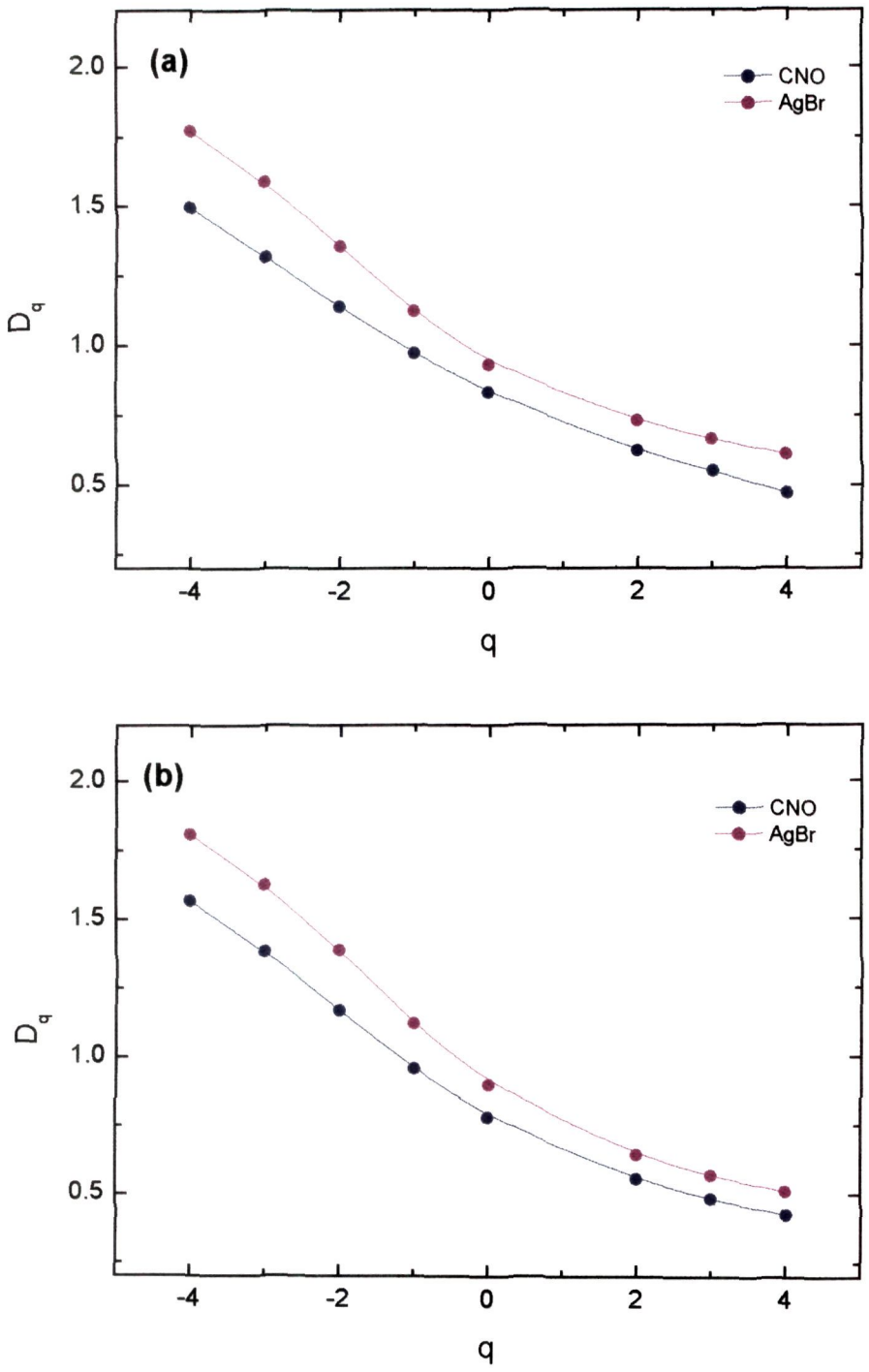

Fig. 4.13 Variations of D_q with q for the interactions of ^{28}Si nuclei with CNO and AgBr at: (a) 4.5A and (b) 14.5A GeV/c.

interactions due to heavier targets for each order of the moment although the effect appears to be rather more pronounced for the situation corresponding to $q < 0$. One of the reasons for the higher values of the generalized dimensions for the interactions due to heavier targets may be attributed to increase in the average multiplicity with increasing target mass [34].

Study of generalized dimensions, D_q, plays a significant role in the fractal analysis. The set of generalized dimensions D_0, D_1 and D_2 corresponding to $q = 0$, $q = 1$ and $q = 2$ respectively, are determined and listed in Table 4.3. These generalized dimensions are regarded to be very sensitive to the dynamics of particle production [27].

Table 4.3 Values of the generalized dimensions D_0, D_1, D_2 for various types of collisions.

Interaction type	Energy (GeV)	D_0	D_1	D_2
Si-Em	4.5A	0.90	0.66	0.60
Si-Em	14.5A	0.92	0.71	0.71
Si-CNO	4.5A	0.91	0.71	0.71
Si-CNO	14.5A	0.94	0.72	0.72
Si-AgBr	4.5A	0.99	0.73	0.73
Si-AgBr	14.5A	0.97	0.77	0.77

4.4.1.4 Dependence of $f(\alpha_q)$ on α_q

Fig. 4.14 shows the variation of the spectral function, $f(\alpha_q)$, with the Lipschitz-Holder exponents, α_q, for 4.5A and 14.5A GeV/c ^{28}Si-Em interac-

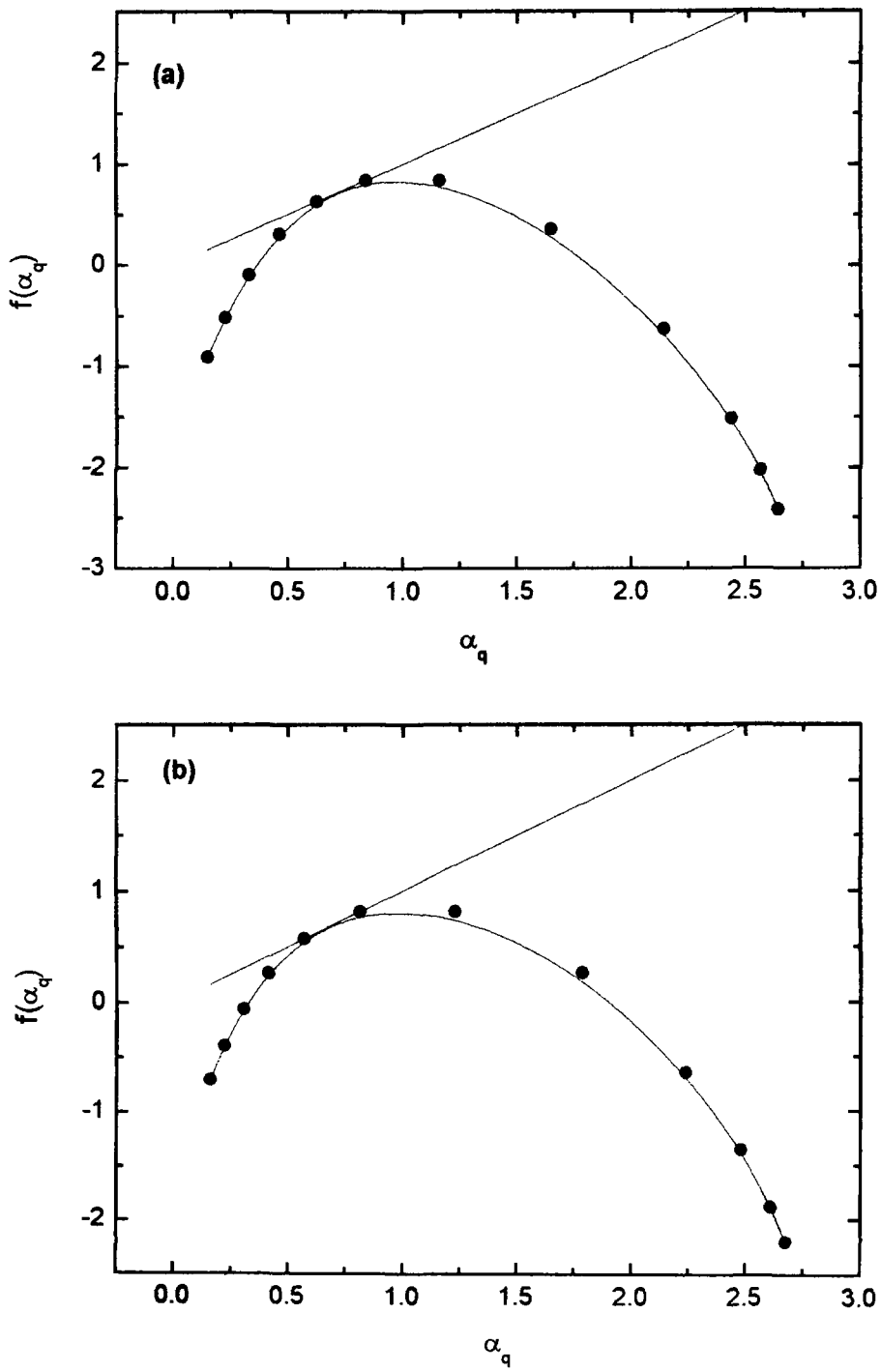

Fig. 4.14 Variations of $f(\alpha_q)$ with q for ^{28}Si-Em interactions at: (a) 4.5A and (b) 14.5A GeV/c.

tions. The spectra are concave downwards centered around α_q corresponding to q = 0 and a common tangent at an angle of $\sim 45^\circ$. This observation agrees fairly well with the predictions of gluon model [15]. However, $f(\alpha_q)$ is not peaked in any of the cases studied which is an indication of non-smooth nature of the multiplicity distribution of the particles produced in the interactions considered in the present study. The left wings (q > 0) of the spectra are sensitive to the peaks whilst the right wings (q < 0) belong to the valleys in their respective pseudorapidity distributions.

Figs. 4.15 and 4.16 represent $f(\alpha_q)$ versus α_q plots for the Monte Carlo and FRITIOF generated data samples. The widths of the multifractal spectra for experimental data sample are relatively wider than those for the simulated data sets, which in turn would mean that $f(\alpha_q)^{dyn}$ has a width characteristic of the non-statistical fluctuations.

Fig. 4.17 shows $f(\alpha_q)$ spectra for ^{28}Si-Em interactions at 4.5A and 14.5A GeV/c plotted for examining the effect of the projectile energy on the shape of the spectra; the spectra at the two energies are nearly similar in the left wings. However, in the right wing corresponding to q < 0, the spectrum for the higher energy tends to broaden.

For investigating whether $f(\alpha_q)$ spectra depend on target mass, the spectra for the interactions of ^{28}Si nuclei with CNO and AgBr targets are plotted in Fig. 4.18 for both the energies. It is observed that for the interactions due to AgBr targets the spectra have larger widths in comparison to the spectra for

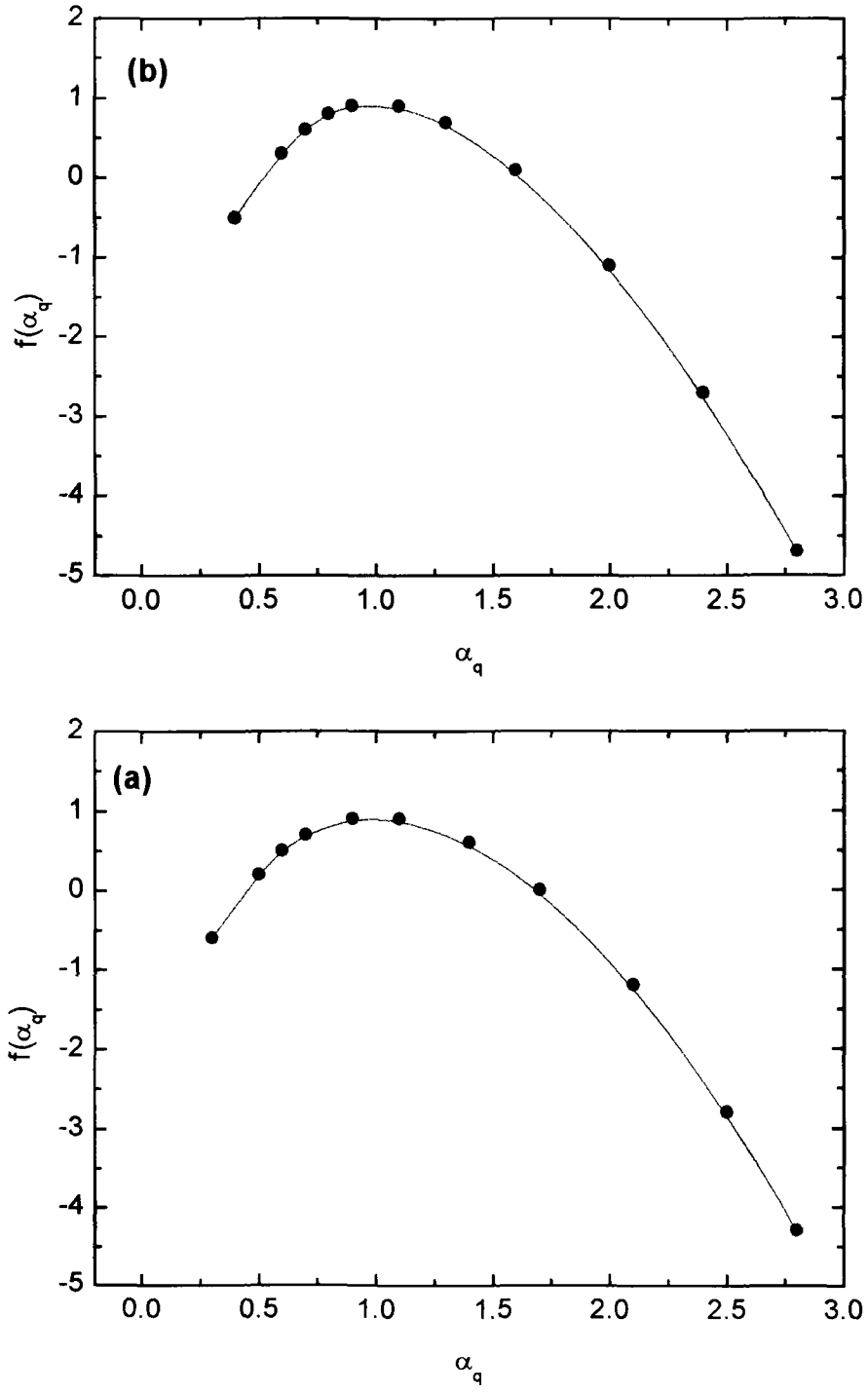

Fig. 4.15 Variations of $f(\alpha_q)$ with α_q for the Monte Carlo generated data on ^{28}Si-Em interactions at: (a) 4.5A and (b) 14.5A GeV/c.

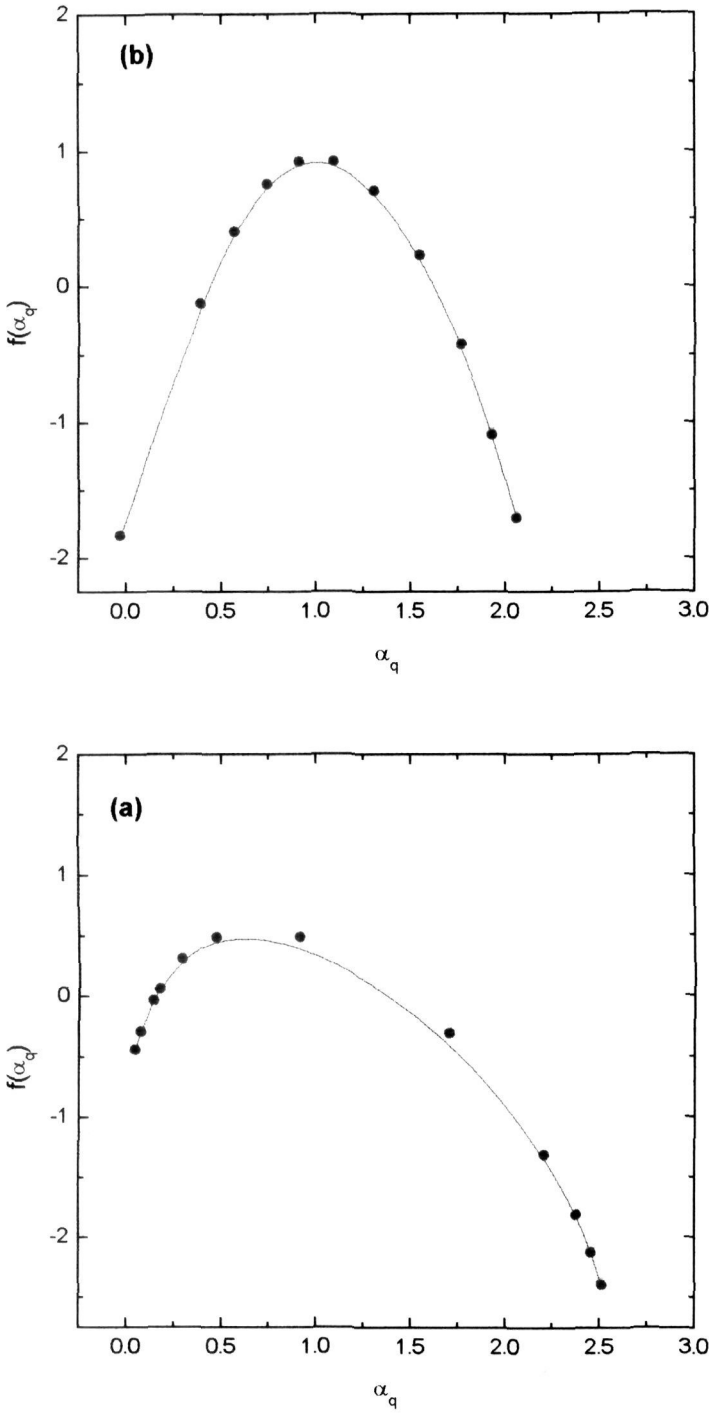

Fig. 4.16 Variations of $f(\alpha_q)$ with α_q for the FRITIOF generated data on ^{28}Si-Em interactions at: (a) 4.5A and (b) 14.5A GeV/c.

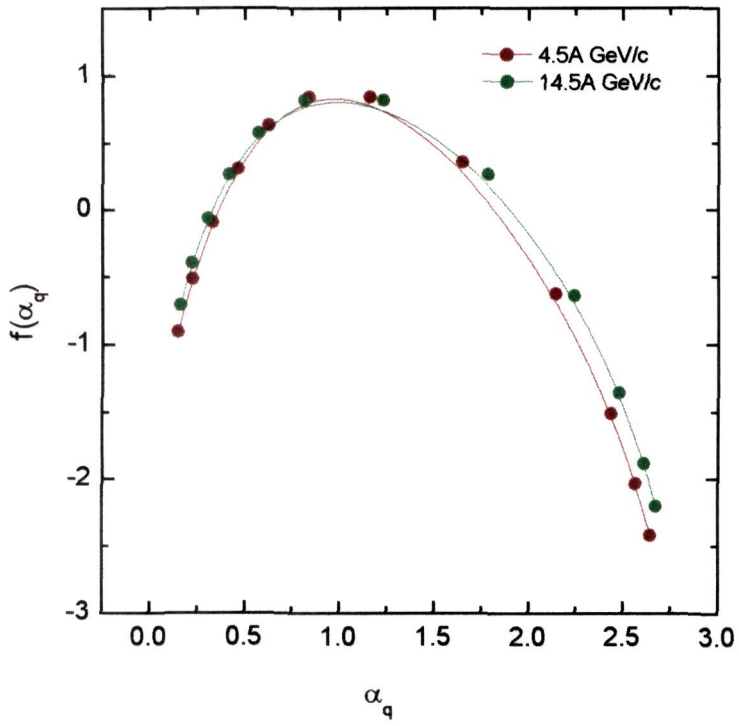

Fig. 4.17 Variations of $f(\alpha_q)$ with α_q for ^{28}Si-Em interactions at 4.5A and 14.5A GeV/c.

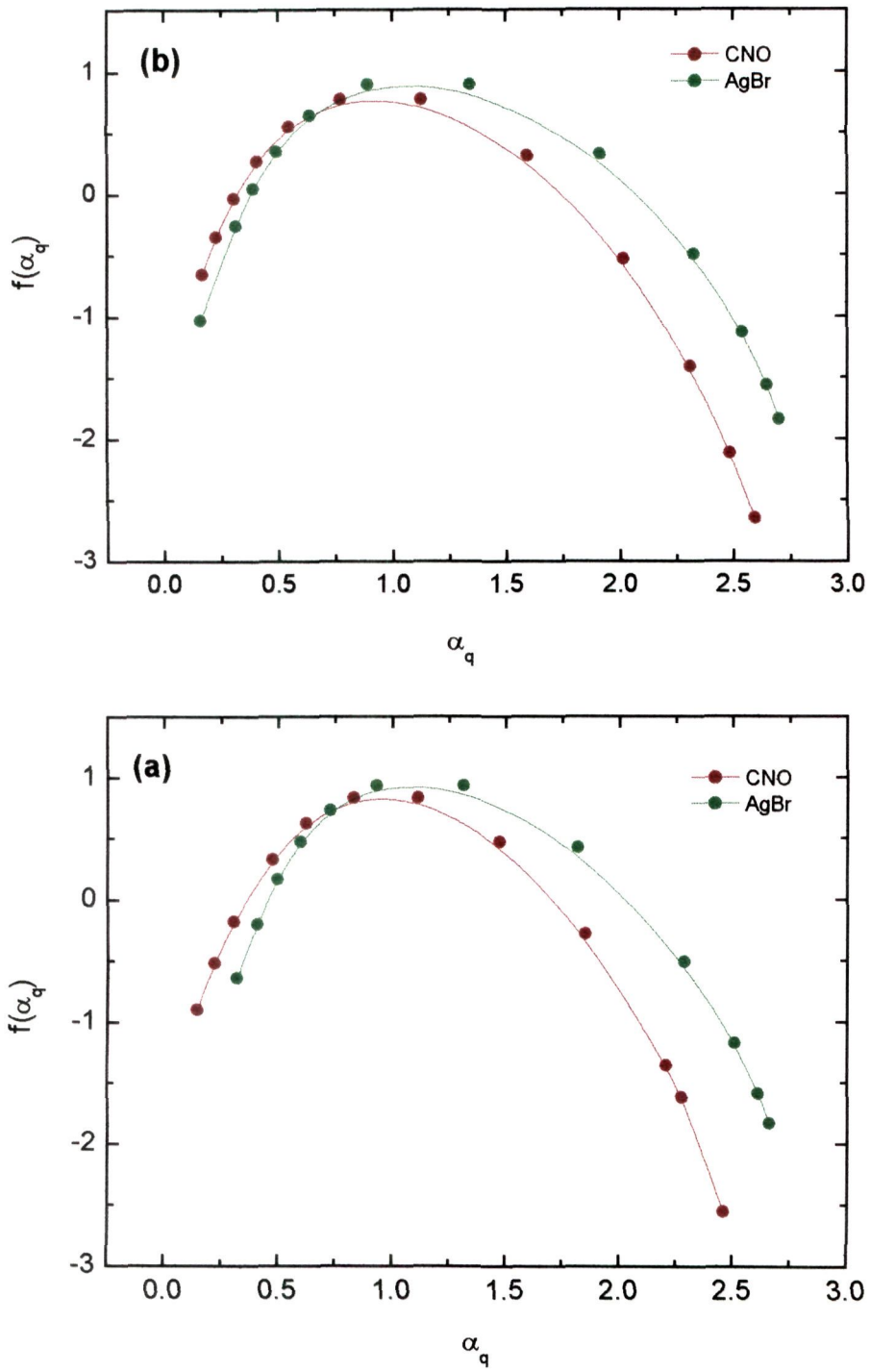

Fig. 4.18 Variations of $f(\alpha_q)$ with α_q for the interactions of ^{28}Si nuclei with CNO and AgBr at: (a) 4.5A and (b) 14.5A GeV/c.

the interactions due to lighter (CNO) targets . It may further be noted that the contribution to the broadening of the width of the spectra with increasing target mass comes mainly from the regions corresponding to $q < 0$. This observation is in disagreement with those reported earlier [34]. However, all the spectra are wide enough to indicate the occurrence of multifractality for the interactions considered.

4.4.2 Modified G_q moments

The G_q moments, discussed in the preceding section, provide a better approach than the usual scaled factorial moments for examining multifractal structure. This is due to the fact that for studying G_q moments one does not take into account the spikes in pseudorapidity distributions only but also include the non-empty valleys which occur in the region characterized by $q < 0$. However, these moments saturate in the limit $\delta\eta \longrightarrow 0$, where the particle multiplicity in the non-empty bins approaches unity and it becomes difficult to separate the statistical contribution to the fluctuations [25,37]. Recently, R. C. Hwa [38] has re-defined the G_q moments as G_q^m and it is written as:

$$G_q^m = \sum_{j=1}^{m} p_j^q \, \theta(n_j - q) \tag{4.17}$$

where θ is the usual step function equal to 1 for $n_j \geq q$ and 0 otherwise. Thus, the moments corresponding only to the values of q being positive integers are considered. The θ function plays a significant role in modifying the ordinary G_q moments, particularly in the cases where particle multiplicity is relatively

small. However, for very large multiplicities, n/M $\gg$ q, G_q and G_q^m moments tend to become identical.

4.4.2.1 Variation of ln $< G_q^m >$ with ln M

Variations of ln $< G_q^m >$ with ln M for 4.5A and 14.5A GeV/c ^{28}Si-Em collisions are displayed in Figs. 4.19 and 4.20. The log-log plots between $< G_q^m >$ and M exhibit a linear behaviour, verifying thereby the following power law:

$$< G_q^m > \propto (M)^{\tau_q^m} \tag{4.18}$$

The statistical contributions to $< G_q^m >$ moments are determined using the simulated data sets, MC-4.5 and MC-14.5. Variations of ln $< G_q^m >$ with ln M for these data sets are also displayed in Figs. 4.19 and 4.20 by the dotted curves. The values of $< G_q >^{stat}$ are observed to be much smaller than the values of $< G_q^m >$, particularly in the region corresponding to higher values of q,that is, q $\geq$ 4. These observations are, thus, in reasonable agreement with those reported earlier [38]; all the quantities involved in the study of multiplicity fluctuations are calculated using Monte Carlo code (ECCO) based on geometrical branching model [38]. It is worthmentioning that for q > 1, the linear dependence of ln $< G_q^m >$ on ln M has been observed in μ-p, $\bar{p}$-p and e^+-e^- interactions[39,40].

The dynamical component of $< G_q^m >$ is expressed [25] as:

$$< G_q >^{dyn} = \frac{< G_q^m >}{< G_q >^{stat}} M^{1-q} \tag{4.19}$$

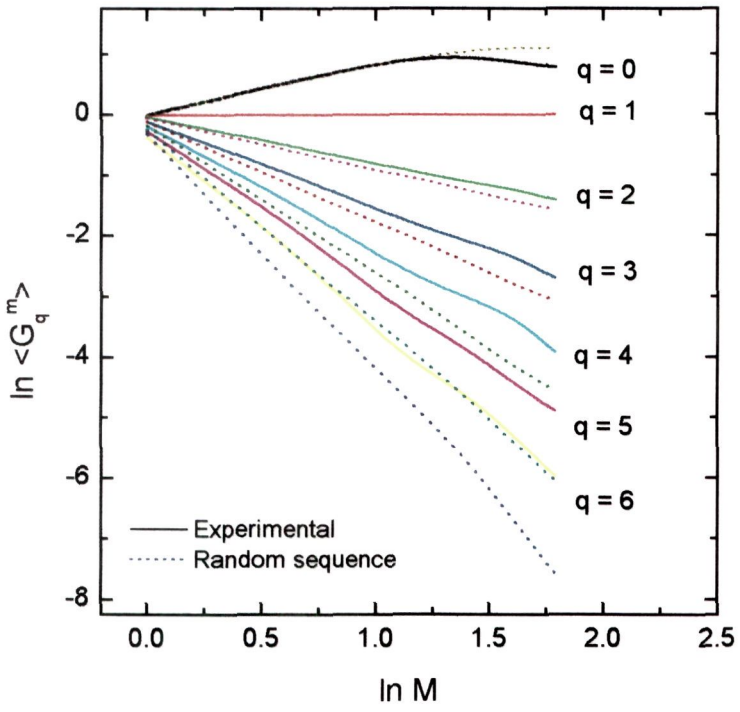

Fig. 4.19 Variation of ln $\langle G_q^m \rangle$ with ln M for 4.5A GeV/c ^{28}Si-Em interactions.

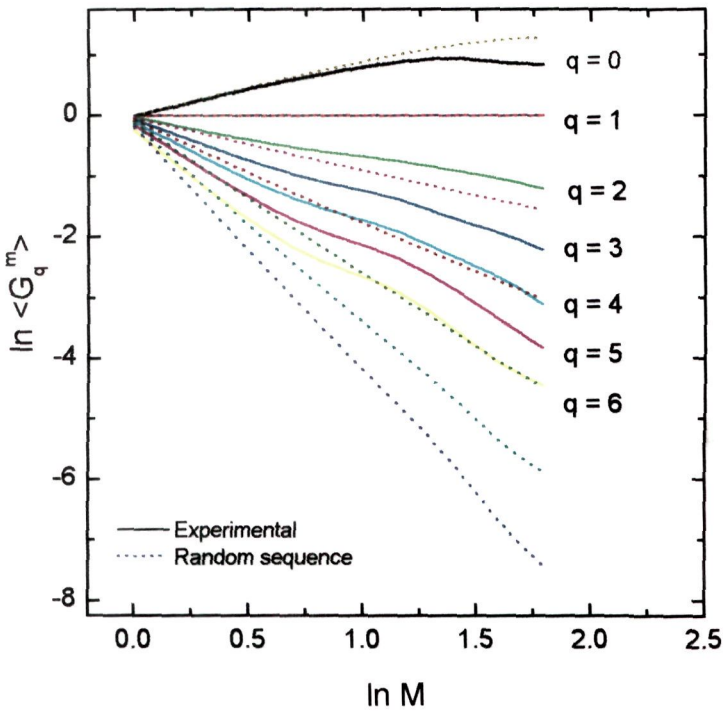

Fig. 4.20 Variation of ln $\langle G_q^m \rangle$ with ln M for 14.5A GeV/c ^{28}Si-Em interactions.

It is, therefore, evident that if $< G_q^m >$ is purely statistical, then $< G_q >^{dyn}$ should vary as M^{1-q}, thereby indicating the involvement of trivial dynamics.

4.4.2.2 Mass exponents

Eq 4.19 indicates the presence of dynamical component of $< G_q^m >$ if $< G_q >^{dyn}$ does not vary as M^{1-q}. This, in turn, would suggest that larger the dynamical contribution, greater will be the deviation in the values of τ_q^m from the line corresponding to $\tau_q^m = q - 1$

Fig. 4.21 shows the variations of τ_q^m, τ_q^{stat}, τ_q^{dyn} with q; τ_q^{dyn} is calculated using the following relationship:

$$\tau_q^{dyn} = \tau_q^m - \tau_q^{stat} + q - 1 \tag{4.20}$$

It is observed that τ_q^{dyn} shows a clear deviation from $q - 1$, thus indicating the presence of dynamical component of fluctuations.

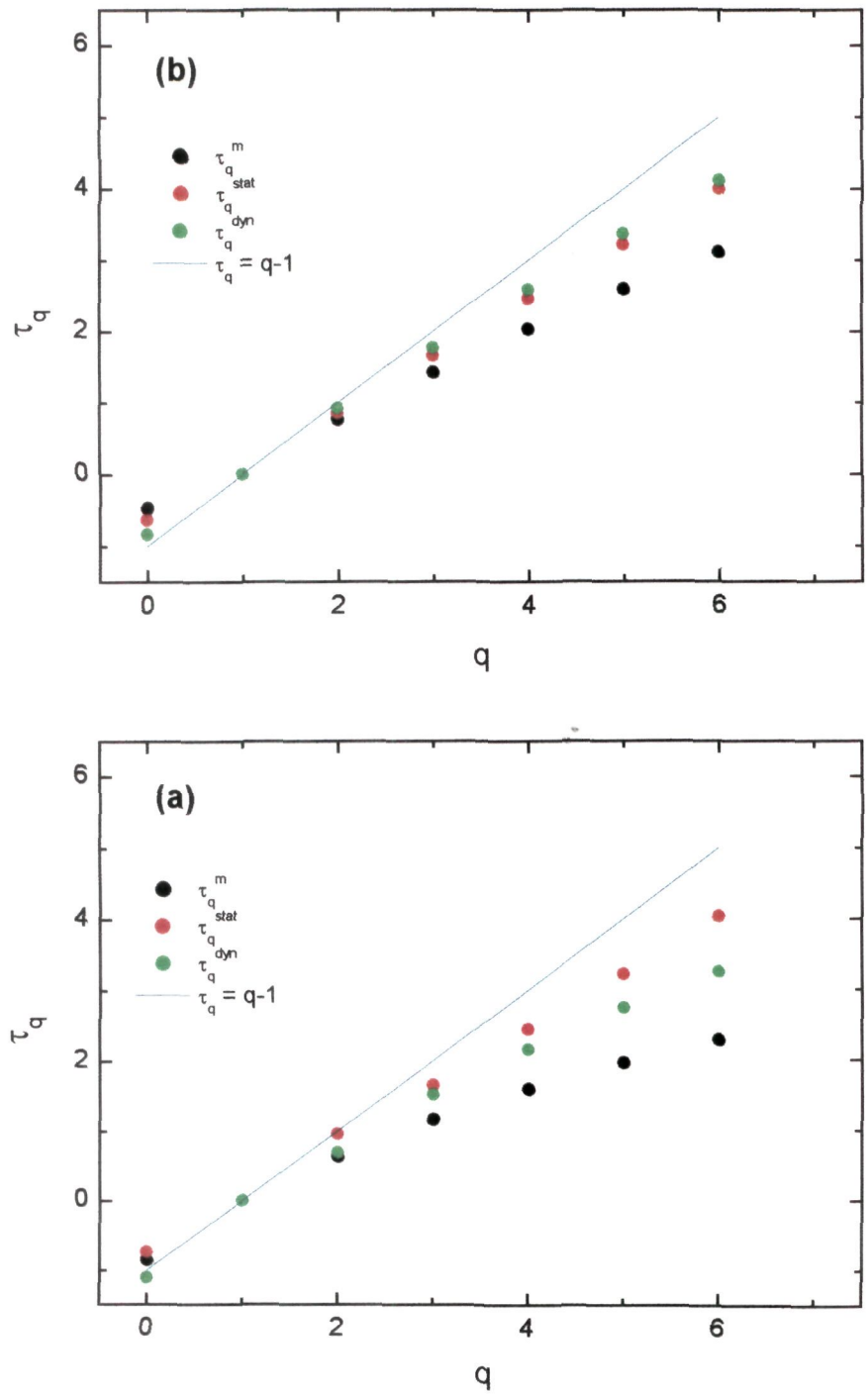

Fig. 4.21. Variations of τ_q^{m}, τ_q^{stat} and τ_q^{dyn} with q for ^{28}Si-Em interactions at: (a) 4.5A and (b) 14.5A GeV/c

References

1. K. Kajantie and L. Mclarran *Phys. Lett.* **B119** (1982) 203.
2. J. D. Bjorken, *Phys. Rev.* **D27** (1983) 140.
3. E. V. Shuryak, *Phys. Rep.* **115** (1984) 152.
4. J. Cleymans, R. V. Gavai and E. Suhanen *Phys. Rep.* **130** (1986) 218.
5. B. Muller, *Rep. Prog. Phys.*, **58**, (1995) 611; S. A. Bass et al, *hep-ph/9810281* (1998), J. P. Blaizot,*Nucl. Phys.* **A661** (1999) 36; C. P. Singh, *Phys. Rep.* **236** (1993) 147; Quark-Gluon Plasma signatures edited by V. Bernard et al, (*Editions Frontiers, Paris, 1990*); Quark-Gluon Plasma, edited by R. C. Hwa, (*World Scientific, Singapore, 1991*)
6. T. H. Burnett et al (JACEE Collaboration) *Phys. Rev. Lett.* **50** (1983) 2062.
7. L. Van Hove, *Z. Phys.* **C21** (1984) 93.
8. M. Gyulassy et al, *Nucl. Phys.* **B237** (1984) 477.
9. G. Paladin, A. Vulpiani, *Phys. Rep.* **56** (1987) 147.
10. A. Bialas and R. Peschanski, *Nucl. Phys.* **B273** (1986) 703.
11. T. Bohr and M. Jenson, *Phys. Rev.* **A36** (1987) 4904.
12. P. Szepfalusy et al *Phys. Rev.* **A36** (1987) 3525.
13. A. Bialas and R. C. Hwa, *Phys. Lett.* **B253** (1991) 3525.
14. *Fluctuations and Fractal Structure*, edited by R.C. Hwa, (World Scientific, Singapore 1992)
15. R. C. Hwa, Phys. Rev. **D41** (1990) 1456.
16. B. Mandelbrot, *The Fractal Geometry of Nature*, (Freeman New York, 1982)
17. R. C. Hwa, *Quark-Gluon Plasma*, Edited by R. C. Hwa (World Scientific, 1990)
18. T. T'el, Z. Naturforsch, **43a**, (1988) 1154.
19. T.C. Halsey, M. H. Jenson, L.P. Kadanoff, I. Procaccia and B. I. Shraiman, *Phys. Rev.* **A33**, (1986) 1141.

20. T.C. Halsey, M. H. Jenson, *Physica*, **D23**, (1986) 112.

21. J Feder, *Fractals*, (Plenum Press, New York, 1988)

22. C. B. Chiu and R. C. Hwa,*Phys. Rev.*, **D43**, (1991) 100.

23. E. A. De Wolf, I. M. Dremin and W. Kittel, *Phys. Rep.*, **270**, (1996), 1.

24. P. Grassberger and I. Procaccia , *Physica*, **D3**, (1984) 34.

25. C. B. Chiu, K. Fialkowski and R. C. Hwa, *Mod. Phys. Lett.*, **A5**, (1990) 2651.

26. Dipak Ghosh et al, *Phys. Rev.*, **D46** (1992) 3712.

27. H. G. E. Hentdchel and I. Procaccia ,*Physica*, **D8**, (1983) 435.

28. N. Prashar, *IL Nuovo Cim.*, **108A**, (1995) 489.

29 P. Carruthers, *Int J. Mod. Phys.*,**A4**, (1989) 5587.

30. P. Grassberger and I. Procaccia ,*Phys. Rev. Lett.* **50** (1983) 346.

31 P. L. Jain, G. Singh and A. Mukhopadhyay,*Phys. Rev.*, **C46** (1992) 721.

32. R. K. Shivpuri and Neeti Prashar,*Phys. Rev.*, **D49**, (1994) 219.

33. Dipak Ghosh et al, *Phys. Lett.*, **B272**, (1991) 5.

34. R. K. Shivpuri and V. K. Verma, *Phys. Rev.*, **D47**, (1993) 123.

35. C. Meneveau and K. R. Srinivasan, *Phys. Rev. Lett.* **59**, (1987) 1424.

36 R Peschanski and R. C. Hwa, *Nucl. Phys.*, **327**, (1989) 144.

37 D. Seibert, *Phys. Lett.*, **B254**, (1991) 253.

38. R. C. Hwa and J. C. Pan, *Phys. Rev.*, **D45** (1992) 1476.

39. I. Derado, R. C. Hwa, G. Jensco and N. Schmitz (EMC), *Phys. Lett.*, **B283**, (1992) 865.

40. G Boca et al (IHSC), *IL Nuovo Cim.*, **105A**, (1992) 865.

CHAPTER V

FLUCTUATIONS IN RAPIDITY DENSITY AND RAPIDITY SPACING SPECTRA

5.1 Introduction

The dynamics of multiparticle production in relativistic nucleus-nucleus collisions is considered to be rather complex and is the least understood in comparison to those involved in hadron-hadron and hadron-nucleus interactions at high energies due to the fact that the number of participating nucleons is believed to play an important role [1]. In a central ^{16}O-Ag collision this number is predicted [1] to be around 70, while only few nucleons may be involved in a peripheral collision. If in a nucleon-nucleon collision inside a nucleus, final state particles are produced instantaneously; all these particles have a fair chance of re-interacting with the nuclear medium. On the other hand, if the formation time is long, that is, longer than the nuclear distances, the energy carried by the incident hadron would continue as a unit while passing through the target. These two pictures of collisions, thus, predict different values of multiplicities of the emitted particles. By studying the various emission characteristics of the produced particles and comparing these with the corresponding values predicted by different models, important conclusions regarding the mechanism of production of these particles may be drawn.

The produced particles are envisaged to be strongly correlated [2,3]. The

observed correlation is expected on theoretical grounds [4] as well due to the production of hot hadronic matter, resonances or quark-gluon plasma. The observation of intermittent behaviour in multiplicity distributions [5,6] have also been interpreted as a possible manifestation of short-range correlations [7,8]. Although these correlations have been extensively studied [1,5,6,9] at different energies, yet no final remarks have been made. It has been suggested to adopt some new approach for a clear and better understanding of the occurrence of fluctuations and correlations in relativistic nucleus-nucleus collisions. Furthermore, even if the required extreme conditions of high temperature and high energy density for QGP formation are achieved, QGP will not be produced in all the events. For selecting the QGP events, a certain analysis on event-by-event basis should, therefore, be carried out. One of the simplest and most useful methods for studying correlations is the study of the maximum density fluctuations in relatively narrow rapidity bins. An attempt is, therefore, made to investigate various features of the maximum charged particle density distributions in 4.5A and 14.5A GeV/c ^{28}Si-nucleus collisions. In order to extract the dynamical contribution to the observed fluctuations, correlation free Monte Carlo events are simulated and analysed. The analytical formalism relating to this approach and the experimental results are presented in Section 5.2.

It has been suggested [10] that the geometry of the nuclear collisions and the number of participating nucleons play a significant role in particle production process resulting in relatively larger fluctuations and random emission.

It is expected that future experiments involving heavier nuclei at sufficiently higher energies, random emission of particles may dominate due to geometrical fluctuations and intranuclear rescattering. Information regarding correlations and random emission of secondary particles may be gleaned in terms of the nearest neighbour spacing spectra of the produced relativistic charged particles. This aspect has been examined in detail for the experimental and the simulated data sets and the results are presented in Section 5.3.

5.2 Maximum density fluctuations

5.2.1 Method of analysis

For investigating various characteristics of maximum particle density distribution in the pseudorapidity space, η distribution of relativistic charged particles for a fixed rapidity interval, $\Delta\eta$, over the entire η–range is plotted for each event and the number of relativistic charged particles in each η-bin of width $\Delta\eta$ is counted and the particle density, $\rho = \frac{\Delta n}{\Delta\eta}$, in each η-bin is calculated. Thus, the maximum particle density, ρ_{max}, for each event is determined. By examining the various features of ρ_{max}, for example, its variation with the total rapidity, $< Y_{tot} >$, of the event, relativistic charged particle multiplicity of the event, n_s, and the distribution of $\frac{dN}{d\rho_{max}}$ as a function of ρ_{max}, presence of fluctuations in each event may be looked into. It is worthmentioning that using a similar approach, events having very high local density have been identified by NA22 collaboration [6].

For examining whether the observed fluctuations are of non-statistical nature, the experimental results are compared with the results obtained using the Monte Carlo (MC) simulated data.

5.2.2 Results and discussion

Variations of $< \rho_{max} >$ with $< Y_{tot} >$ for various values of pseudorapidity window, $\Delta\eta$, for 4.5A and 14.5A GeV/c ^{28}Si-nucleus interactions are exhibited in Fig. 5.1: $< Y_{tot} >$ denotes the average value of Y_{tot} in the interval of 1 and Y_{tot} is the total rapidity which is calculated using $Y_{tot} = 2\sum_{i=1}^{n_s} \eta_i/n_s$, where n_s represents the number of relativistic charged particles in a collision. It may be noticed in the figure that value of $< \rho_{max} >$ decreases exponentially with $< Y_{tot} >$ for the two data sets for various $\Delta\eta$ values. Furthermore, the value of $< \rho_{max} >$ is found to be relatively larger for the data on the higher beam energy. However, for $< Y_{tot} > \geq 10$, $< \rho_{max} >$ turns out to be essentially energy independent.

The curves in the figures represent the best fits to the data satisfying the following relationship:

$$< \rho_{max} >= a + be^{-(<Y_{tot}>-Y_0)/d} \qquad (5.1)$$

where Y_0 is the minimum experimental value of Y_{tot} used for obtaining the best fits. The values of the constants a, b and d and χ^2/D.F. obtained for each fit are listed in Table 5.1.

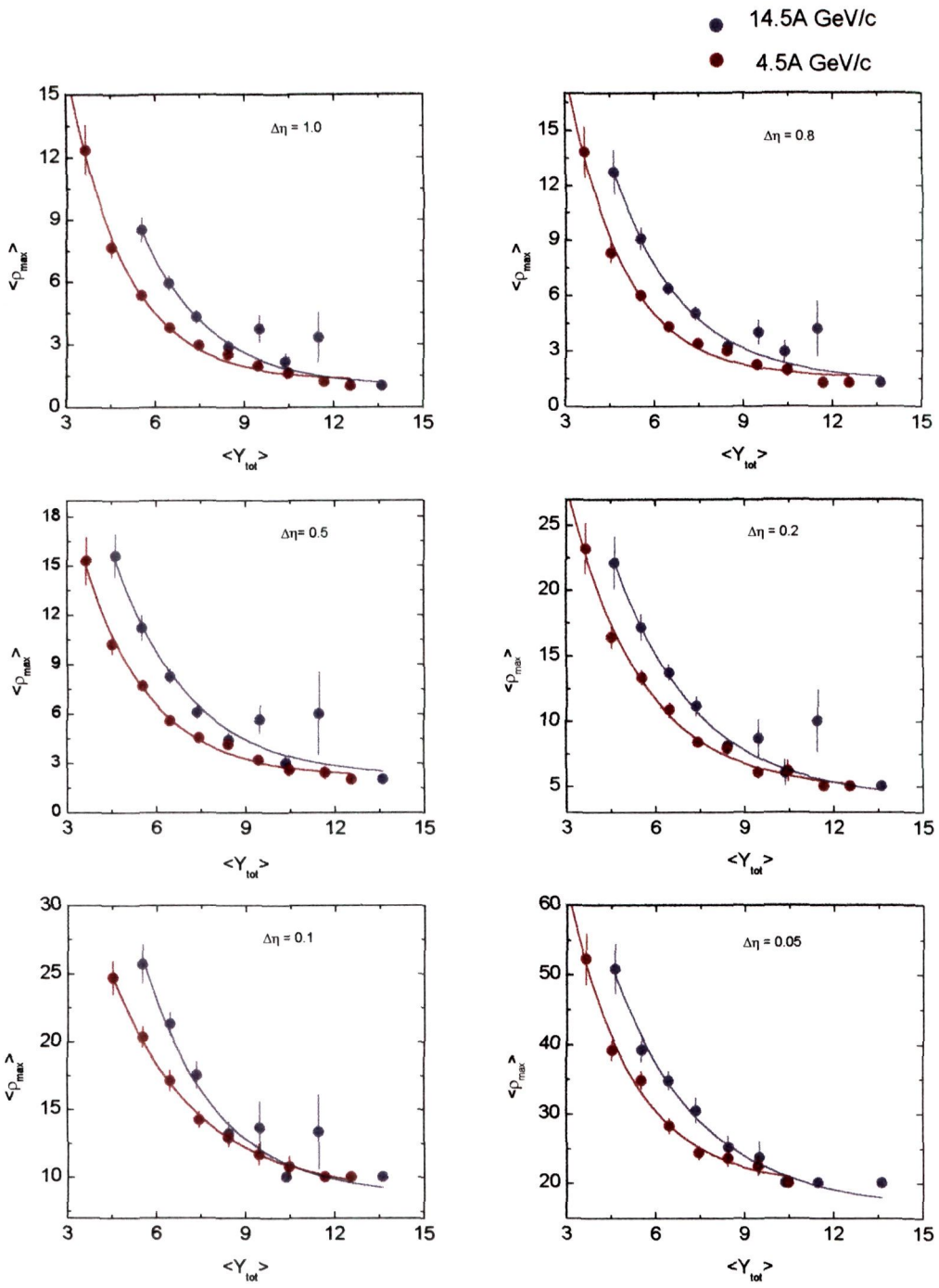

Fig.5.1 Variations of $<\rho_{max}>$ with average total pseudorapidity $<Y_{tot}>$ for 4.5A and 14.5A GeV/c ^{28}Si-Em interactions.

Table 5.1. Values of the constants a, b and d appearing in Eq. 5.1 and χ^2/D.F. for each fit.

Interaction type/ beam energy	$\Delta\ \eta$	a	b	d	χ^2 /D.F
	1.0	1.25±0.19	18.76±0.91	1.93±0.14	0.05
Si-Em	0.8	1.51±0.27	20.88±1.33	1.89±0.18	0.19
4.5A GeV	0.5	2.13±0.25	12.87±0.36	2.48±0.16	0.13
	0.2	4.63±0.45	27.70±1.18	2.49±0.21	0.16
	0.1	8.81±0.25	15.99±0.26	2.86±0.13	0.04
	0.05	19.41±1.46	52.00±3.43	2.20±0.30	1.78
	1.0	0.95±0.27	7.52 ±0.30	2.27±0.23	0.05
Si-Em	0.8	1.33±0.41	11.34±0.25	2.34±0.49	0.16
14.5A GeV	0.5	2.15±0.98	13.22±1.12	2.48±0.56	0.85
	0.2	3.96±0.51	18.22±0.36	2.78±0.16	0.30
	0.1	8.60±1.26	17.55±0.54	2.43±0.21	1.04
	0.05	10.27±3.12	33.74±1.39	2.92±0.49	1.84

Distributions of $\frac{dN}{d\rho_{max}}$ as a function of ρ_{max} for various $\Delta\eta$ values are displayed in Figs. 5.2 and 5.3 respectively for the interactions of 4.5A and 14.5A GeV/c ^{28}Si nuclei with emulsion. These figures also exhibit similar distributions for the MC generated events. It may be seen in these figures that the distributions tend to become wider and have longer tails with decreasing bin widths, $\Delta\eta$, for both the incident energies. Although the experimental distributions and the distributions for the simulated data are observed to have

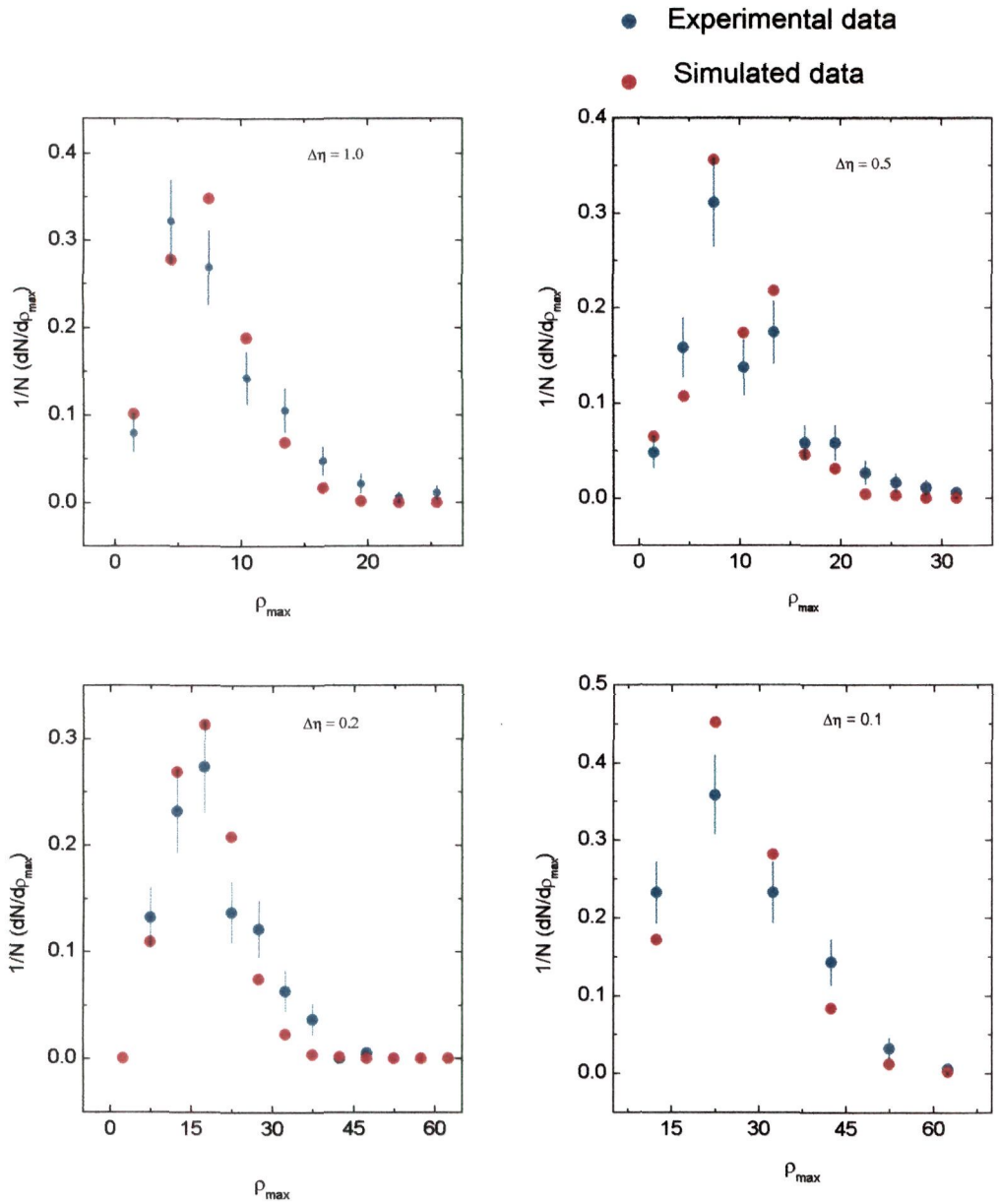

Fig. 5.2 Distributions of $1/N\ (dN/d\rho_{max})$ as a function of maximum particle density ρ_{max} for 4.5A GeV/c ^{28}Si-Em interactions and the simulated data.

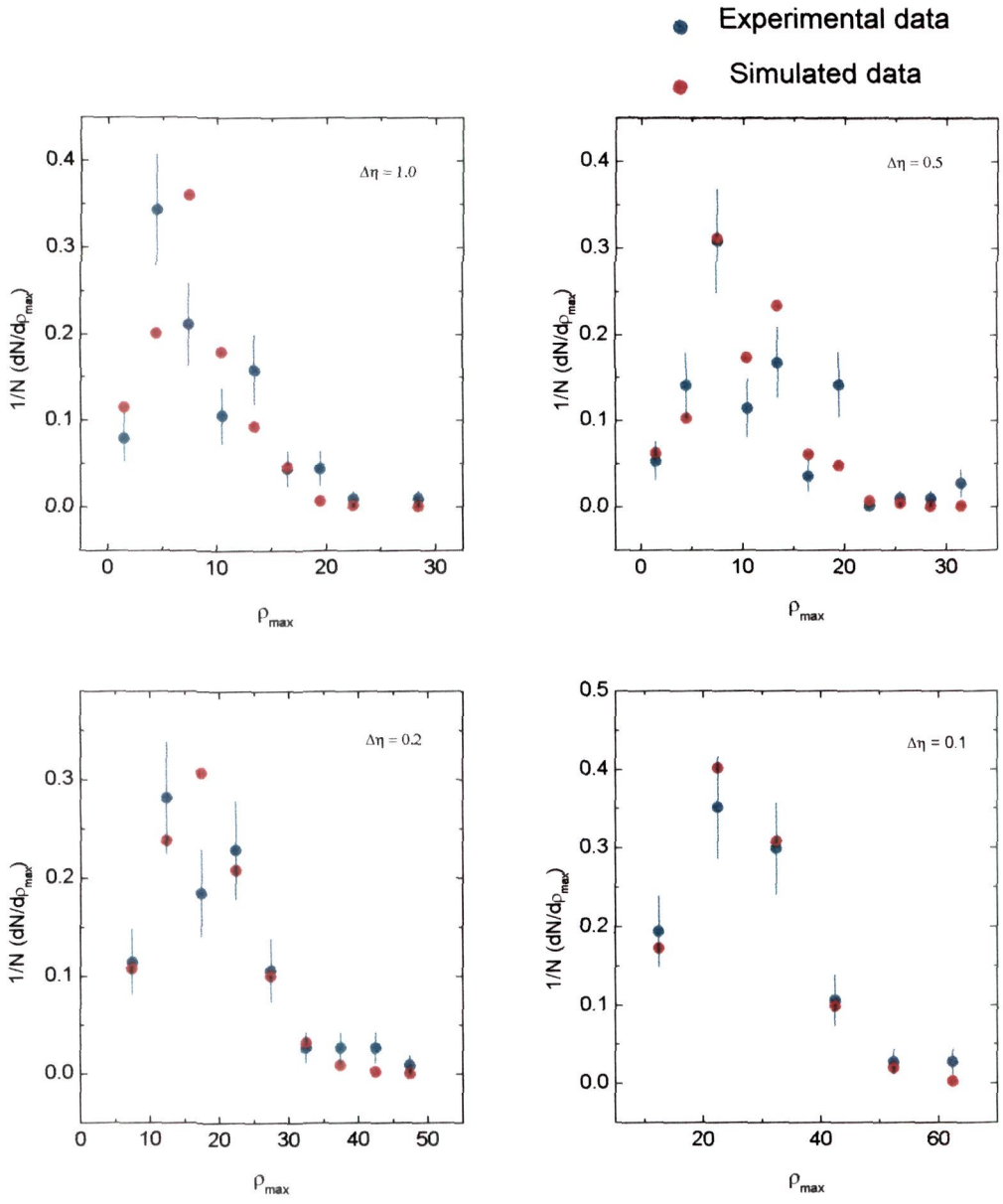

Fig. 5.3 Distributions of $1/N\ (dN/d\rho_{max})$ as a function of the maximum particle density ρ_{max} for 14.5A GeV/c ^{28}Si-Em interactions and the simulated data.

similar shapes, yet the values of $\frac{dN}{d\rho_{max}}$ obtained for the experimental data are quite different from those obtained for the simulated data, particularly in the mid-regions of the distributions. The mean values of the maximum particle density, $< \rho_{max} >$, and dispersion, $D(\rho_{max})$, for each distribution, experimental as well as MC generated, are listed in Table 5.2. It may be of interest to mention that the experimental values of both $< \rho_{max} >$ and $D(\rho_{max})$ are comparatively higher than those for the simulated events. The observed higher values of the two parameters in comparison to the corresponding values for the correlation free simulated events, in turn, reveal the occurrence of high particle densities in small η-bins for the experimental data. This may be due to the presence of dynamical correlations and clusterization of the particles produced in relativistic A-A collisions.

Using the value of ρ_{max} for each event for a fixed pseudorapidity interval, mean values of ρ_{max} for the events having multiplicities in the interval, 4 8, 9 12, 13 16, etc., are calculated. Variations of $< \rho_{max} >$ with $< N_s >$ for various $\Delta\eta$ values are plotted in Figs. 5.4 and 5.5; $< N_s >$ denotes the mean number of relativistic charged particles in the multiplicity interval considered. It may be noted from the figures that $< \rho_{max} >$ increases linearly with $< N_s >$ for both the data sets. The straight lines in the figures are the least squaresfits having the form:

$$< \rho_{max} > \quad = \quad a + b < N_s > \qquad (5.2)$$

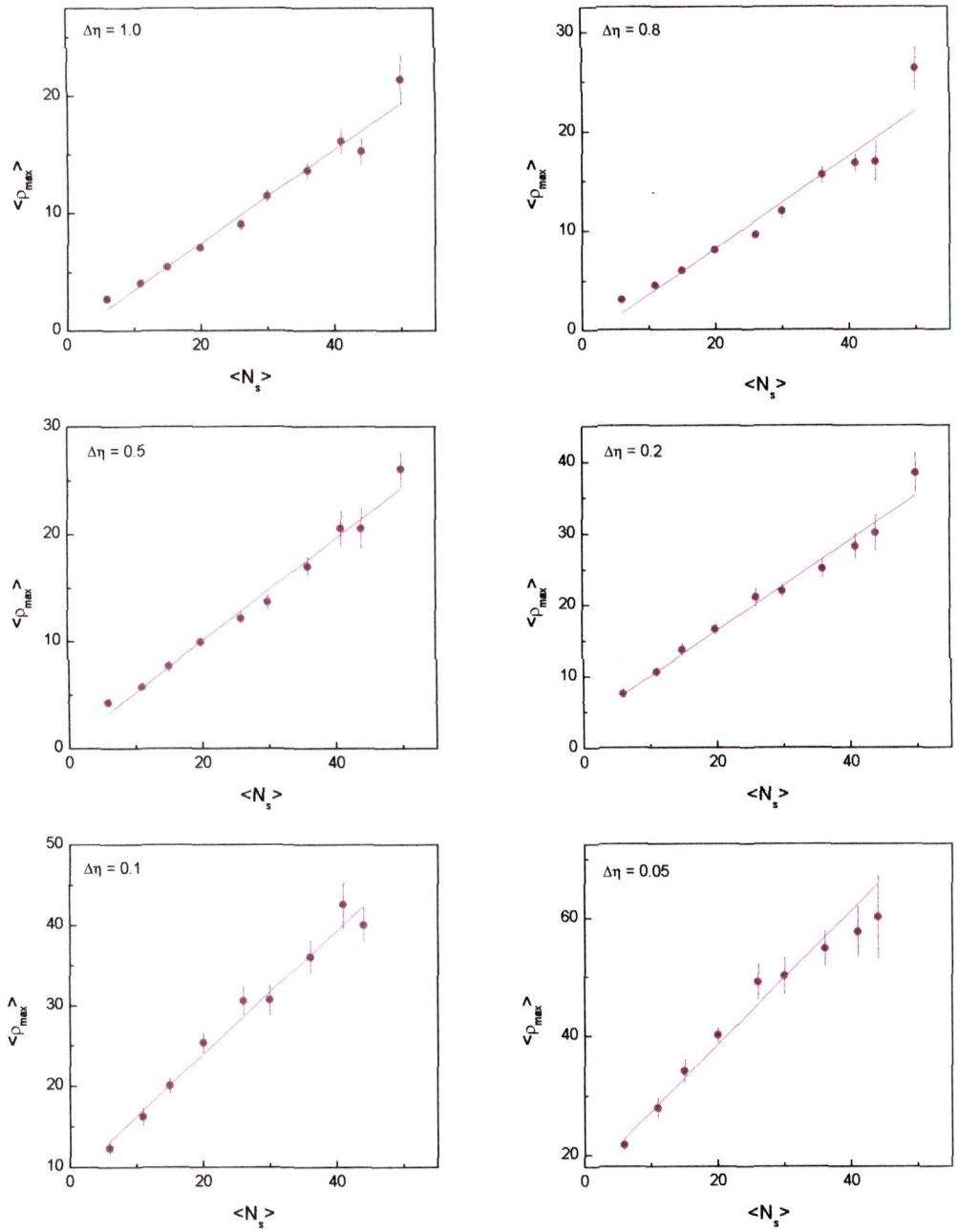

Fig. 5.4 Variations of $<\rho_{max}>$ with $<N_s>$ for different pseudorapidity windows in 4.5A GeV/c ^{28}Si-Em interactions.

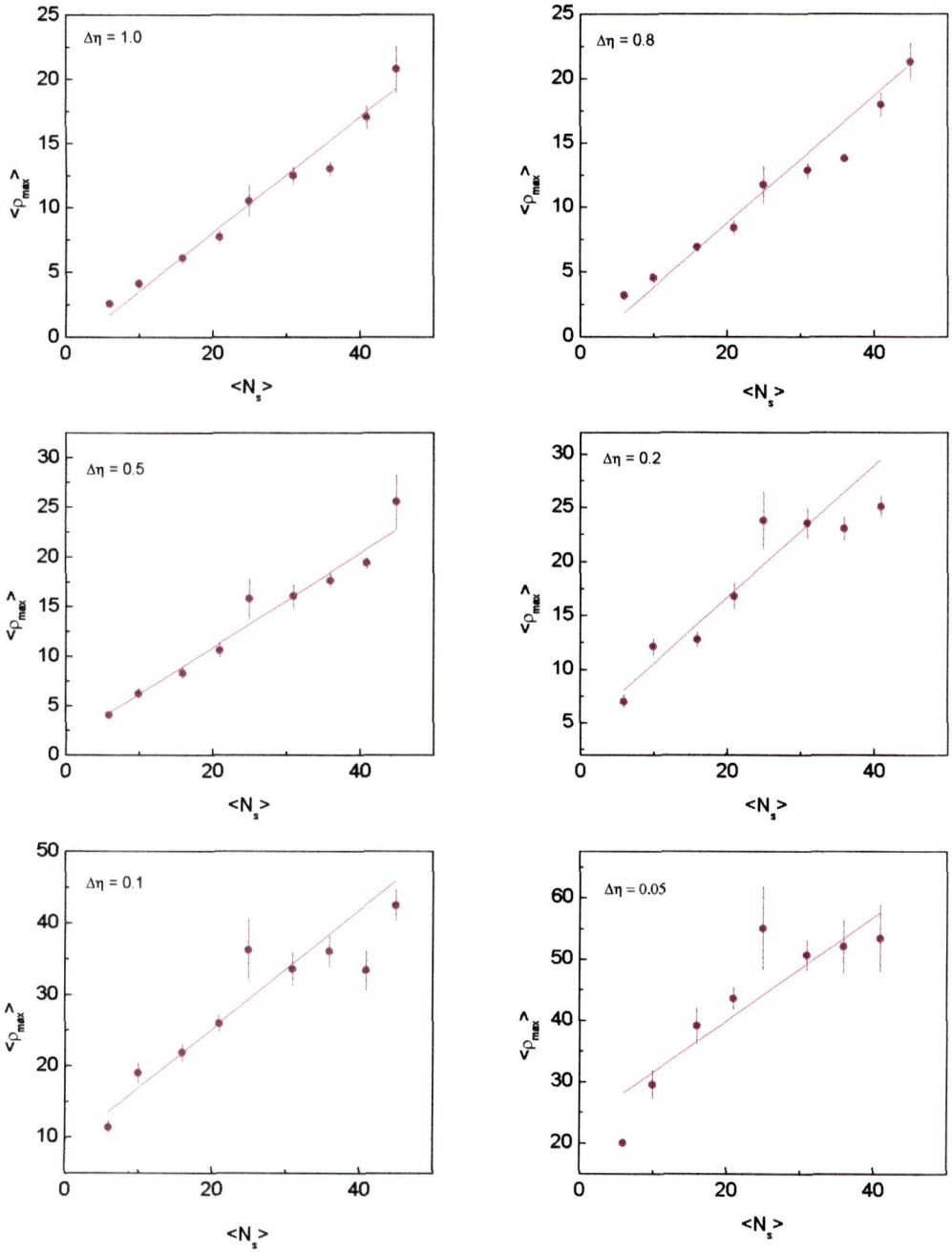

Fig. 5.5 Variations of $<\rho_{max}>$ with $<N_s>$ for different pseudorapidity windows in 14.5A GeV/c ^{28}Si-Em interactions.

Table 5.2 Values of $< \rho_{max} >$ and $D(\rho_{max})$ in different pseudorapidity intervals for the experimental and simulated events at the two energies.

Energy/Type of interaction	$\Delta\eta$	observed events		simulated events	
		$< \rho_{max} >$	$D(\rho_{max})$	$< \rho_{max} >$	$D(\rho_{max})$
14.5A GeV	1.0	6.29± 0.27	4.51± 0.20	5.72±0.05	3.14±0.03
^{28}Si Em	0.8	6.82± 0.28	4.63± 0.20	6.30±0.05	3.36±0.03
	0.5	8.60±0.33	5.60±0.24	7.83±0.06	4.00±0.04
	0.2	13.85±0.45	7.60±0.32	13.11±0.08	5.93±0.06
	0.1	21.10±0.61	10.29±0.43	20.81±0.12	8.68±0.09
4.5A GeV	1.0	4.82±0.17	3.87±0.12	4.82±0.04	2.67±0.03
^{28}Si Em	0.8	5.40±0.19	4.27±0.13	5.33±0.04	2.87±0.03
	0.5	6.80±0.21	4.85±0.15	6.77 ±0.05	3.42±0.03
	0.2	11.92±0.32	7.27±0.22	11.71±0.08	5.30±0.05
	0.1	18.60±0.42	9.77±0.30	19.00±0.12	8.06±0.08

The values of a, b and χ^2/D.F. for various fits are presented in Table 5.3. It may be seen from the table that, in general, the value of 'b' increases with decreasing $\Delta\eta$, however, its value is found to be essentially independent of the beam energy. Thus, for a fixed value of $\Delta\eta$, an energy independent relationship between $< \rho_{max} >$ and $< N_s >$ is obtained. Similar behaviour for the dependence of $< \rho_{max} >$ on $< N_s >$ has been reported by NA22 collaboration

[6] for π^+-p, k^+-p and p-p collisions at 250 GeV projectile energy.

Table 5.3 Values the constants a and b appearing in Eq. 5.2 and χ^2/D.F. for each fit.

Energy/Type of interaction	$\Delta\eta$	a	b	χ^2/D.F.
14.5A GeV	1.0	-0.11±0.72	0.43±0.01	0.85
^{28}Si Em	0.8	-0.47±1.67	0.48±0.01	2.43
	0.5	2.11±0.91	0.45±0.01	1.13
	0.2	5.29±3.99	0.59±0.01	1.69
	0.1	9.15±1.38	0.81±0.01	2.35
	0.05	23.71±9.90	0.81±0.01	2.31
4.5A GeV	1.0	-0.53±0.80	0.40±0.03	2.91
^{28}Si Em	0.5	-1.06±1.35	0.46±0.04	4.02
	0.5	0.44±0.76	0.48±0.02	2.57
	0.2	3.71±1.02	0.63±0.03	1.90
	0.1	9.31±1.06	0.75±0.03	1.06
	0.05	16.86±2.67	1.10±0.09	1.03

5.3 Fluctuations in rapidity gap spectra

5.3.1 Method of analysis

In order to look for the occurrence of fluctuations in rapidity gap spectra, the pseudorapidities of the particles produced in a collision are arranged in decreasing order. If n represents the number of particles in a limited pseudorapidity bin, $\Delta\eta$, with pseudorapidity values $\eta_1, \eta_2, \eta_3, ...\eta_n$, then the average

spacing between two consecutive particles is given by $\bar{s} = \frac{\Delta\eta}{n}$. The η-windows are selected in such a way that $|\eta_{min} - \eta_0| = |\eta_{max} - \eta_0| = \frac{\Delta\eta}{2}$, where η_0 is the centre-of-mass hadron-nucleon rapidity.

A comparison of the detailed structure of the nearest neighbour spacing in different collisions is carried out in terms of a re-scaled variable [3], $x_i = \eta_i/\bar{s}$, where i = 1, 2,.....n. The range of the re-scaled arguments of the particles is, thus, defined by $|x| \leq n/2$. The k-order spacing between the particles in terms of the re-scaled arguments is given by $s_k = x_{i+k+1} - x_i$, which denotes the nearest neighbour spacing for k = 0. It may be mentioned that if N(x) is the number of particles with positions from $-n/2$ to x, then

$$N(x) = \int_{-n/2}^{x} dx' \rho(x') \text{ where } \rho(x) = \bar{s}\rho(\eta)$$

For a sequence of particles with pseudorapidities η_i with constant average spacing, the averaged value of N(x), $< N(x) >$, would lie on a straight line, with slope $1/\bar{s}$ Thus, the intensity of fluctuations in each event around a straight line may be measured in terms of the least squares deviation [10]:

$$D(n) = \min \frac{1}{n} \int_{-n/2}^{n/2} d(x)[N(x) - (a + bx)]^2 \qquad (5.4)$$

According to the Random Matrix Theory [10,11], for a purely random sequence of correlation free particles with uniform density, which is essentially a Poisson ensemble, is calculated from $< D(n) >_{Poisson} = n/15$, n being the particle multiplicity in an event.

In the present study, in addition to the experimental results on 4.5A and

14.5A GeV/c ^{28}Si-nucleus interactions, results on two randomly simulated data samples, Set1 and Set2, each comprising of 3000 identical events are presented: both the data sets are so simulated that the multiplicity distribution of the charged particles are similar to the corresponding multiplicity distribution observed for 14.5A GeV/c ^{28}Si-nucleus collisions. However, for Set1, relativistic charged particles in each event are set to have uniform pseudorapidity distribution in the η-range covered. For Set2, pseudorapidity values in each event are set to have Gaussian like distribution having the mean values and the dispersion equal to the corresponding experimental values obtained for 14.5A GeV/c ^{28}Si-nucleus interactions.

5.3.2 Results and Discussion

Scatter plots of D(n) against n for various η-windows, W obtained for Sets 1 and 2 are exhibited in Figs. 5.6 and 5.7. The shaded circles in the figures correspond to the average values of D(n) for the events having a fixed multiplicity, whereas the straight lines are due to Poisson type distribution. It is noticed from the figures that for Set1 , values of $< D(n) >$ lie on straight line as a consequence of Poisson distribution irrespective of the window size. However, for Set2 having Gaussian type η distribution , $< D(n) > \sim n/15$ only for $W \sim 1.0$, while for larger η-windows, the values of $< D(n) >$ are found to be significantly away from the straight line resulting from Poisson distribution. It is worthmentioning that this trend of departure of the values of $< D(n) >$

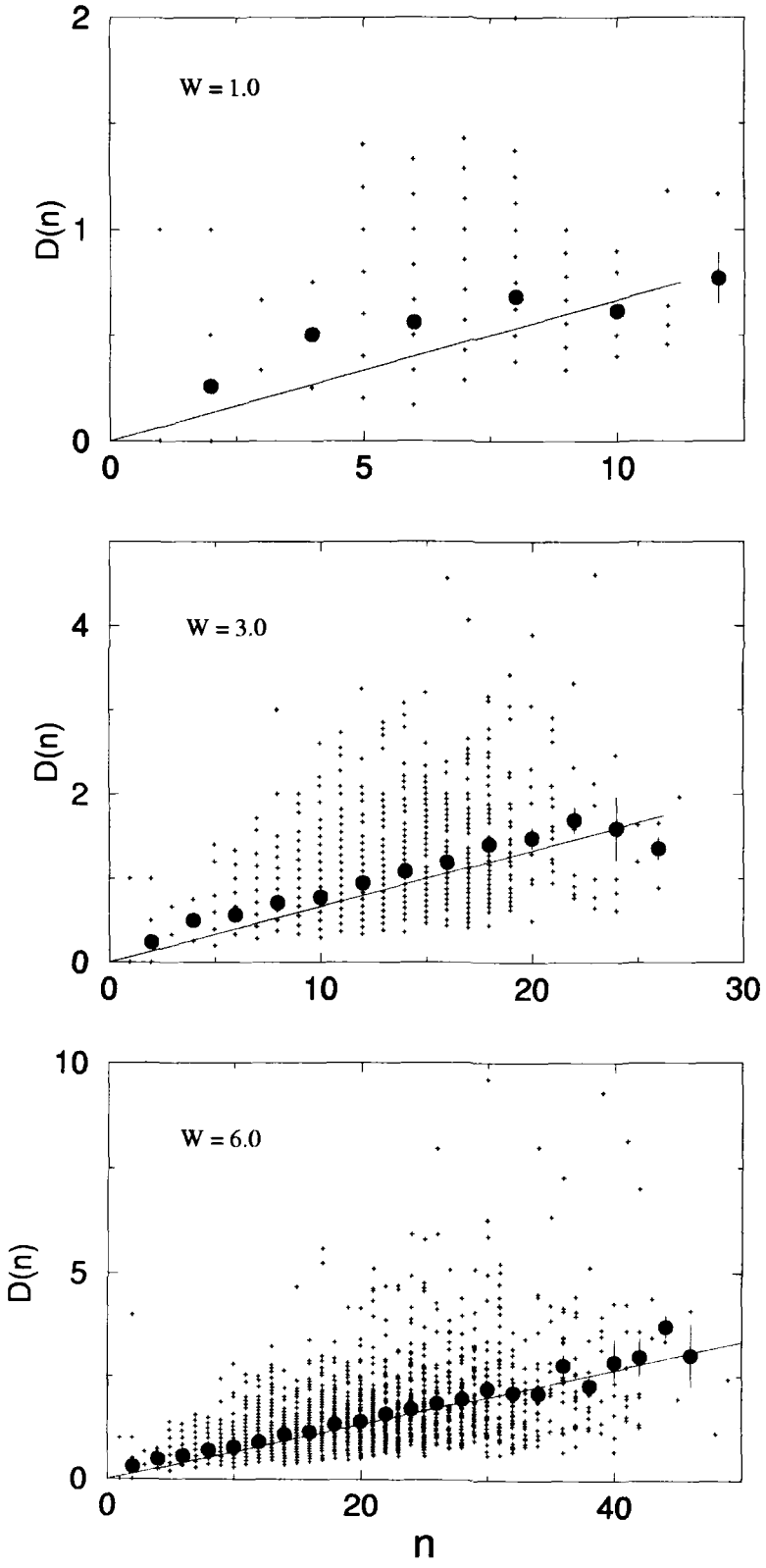

Fig. 5.6 Scatter plots of D(n) and n for the simulated events for set1.

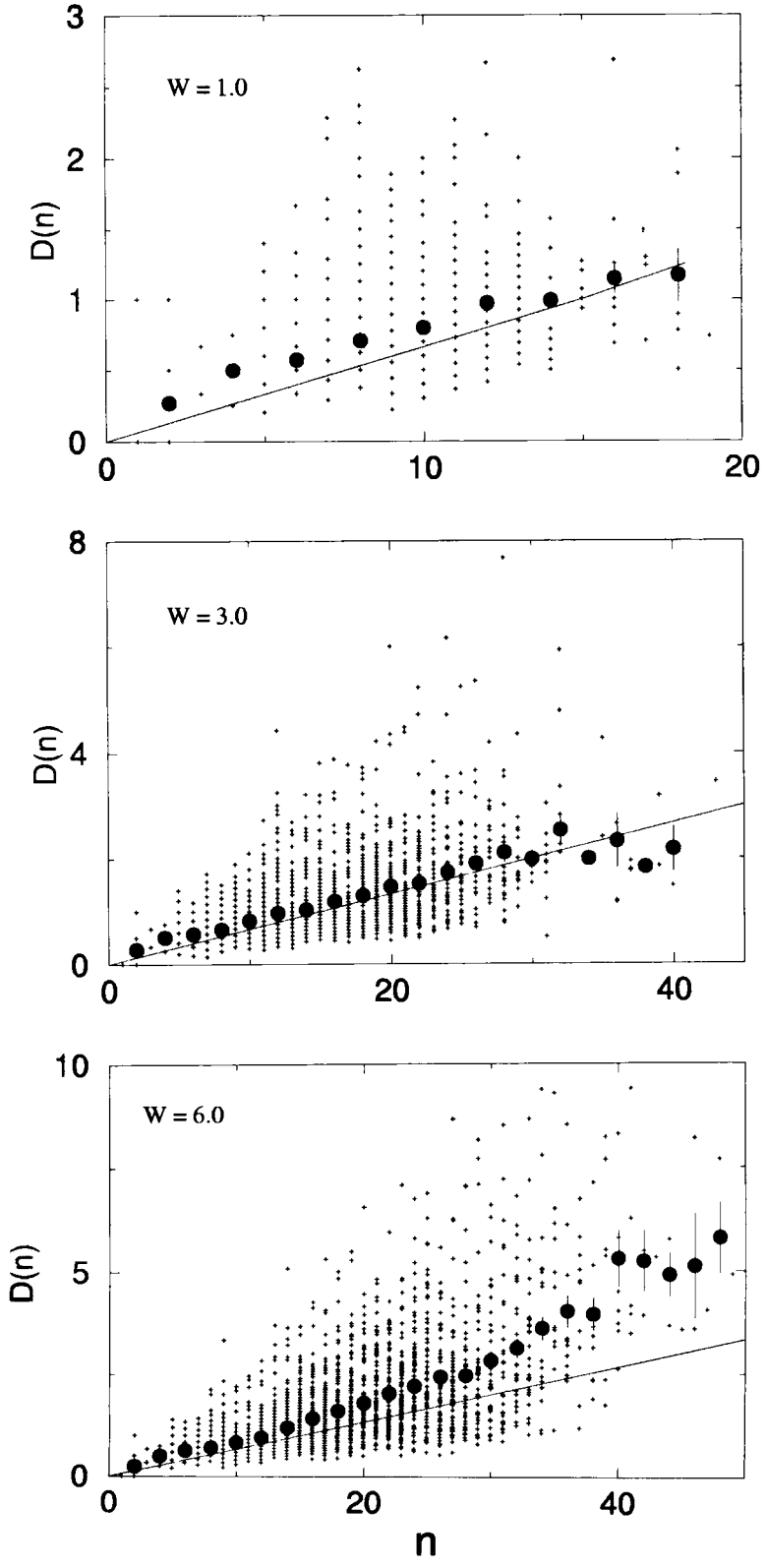

Fig. 5.7 D(n) vs n plots for the simulated events for Set2.

from the straight line is expected as the single particle inclusive distribution for smaller windows are rather more even.

Dependence of $< D(n) >$ on n for different pseudorapidity windows for the experimental data on 4.5A and 14.5A GeV/c ^{28}Si-nucleus interactions are exhibited in Fig. 5.8. Two data samples each comprising of 3000 events each corresponding to 4.5A and 14.5A GeV/c are generated using FRITIOF of Lund Model [11] for a comparison with the experimental results. The plots of $< D(n) >$ versus n for the simulated data are also exhibited in Fig. 5.8. It is worthmentioning that the values of $< (D(n) >$, for both experimental and FRITIOF data, are observed to lie on a straight line for all η-windows having the widths lying in the central region of the pseudorapidity spectra except that the fluctuations are large in the region of large multiplicity values. This might be due to the statistical reasons as the number of events is very small in this region. However, on increasing the window size, covering all the regions of η-spectrum, values of $< D(n) >$ turn out to be higher than those expected on the basis of Poisson distribution.

In order to examine the correlation effects at higher beam energy and in the case of heavy colliding nuclei, data samples, each having 2000 events, corresponding to the ^{16}O-Em and ^{32}S-Em interactions at 200A GeV and ^{208}Pb-^{208}Pb collisions at 158A GeV have been generated using FRITIOF. A sample of 2000 events corresponding to the 158A GeV/c ^{207}Pb-^{207}Pb interactions has also been generated using the event generator VENUS, based on the multi-string model

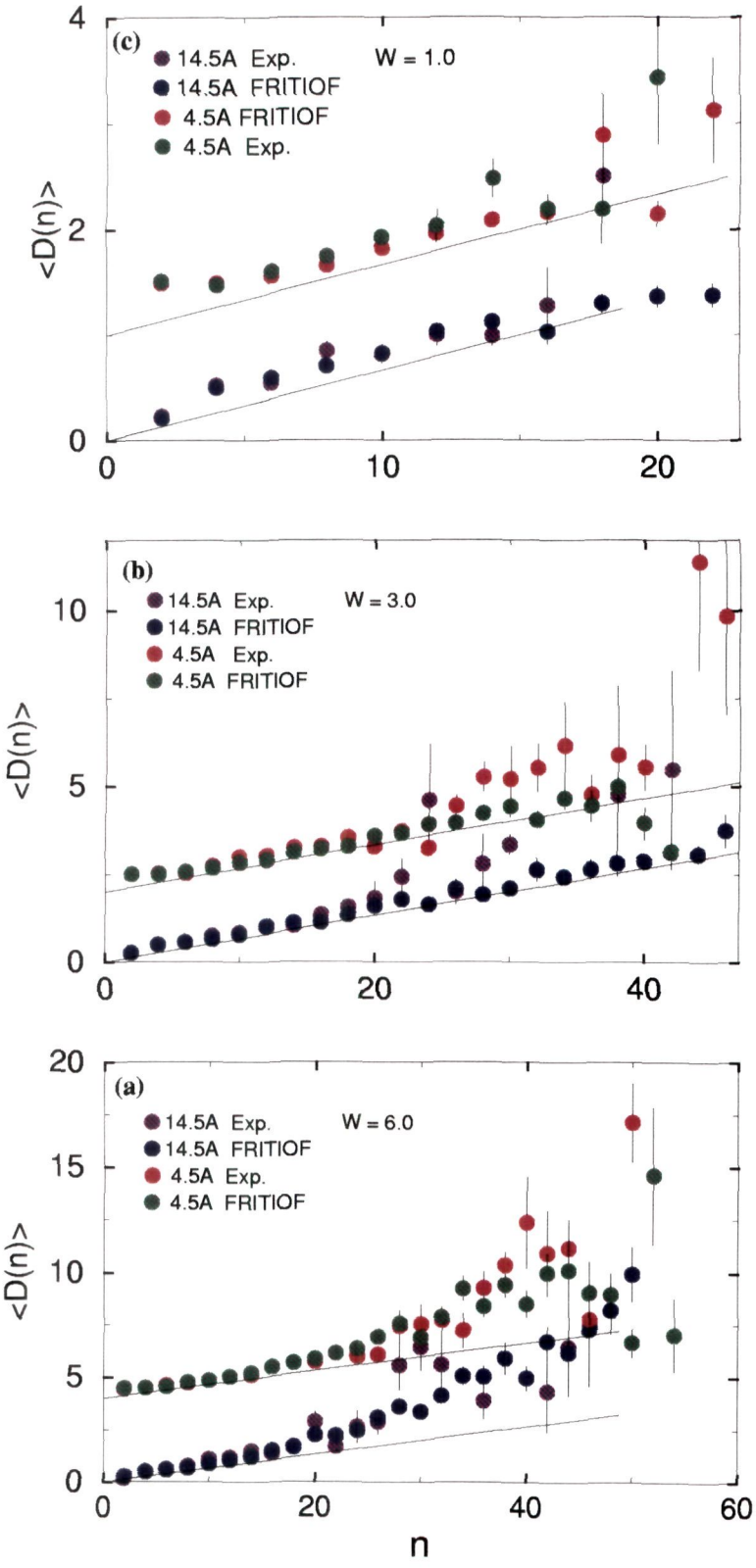

Fig.5.8 Plots of <D(n)> and n for selected rapidity windows for 4.5A and and 14.5A GeV/c Si–Em collisions.

[12]. Variations of $< D(n) >$ with n for all these data sets have been displayed in Figs. 5.9 and 5.10 for various rapidity windows considered; the window size is chosen such that the η values lie in the central region of η distribution. It may be of interest to note that the data corresponding to the different incident energies and for the various projectiles lie on the line corresponding to $< D(n) > \sim n/15$. These observations, therefore, tend to suggest that in the central region, the random emission of particles does dominate and the correlation between the produced particles, if any, appears to be suppressed.

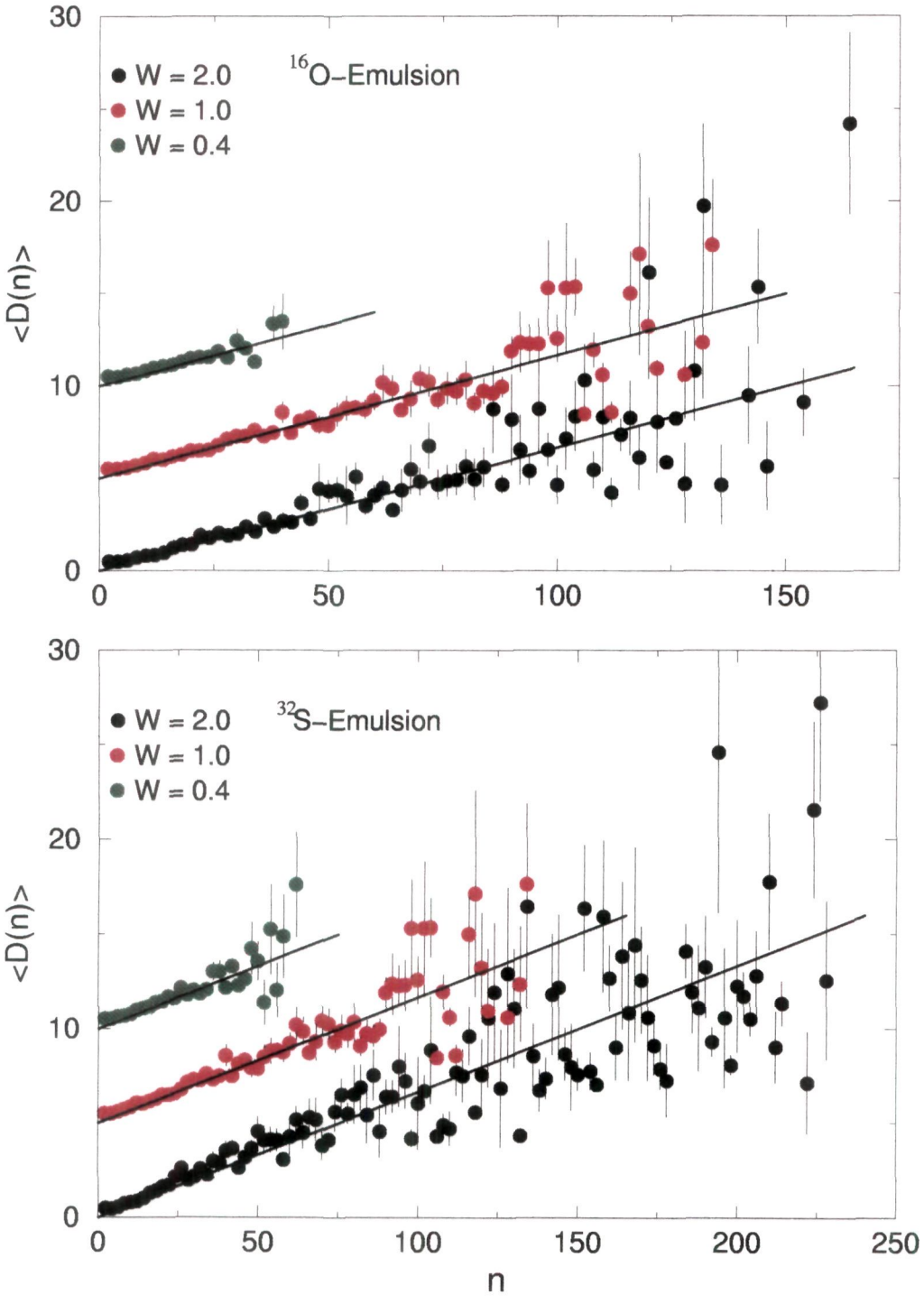

Fig. 5.9 Plots of <D(n)> and n in different rapidity windows for FRITIOF events for ^{16}O–Em and ^{32}S–Em collisions at 200A GeV/c.

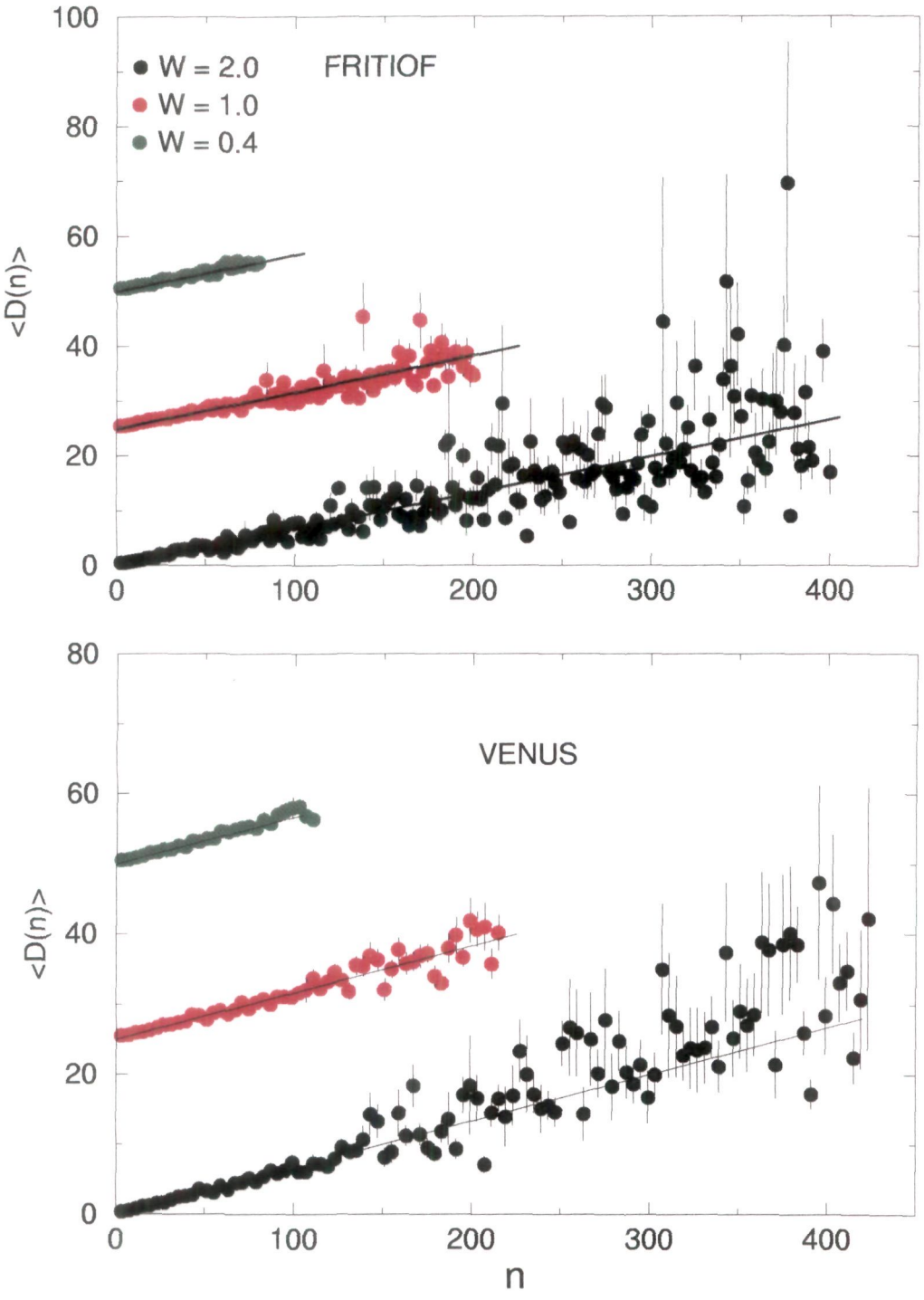

Fig. 5.10 Plots of D(n) and n in fixed rapidity windows for FRITIOF and VENUS data for 158A GeV/c Pb–Pb interactions.

References

1. G. Singh, K. Sengupta and P. L. Jain, *Phys. Rev. Lett.*, **61**, (1988) 1073.
2. E. A. De Wolf, I. M. Dremin and W. Kittle, *Phys, Rep*, **270**, (1996) 1.
3. Dipak Ghosh, Argha Deb, J. Ghosh, Rini Chattopadhyay et al, *Phys. Rev.*, **C61**,(2000) 037902.
4. R. C. Hwa , *Phy. Rev.*, **D 41**, (1990)1 456; **D 45** (1990) 475.
5. T. H. Burnett et al (JACEE Collaboration), *Phys. Rev. Lett.*, **50**, (1983) 2062.
6. M. Adamus et al (NA22 collaboration), *Phys. Lett.*,**B185**, (1987) 200.
7. A. Bialas and R. Peschanski, *Nucl. Phys.*, **B 273**, (1986) 703; **B 308**, (1987) 857.
8. D. Ghosh et al, *Phys. Lett.*, **B272**, (1991) 5.
9. D. Ghosh et al, *Phys. Rev.*, **D47**, (1993) 1235.
10. X. Cai, *ALICE/93-30 internal note/PHY* 20 sept., 1993.
11. B. Anderson, *Nucl. Phys.*, **A 447**, (1986) 1658.
12. K. Werner: Proc. 2^{nd} Int. Conf. Phys. & Astrophys. of Quark-Gluon Plasma, jan 19 23,1993 Calcutta, India.

CHAPTER VI

SUMMARY AND CONCLUDING REMARKS

Interest in the study of relativistic heavy-ion collisions has increased manifold during the recent years. It is because of the realization that nuclear collisions at relativistic energies may provide a unique opportunity to disentangle information regarding quark-gluon plasma, speculated to be formed in these collisions. Quark-gluon plasma (QGP) is elusive in nature as it is very short lived and very small in size; QGP is a few fermi in diameter and survives for about 5 to 10 fm/c only. Study of relativistic nuclear collisions in the fixed target mode became possible with the availability of ion beams from the AGS and SPS Currently RHIC is producing ultra-relativistic collisions at the centre-of-mass energy of ~200 GeV per nucleon. On the other hand, LHC, which is scheduled to become operational in 2005, would provide centre-of-mass energy of about 6.4 TeV per nucleon pair for Pb-Pb collision. Several large detectors are under construction to analyze the products of these interactions for investigating the formation of quark-gluon plasma.

It has been suggested that QGP may be formed at an early stage of relativistic heavy-ion collisions, which as a result of expansion and cooling, hadronizes so that hadrons are observed in the final state of the collisions. It is, therefore, difficult to attain conclusive evidence about the formation of QGP in these collisions. However, despite these difficulties, many signatures

of the formation of QGP have been proposed.

Study of non-statistical fluctuations in multiplicity and pseudorapidity distributions of relativistic charged particles produced in relativistic heavy-ion collisions is considered as one of the most useful procedures to examine the formation of QGP in these collisions. Particular emphasis in this regard is, therefore, given to look into the presence of non-statistical fluctuations which is envisaged to yield valuable information about QGP formation. The idea of using fluctuations as a probe for the production of QGP is based on the fact that QGP, if formed in a collision, would manifest itself in the form of non-linear emission of particles producing unusual peaks and valleys in the multiplicity distributions.

Fluctuations in the multiplicity and pseudorapidity distributions of the particles produced in relativistic nuclear collisions may not be entirely due to dynamical reasons only; there may be other reasons as well which may be purely statistical ones, like the fluctuations due to the difference in the impact parameter of the various collisions from which these particles originate. It may be of interest to mention that for looking at the fluctuations which might result due to occurrence of some physical processes in the collisions, statistical contribution to these fluctuations must be separated out.

Power law behaviour for the scaled factorial moments, F_q, with decreasing pseudorapidity bins, $\delta\eta$, called intermittency, has been proposed to be an indication for the presence of dynamical fluctuations. In the present study,

this approach is used to look for the presence of non-statistical fluctuations in the interactions of 4.5A and 14.5A GeV/c ^{28}Si nuclei with emulsion, CNO and AgBr targets. The plots of ln $< F_q >$ against $-\ln \delta\eta$ for the three categories of the interactions show linear rise confirming thereby power law behaviour and thus indicating the presence of intermittency in these interactions. Scaled factorial moments are observed to have higher values for the interactions due to CNO as compared to their values for the interactions due to AgBr targets. This is attributed to the fact that multiplicity resulting from the interactions due to CNO will be comparatively low.

The strength of the intermittency effect is investigated in terms of the slopes of log-log plots between $< F_q >$ and $-\delta\eta$. The slope parameter, ϕ_q, is observed to increase with the order of the moment, q. Further, for each order of the moment, the value of ϕ_q is found to be higher for the case of higher incident energy.

The fractal nature of particle emission source is examined in terms of anomalous dimensions, d_q, which are directly obtained using the slope parameters, ϕ_q. The anomalous dimensions are found to increase with the order of the moment, q. Furthermore, the value of d_q is found to be higher for 14.5A GeV/c ^{28}Si-nucleus collisions as compared to those for 4.5A GeV/c ^{28}Si-nucleus collisions for each order of the moment.

The intermittent behaviour in the final state of multiparticle production in relativistic nuclear collisions may be a projection of the occurrence of a

non-thermal phase transition. This aspect is investigated in terms of the behaviour of $\lambda_q(=\frac{\phi_q+1}{q})$ by plotting λ_q as a function of q. In the present study, for the interactions of ^{28}Si nuclei with emulsion, λ_q versus q plots show a distinct minimum whereas for other types of interactions, the resulting curves are observed to saturate. The observed distinct minimum may be an indication for the occurrence of a non-thermal phase transition in the collisions and the saturation effect may be because of the fact that analysis is carried out only upto q = 6.

The scaling behaviour of scaled factorial moments with respect to the second order scaled factorial moments is studied in terms of the Ginzburg-Landau description. The value of ln $< F_q >$ is found to increase linearly with ln $< F_2 >$ for all the three types of interactions considered. The slopes, β_q , are found to exhibit power law behaviour with (q-1). The values of the slopes of lnβ_q versus ln(q-1) plots for the various interactions are found to be positive.

Multiparticle production data may exhibit fractal behaviour analogous to the well known phenomenon of self-similarity in geometrical and statistical systems. In the present work, characteristics of multifractality in 4.5A and 14.5A GeV/c ^{28}Si-nucleus collisions are investigated using the multifractal moments, G_q, as a function of the phase space interval $\delta\eta$. It is found that ln $< G_q >$ rises linearly with $-\ln \delta\eta$ to a certain extent and thereafter the plots are observed to saturate. The linear rise manifests self-similarity in the mechanism of multiparticle production in the interactions considered. The saturation effect

is due to increase in the number of bins with multiplicity 0 or 1 with decreasing bin size Similar trends are also observed in the case of FRITIOF simulated data.

The dynamical component of the mass exponents, τ_q^{dyn}, is observed to deviate distinctly from (q-1), indicating thereby the occurrence of dynamical fluctuations. Furthermore, the generalized dimensions, D_q, are observed to satisfy the condition of multifractality, i.e., $D_q > D_{q'}$ for $q < q'$ for the various interactions considered in the present work. Further, the generalized dimensions are found to be positive for all the orders of the moment and demonstrate a decreasing trend with increasing q, which is a general property of the multifractals.

The spectral function, $f(\alpha_q)$, which gives a quantitative description of the fluctuations in the dense and sparse regions of multiplicity distribution, is found to be smooth, concave downwards with its maximum taking place around $q = 0$. The spectral function is not observed to peak in for all the three types of interactions considered, indicating thereby non-smooth nature of the multiplicity distribution of the particles produced in these interactions.

Correlation and clusterization amongst the relativistic charged particles produced in various interactions considered are investigated in terms of the maximum rapidity density distribution of relativistic charged particles in narrow pseudorapidity bins, $\Delta\eta$. It is found that maximum charged particle multiplicity, ρ_{max}, decreases exponentially with the total pseudorapidity for

each event. The distribution of maximum particle density, $dN/d\rho_{max}$ with respect to ρ_{max} exhibits almost a similar trend irrespective of the bin size, $\Delta\eta$. These distributions when looked into the Monte Carlo background, indicate the presence of dynamical fluctuations and clusterization. The average value of the maximum particle density, $< \rho_{max} >$ increases linearly with increasing multiplicity of relativistic charged particles. On the other hand, for a given multiplicity, $< \rho_{max} >$ is observed to increase with decreasing η bin width.

List of Publications

1. Publications in International Journals

1. Cluster Production in 14.5A GeV/c Si-nucleus collisions.
   A. Shakeel, **W. Bari**, N. Ahmad, A. R. Khan, M. Zafar and M. Irfan
   Int. J. Mod. Phys. E, Vol. 8, No. 2, 1999
2. Maximum charged particle density fluctuations in relativistic heavy ion collisions
   Shakeel Ahmad, **W. Bari**, N. Ahmad, M.M. Khan, M. Zafar and M. Irfan
   Journal of Phyisical Society of Japan, **Vol. 71, No. 4**, (2002) 1059.
3. Intermittency in 4.5A and 14.5A GeV/c ^{28}Si-nucleus interactions.
   W. Bari, N. Ahmad, M. M. Khan, Shakeel Ahmad, M. Zafar and M. Irfan
   Int. J. Mod. Phys., **E, Vol. 11, No. 2**, (2002) 131.
4. Non-statistical fluctuations in relativistic nucleus-nucleus collisions.
   W. Bari, N. Ahmad, A. Shakeel, M. Zafar and M. Irfan
   Communicated to the Canadian Journal of Physics, Canada
5. Cluster size dependence on relativistic charged particle multiplicity in nucleus-nucleus collisions.
   N. Ahmad, **W. Bari** and Shakeel Ahmad
   Submitted to the Canadian Journal of Physics, Canada

2. Papers presented at International/National Symposia/Conferences

1. Multiplicity and Compound Multiplicity in 14.5A GeV/c ^{28}Si-emulsion nuclei.
   Shakeel Ahmad, **W. Bari**, N. Ahmad, M. Zafar and M. Irfan
   DAE Symposium on Nuclear Nuclear Physics, Bangalore University, Dec. 26-30, 1997, Bangalore, India.
2. Angular Characteristics of charged shower particles produced in 4.5A and 14.5A GeV/c Si-nucleus collisions.

W. Bari, A. Tufail, A. Ahmad and A. R. Khan. XIII DAE Symposium on High Energy Physics, Punjab University, Chandigarh, Dec. 26-30, 1998, Chandigarh , India.

3. Fabrication and testing of a large area cathode pad chamber.
   P. Bhattacharya, S. Bose, S. Chattopadhyay, N. Majumdar, S. Sarkar, P. Sen, S. Sen, T. Sinha, B. C. Sinha, A. Bhasin, A. Gupta, L. K. Mangotra, N. Ahmad and **W. Bari** DAE Symposium on Nuclear Physics, Punjab University, Chandigarh, Dec. 27-31, 1999, Chandigarh , India.

4. Position resolution studies of a cathode pad chamber.
   P. Bhattacharya, S. Bose, S. Chattopadhyay, N. Majumdar, S. Sarkar, P. Sen, S. Sen, T. Sinha, B. C. Sinha, N. Ahmad and **W. Bari** DAE Symposium on Nuclear Physics, Punjab University, Chandigarh, Dec. 27-31, 1999, Chandigarh , India.

5. Characteristics of events accompanied by hadrons in the backward hemisphere in relativistic nucleus-nucleus collisions.
   Shakeel Ahmad, **W. Bari**, N. Ahmad, A. Tufail, and A. R. Khan. DAE Symposium on Nuclear Nuclear Physics, Punjab University, Chandigarh, Dec. 27-31, 1999, Chandigarh , India.

6. Multifractals in relativistic heavy-ion collisions.
   W. Bari, M. M. Khan, N. Ahmad, Shakeel Ahmad and A. R. Khan.
   International Symposium on Nuclear Physics, Bhaba Atomic Research Centre, Mumbai, Dec. 18-22, 2000, Mumbai, India.

7. Design and fabrication of ultrathin cathode pad chamber (CPC) Muon Arm Project in ALICE,
   SINP, Kolkata, **AMU, Aligarh** and Jammu University, Jammu.
   International Symposium on Nuclear Physics, Bhaba Atomic Research Centre, Mumbai, Dec. 18-22, 2000, Mumbai, India.

8. Multiparticle response of cathode pad chamber (CPC).
   Muon Arm Project in ALICE,
   SINP, Kolkata, **AMU, Aligarh** and Jammu University, Jammu.
   International Symposium on Nuclear Physics, Bhaba Atomic Research Centre, Mumbai, Dec. 18-22, 2000, Mumbai, India.

9. Multiplicity fluctuations in high energy heavy ion collisions.
   Shakeel Ahmad, **W. Bari**, N. Ahmad, M. M. Khan, M. Zafar and

M. Irfan.
XIV DAE Symposium on High Energy Physics, Hyderabad University, Hyderabad, Dec. 18-22, 2000, Hyderabad, India.

10. Intermittency in relativistic heavy–ion collisions.
W. Bari , N. Ahmad, T. Ahmad, S. Ahmad and M. Zafar
IV International Conference on Physics and Astrophysics of QGP, Jaipur (India) Nov. 26-30, 2001.

11. Multifractal analysis of multiparticle production at relativistic energies.
W. Bari, N. Ahmad, M. M. Khan, Shakeel Ahmad and A. Tufail
DAE Nuclear Physics Symposium, SINP, Kolkata, Dec. 26-30, 2001, Kolkata, India

12. Evidence of clusterization in ^{28}Si-nucleus collisions at 14.5A GeV/c.
N. Ahmad, **W. Bari**, M. M. Khan and Shakeel Ahmad.
DAE Nuclear Physics Symposium, SINP Kolkata, Dec. 26-30, 2001, Kolkata, India